REPUBLIC OF CAMEROON
REPUBLIQUE DU CAMEROUN

UNIVERSITY OF YAOUNDE 1
UNIVERSITE DE YAOUNDE 1

FACULTY OF SCIENCE
FACULTE DES SCIENCES

DEPARTMENT OF PHYSICS
DEPARTEMENT DE PHYSIQUE

Spatio-temporal Variabilities of precipitation Indices in Cameroon and Neighbouring Areas

THESIS

Submitted and defended publicly in fulfilment of the requirements for the award of the Doctorate Degree/Ph.D in Physics.

Option: **Environmental Modelling and Atmospheric Physics**

by

GUENANG Guy Merlin
Master degree in Physics
Registration number: 97Q018

Supervised by

MKANKAM KAMGA François
Professor

JURY:

President :	MANGUELLE-DICOUM Eliezer	Professor	University of Yaoundé I, Cameroon;
Rapporteur:	MKANKAM KAMGA François	Professor	University of Yaoundé I, Cameroon;
Members:	TCHAWOUA Clément	Associate Professor	University of Yaoundé I, Cameroon;
	TABOD Charles	Associate Professor	University of Yaoundé I, Cameroon;
	NZEUKOU Armand	Associate Professor	University of Dschang, Cameroon;
	MONKAM David	Associate Professor	University of Douala, Cameroon;

Year 2014

Dedications

To my mother mum NANA Rosalie and my late father dad NGUENANG David for sacrifices endured for my education.

Acknowledgements

I am thankful to Professor MKANKAM KAMGA Francois, my Supervisor, for his guidance, suggestions, and miscellaneous support during this work. A lot of time he invested for me cannot receive a human reward.

I send particular gratitude to all the members of jury (Pr. MANGUELE-DICOUM Eliezer, Pr. MKANKAM KAMGA Francois, Pr. TCHAWOUA Clément, Pr. TABOD Charles, Pr. NZEUKOU Armand and Pr. MONKAM David) who accepted to evaluate this work.

I acknowledge all the entire members of the Laboratory of External Geophysics for their kind collaboration and support.

I also acknowledge all my friends and the members of my family that encouraged me to persevere in the research.

This work is the result of cumulative knowledge received during all my studies. So I thank all my teachers especially those of the University of Yaounde I from whom I received the best qualities of teaching during my under- and post-graduate academic years.

I am gratefull to my institution the University of Yaounde I and to Atmospheric Science Letters (ASL) journal, for their support in publication.

I am also grateful to the anonymous reviewers of the ASL who helped improve the content, grammar and syntax of the report of my researches.

Many thanks to the National Meteorological Services of Cameroon (DNMC) for providing observed daily precipitations data.

Many more thanks also go to the following: the modelling groups for making their model output available for analysis, the Program for Climate Model Diagnosis and Intercomparison (PCMDI) for collecting and archiving this data, and the WCRP's Working Group on Coupled Modelling (WGCM) for organizing the model data analysis activity. The WCRP CMIP3 multi-model dataset is supported by the Office of Science, U.S. Department of Energy.

Contents

Résumé

Dans ce travail de recherche réalisé dans un domaine centré sur le Cameroun et ses environs, nous avons calculé quelques indices climatiques relatifs aux précipitations. Les résultats obtenus ont été soumis à des analyses spatiales et temporelles à partir des outils mathématiques appropriés. Les données utilisées sont celles des précipitations provenant de trois sources différentes: celles enregistrées dans 24 stations météorologiques du Cameroun, celles des simulations de quatre modèles climatiques de circulation générale (modèles MPI-echam5, MRI-cgcm2.3.2a, BCCR-bcm2.0 et CSIRO-mk3.5) et les données du 'Climatic Research Unit (CRU)'. Ces données s'étendent sur une période allant de 1951 à 2005. Pour les modèles climatiques, nous disposons en plus les données de projection pour les deux dernières décennies du 21^e siècle, simulées selon le scénario SRES A2 sur l'émission des gaz à effets de serre. Le calcul des dates de début et de retrait de la saison des pluies nous a permis de définir un zonage du domaine en trois grandes régions climatiques et d'établir un calendrier utile aux activités agricoles. Les résultats des autres paramètres statistiques montrent que dans tout le domaine d'étude, la fréquence et l'intensité des précipitations diminuent pendant que les pluies extrêmes deviennent plus fréquentes. Les modèles climatiques CSIRO-mk3.5 et MPI-echam5 simulent mieux ces indices et les meilleures corrélations sont obtenues par le modèle CSIRO-mk3.5. D'après les projections des modèles pour l'horizon 2082-2098, le début et le retrait des pluies connaîtront des retards respectifs d'au moins 5 jours et d'au plus 2,5 jours dans les régions du centre et du sud Cameroun, ce qui réduirait dans ces régions la durée de la saison des pluies. Dans la zone sahélienne du pays, c'est la situation inverse qui est projetée avec comme conséquence une augmentation de la durée des pluies. Les projections des autres paramètres prévoient des modifications spatiales futures de la fréquence et de l'intensité des pluies, à l'exception des régions autour du plateau de l'Adamaoua et dans la partie Est du domaine. Dans la dernière partie du travail visant à poser les bases pour le calcul de l'indice standardisé des précipitations au Cameroun, les précipitations ont été premièrement ajustées par quatre fonctions de distributions statistiques (gamma, weibull,

exponentielle et lognormale). La distribution appropriée pour chaque station a été ensuite utilisée pour le calcul de cet indice. Il ressort que pour des précipitations cumulées sur 6-mois ou moins, la fonction gamma convient pour la distribution des précipitations de la zone Sahélienne (>10°N) et la fonction weibull pour celles des autres zones. Sur plus de 6-mois, la répartition spatiale des fonctions de distribution devient inconsistante et le nombre de stations montrant une préférence pour la loi lognormale augmente avec le nombre de mois. L'analyse des résultats de l'indice standardisé des précipitations montre qu'en générale la sécheresse survient rarement et que les décennies 1970 et 1980 ont été les plus sèchent. Les calculs faits avec les données de précipitations de CRU donnent des résultats similaires avec de bonnes performances pour les cumuls sur de courtes périodes. L'étude des seuils opérationnels de sécheresse montre qu'ils varient avec l'espace et la longueur de la période temporelle considérée et impose donc la nécessité d'une définition objective pour l'utilisation en agriculture et en gestion des ressources hydrologiques.

Mots clés: Indices Climatiques; Variabilités climatiques; Changements Climatiques; Validation des Modèles Climatiques; Projections Climatiques; Fonctions de distributions statistiques; Indice standardisé des précipitations; Cameroun.

Abstract

In this work, some climatic indices related to precipitation were calculated over Cameroon and some neighboring areas. Results underwent spatial and temporal analyses through appropriate mathematical tools. We used three datasets: precipitation data from 24 meteorological stations in Cameroon, simulated precipitation from four general circulation climate models (namely MPI-echam5, MRI-cgcm2.3.2a, BCCR-bcm2.0 and CSIRO-mk3.5) and CRU (Climatic Research Unit) gridded precipitation. These data cover different time periods from the range 1951-2005. Model data are also available for the last two decades of the 21^{st} century, simulated under the SRES A2 emission scenario. The study of onset, retreat and length of the rainy season led to the grouping of stations into three different climatic zones and to the definition of an agricultural calendar. Results for other statistical parameters show that over the entire domain, precipitation frequency and intensity decreased while heavy rainfall increased. The two models CSIRO-mk3.5 and MPI-echam5 reproduce quite well observed patterns and gradients, however CSIRO-mk3.5 shows higher correlations. For the future period 2082-2098, onset dates are expected to be later by one pentad (5 days) or more and retreat dates later by less than half a pentad in most locations. This will lead to a slight decrease in the duration of the rainy season. The situation is reverse in Sahelian zone, where the season will be longer. Model projections for other statistical parameters show spatial variation in rainfall frequency and intensity except around Adamawa Plateau and in the Eastern part of domain. In the last part of the study aimed to lay a basis for the calculation of the Standardized precipitation index (SPI), data were firstly fitted to four probability density functions (i.e. gamma, exponential, weibull and lognormal). The appropriate distribution for each station was afterwards used for computation of the SPI. It appears that for short time scales (up to 6-month) and for stations above 10°N, the gamma distribution is the most frequent choice, while below this belt, the weibull distribution predominates. For longer than 6-month time scales, there are no consistent patterns of fitted distributions and the number of stations showing bias to lognormal increases with the number of month. Results of SPI show that

droughts were generally rarer than wetness. Long episodes of severe droughts and short episode of extreme droughts are identified in the decades 1970 and 1980 in many stations. Similar studies with CRU grid precipitation show good results with the best performances on short time scales. The study of operational drought thresholds shows the necessity of their objective definition because they change with space and with the considered time period. This will be useful in agriculture and water resource management.

Keywords: Climatic indices; Climate variability; Climate Change; Climate Model validation; Climate Projection; Statistical distribution functions; Standardized precipitation index (SPI); Cameroon.

Abreviations list

4AR	Fourth Assessment Report
AOGCM	Atmosphere-Ocean General Circulation Model
ASL	Atmosperic Science Letters
BCCR	Bjerknes Centre for Climate Research
CDF	Cumulative Density Function
CMIP3	Coupled Model Inter-comparison Project phase 3
CO2	Carbon dioxide
CRU	Climatic Research Unit
CSIRO	Commonwealth Science and Industrial Research Organisation
DJF	December–January–February
ECDF	Empirical Cumulative Density Function
GCM	General Circulation Model
GHG	Green House Gases
HADCM2	Hadley Circulation Model 2
IPCC	Intergovernmental Panel on Climate Change
IR	infra-red radiation
ITCZ	Inter-Tropical Convergence Zone
JJA	June–Juilly–August
LLNL	Lawrence Livermore National Laboratory
MAM	March–April–May
MPI	Max Planck Institute
MRI	Meteorological Research Institute
NCL	NCAR Command Language
NMSC	National Meteorological Services of Cameroon
PCMDI	Program for Climate Model Diagnosis and Intercomparison

RCM	regional Climate Model
SON	September–October–November
SPI	Standardized Precipitation Index
SRES	Special Report on Emissions Scenarios
TOA	Top of the Atmosphere
USA	United States of America
WAM	West African Monsoon
WCRP's	World Climate Research Program's
WGCM	Working Group on Coupled Modelling

List of Tables

List of Figures

General Introduction

Variations in meteorological elements as a result of atmospheric processes, determine the weather and the climate. In the coming decades, because of increases in atmospheric greenhouse gases (GHGs) and aerosols affecting atmospheric components, the climate is expected to change. A great challenge nowadays is the capability to translate this change in terms of climatic indices such as weather start and end, weather sequences/frequencies and extreme weather that may occur, so that these in turn can be translated into impacts on various sectors of society, economy and human endeavor.

In sub-Saharan African Countries, agriculture is the main socio-economic activity. According to Tarhule et al. (2009), about 95% of the land used is devoted to agriculture which is the main occupation of about 65% of the population. Good crop development depends on precipitation to maintain the needed level of soil water reserve. Perturbations of the hydrological cycle, in response to climate change, may involve perturbations of frequency and intensity of precipitation and then, directly affect the availability and quality of fresh water (Indrani et Abir 2011). Droughts are apparent after a long period with a shortage of precipitation or without any precipitation (Sergio et al. 2009). In recent years, severe droughts were recorded in the Sahel region in the decades 1970 and 1980, whereas in the Horn of Africa, they have been even more frequent in the late 20^{th} to early 21^{th} centuries. Another modification of the climate is observed in the perturbation of the rainy season that has become unpredictable. Start and end dates are uncertain. There are long dry spells in the middle of the rainy season. When rain comes, it can be so heavy that the soil is washed away and crops are destroyed. For farmers, it is becoming more difficult to know when to plant, or even what to plant. Substantial climate modifications as a result of global warming will affect the onset and retreat of the rainy season which has become irregular over the years (Salack et al. 2011), making it difficult for farmers to optimize the seed planting period and adjust to the length of the growing season (Olaniran 1983a; Mugalavai et al. 2008; Ndomba 2010). The sad consequences of these climate variabilities will be the decrease of agricultural production and thus, wide-spread starvation and

death (Leonard 2010; UNEP 2004). Extreme precipitation events are also among the main causes of losses and injuries attributed to weather and climate in African countries. In the subtropical zone, they are responsible for flooding, landslides, and collapse of houses, hail damages to crops, etc. Rainfall must be taken into account in the design of some types infrastructures, especially in urban areas. Knowledge of the frequency, amount and spatial distribution of rainfall can help in the forecast of catastrophes and the management of water resources and related activities in agriculture, hydroelectric energy production and tourism. Therefore, there is the need to better understand the precipitation indices and to study their temporal and spatial variabilities under the current and future perturbed climate, in order to guide vulnerability and adaptation assessment and measures.

Although the time scale of events leading to flooding and other weather related destructions is of the order of a few hours, most studies are based on the more readily available daily data (Gordon et al. 1992; Jolliffe et Hope 1996; Osborn et al. 2000; Brunetti et al. 2001; Burgueño et al. 2004; Seleshi et Zanke 2004). In studies on Africa, only a limited number of stations and data on short periods are available. The use of satellite data or climate model outputs are alternative solutions to these issues. However, satellite data are limited to recent periods while model outputs can cover longer periods in both the present and the future. In view of the ongoing global warming and its consequences on regional climate variability, the use of model outputs to investigate characteristics of the rainy season (e.g. rainfall totals, rainy day frequencies, onset, retreat and length of the rainy season) is necessary in order to assess future changes and guide adaptation measures and long term planning. This is why much work has been devoted to developing model projections at global (Emori et al. 2005) and regional scales (Jones et al. 1997). Climate models project intensification of the water cycle and of extreme events as consequences of the rising temperature (Zwiers et Kharin 1998; Voss et al. 2002).

Global and regional climate models with various IPCC emission scenarios have been used by many authors for projecting future climate change. In the Iberian Peninsula, it was found that 5/24 IPCC GCMs (MIROC3.2-HIRES, MPI-ECHAM5, GFDL-CM2.1, BCCR-BCM2.0 and UKMO-HADGEM1) best reproduced current climate (Errasti et al. 2011) and could be used for future climate projections. Mkankam (2000) concluded that two IPCC coupled atmosphere-ocean general circulation models (ECHAM4 and HADCM2), simulated well the present climate in Cameroon and neighbouring areas. Thus, he used their outputs to evaluate projected changes in rainfall and temperature resulting from increased concentration of greenhouse gases in the atmosphere for the period 2040-2070. The results revealed changes in annual rainfall within the range of present

climate variability while the projected temperature increases were larger than observed variability. An evaluation of the ability of 18 GCMs to capture the West African monsoon system found that three models (amongst which MPI-ECHAM5) gave reasonable simulations of the twentieth-century climate while others comprising CSIRO-Mk3.0 and MRI-CGCM2.3.2 failed to do so (Cook et Vizy 2006). Errasti et al. (2011) found that all IPCC models do not describe the present climate with similar accuracy. Furthermore, the best models for a particular region of the earth do not always achieve the same degree of performance in other regions. Additionally, the skill of the models is different according to the meteorological variables examined.

Following the scientific challenge stated in the first paragraph, the contribution of this work is to translate observed climatic variables into indices that characterize the climate and to assess their future changes under a perturbed climate. Thus we will study spatial and temporal variabilities of some precipitation indices under a current and future climate. The study is done over Cameroon and some of its neighboring areas. The precipitation indices include: precipitation intensity and frequency; onset, retreat and length of the rainy season; the standardized precipitation index (SPI). The work is organized as follows: In chapter 1, literature review on climate change, climatic variabilities and climate models are presented. Chapter 2 is devoted to description of data and methodology of investigation. The results are shown and discussed in chapter 3. The study ends with general conclusion and perspectives.

Chapter 1

Literature Review on Climate Variability and Change

1.1 Climate Variability definition

Climate variability can be defined as the way climatic variables (such as temperature or precipitation) depart from some average state, either above or below it. For illustration, the average maximum temperature in July in a given region, may be 25°C (averaged over the last 30 years), but each year, July's daily maximum average temperature will be less than or greater than this long-term average value. Climate variability can be observed at various time scales: daily, monthly, yearly or decadal.

1.2 Climate change definition and impacts

Climate change is a long-term (decadal or longer) modification in climate. It can be defined as a trend in one or more climatic variables characterized by a fairly smooth continuous increase or decrease of the average value during the period of record. As defined in the Third Assessment Report (TAR) of the Intergovernmental Panel on Climate Change (IPCC 2001a), the concept of climate change detection is the process of demonstrating that climate has changed in some defined statistical sense, without providing a reason for that change. There are many alerts today about the changing of the weather. The weather is the condition of the atmosphere in one area at a particular time. The report of the IPCC (1995) has been taken as a starting point for the assessment of the scientific knowledge concerning climate change and its impacts regarding the weather and weather extremes in particular (Vellinga et van Verseveld 2000). Since 1995 many new observations

and reports have become available.

1.2.1 Causes of climate change: greenhouse gases (GHG)

Greenhouse gases are atmospheric gases which allow direct sunlight (relative shortwave energy) to reach the Earth's surface unimpeded. They also contribute to the greenhouse effect by absorbing infrared radiation produced by solar warming of the Earth's surface and this gradually increases the temperature of the Earth's surface and the air in the lower atmosphere.

Most of the observed increase in global average temperatures since the mid-20^{th} century is very likely due to the observed human induced increase in greenhouse gas concentrations (IPCC 2007b). Human activities have contributed to a number of the observed changes in climate. According to the IPCC (2007b), this contribution has principally been through the burning of fossil fuels, which has led to an increase in the concentration of GHGs in the atmosphere. Another human influence on the climate are sulfur dioxide emissions, which are a precursor to the formation of sulfate aerosols in the atmosphere. They all alter the amount of energy within the climate system and cause changes to the climate.

Illustration of the greenhouse gas effect on global warming

Let T_s be the surface temperature and T_a the temperature of the atmosphere (Figure 1).

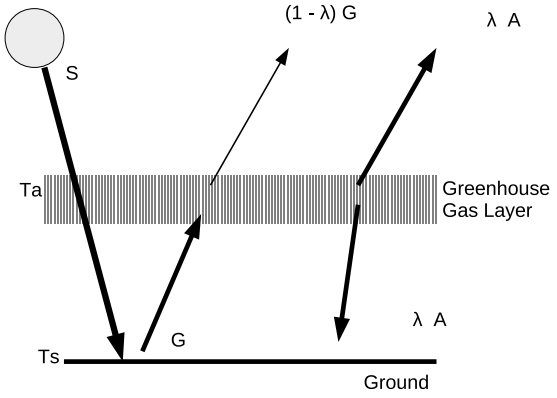

Figure 1: Greenhouse effect in the energy balance models.

The surface emission is $G = \sigma T_s^4$, where λ is the emissivity of the atmosphere (depending on the strength of the greenhouse effect) and $\sigma = 5.6697 \times 10^{-3} W.m^{-2}.K^{-4}$ is the Stephan-Boltzmann constant.

the following equations can be written in terms of the energy fluxes

- for the surface

$$S + \lambda A = G \tag{1.1}$$

A is the emission from the atmosphere and S is the solar radiation

- for the atmosphere

$$\lambda G = 2\lambda A \tag{1.2}$$

- for the planet

$$S = \lambda A + (1 - \lambda)G \tag{1.3}$$

Combining Equations 1.2 and 1.3, we deduce

$$G = \sigma T_s^4 = \frac{S}{(1 - 0.5\lambda)} \tag{1.4}$$

and then

$$T_s = [\frac{S}{\sigma(1 - 0.5\lambda)}]^{1/4} \tag{1.5}$$

This simple model readily determines the effect of changes in solar output or change of earth albedo or effective earth emissivity on average earth temperature. It says nothing, however about what might cause these things to change.

1.2.2 Sources of greenhouse gases

Many greenhouse gases occur naturally in the atmosphere, such as carbon dioxide (CO2), methane (CH4), water vapor (H2O), and nitrous oxide (NOx), while others are purely man made. These anthropogenic GHGs include the chlorofluorocarbons (CFCs), hydrofluorocarbons (HFCs) and Perfluorocarbons (PFCs), as well as sulfur hexafluoride (SF6).

Natural sources

The natural sources of the greenhouse gases are those that are continuously being recycled in the atmosphere through biogeochemical cycles that operated for millions of years before humans. These processes include:

* volcanism that produces GHG and aerosols (Aerosols are small particles present in the atmosphere with widely varying sizes), and then increases their rate in the atmosphere

* increase in the sun's radiation that increases the water vapor rate in the atmosphere

* animal and plant respiration that produces carbon dioxide

Anthropogenic sources

Human activities accelerate the natural process by creating more greenhouse gases in the atmosphere. These activities include:

* Fossil fuel combustion for electricity, heat, and transportation, raising the level of carbon dioxide in the atmosphere

* Land-use changes that increase the levels of methane and nitrous oxide.

* Industrial processes that emit synthetic fluorinated gases: Hydrofluorocarbons, perfluorocarbons, and sulfur hexafluoride.

1.2.3 Recent climate trends

Trends have been observed in many climatic variables. The most sensible variables we focus on are temperature, precipitation and sea level rise.

a) Temperature

The climate and the mean temperature on the Earth's surface depend on the balance between incoming (short wave) solar energy and outgoing energy (infrared radiation) emitted from the Earth's surface. Greenhouse gases trap some of the infrared radiation emitted by the Earth and keep the planet warmer than it would be otherwise. The mean global temperature, about 15°C, would be far below zero without this natural greenhouse effect (Vellinga et van Verseveld 2000).

It has been observed from the year 1880 to 2009 that the global mean surface temperature has increased and will probably continue to increase during the coming years (Hansen et al. 2010) (Figure 2).

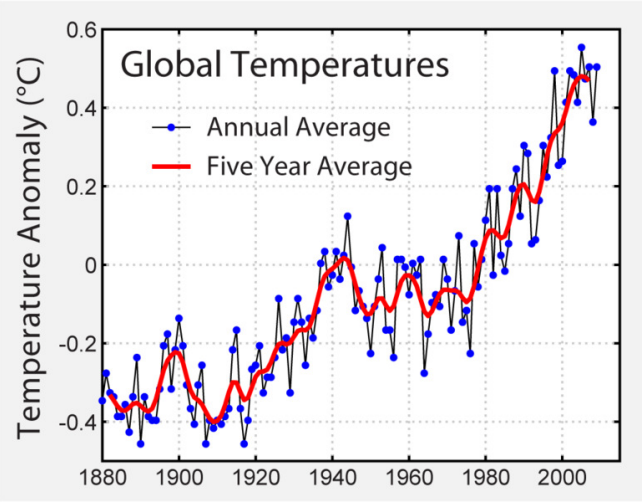

Figure 2: Global mean surface temperature difference from the average for 1880-2009 (Hansen et al. 2010.)

Over the past 130 years, the mean temperature of the Earth's surface has risen between 0.3 and 0.6°C, as reported by IPCC (1995). More recent analysis, including the temperature record up to 1999, indicates that the global average temperature has now risen by about 0.6°C over the whole period of record since 1860 (Wigley 1999; Kevin et al. 2000). However, most of this temperature increase occurred during the last few decades, when the global average temperature rose by about 0.2°C per decade. The top ten warmest years ever measured worldwide (over the last 120 years) all occurred after 1981 with the peak in the year 1998, the six warmest of these years occurred after 1990 (Vellinga et van Verseveld 2000).

The global temperature change is not equally distributed. The largest recent warming is between 40°N and 70°N (Vellinga et van Verseveld 2000). In a few areas, such as the North Atlantic Ocean, north of 30°N, the temperature decreased during the last decades (Houghton et al. 1995).

b) Precipitation

An increase in the average global temperature is very likely to lead to more evaporation and precipitation. However, it is difficult to predict and measure the precise changes in the hydrological cycle because of the complex processes of evaporation, transport, and precipitation and also because of the limited quality of data, short periods of measurements, and gaps in time series. In spite of these limitations, some specific changes in the amounts and patterns of precipitation have been found over the last few decades. It has been observed an increase in the mean precipitation from 30°N to 70°N and 0°S to 70°S while in the area between 0°N and 30°N (comprising our study domain 0°-14°N), a general decrease in the mean precipitation has occurred (Houghton et al. 1995).

c) Sea level rise

Sea level has risen between 10-25 cm over last 100 years. It has risen most sharply over the last 50 years (Vellinga et van Verseveld 2000). According to Vellinga et van Verseveld (2000), the recent increase in the rate of sea level rise is related to the observed increase of the Earth's global temperature and the ocean sea surface temperature. The volume of the ocean surface water layer expands per 0.1°C warming of the surface layer of the oceans, such that the sea level rises about 1 centimeter. Thus, the measured 0.6°C−sea surface temperature increase explains a 6 centimeters sea level rise. The observed melting and retreating of glaciers and ice sheets indicates an additional sea level rise between 2

and 5 centimeters.

Observations of other components of the climate system (Snow and Ice changes, Circulation patterns, (Extra)-tropical cyclones, Observed changes in ecosystems, Extreme weather events and damage cost) can be found in Vellinga et van Verseveld (2000). Recent studies show that inter-annual and synoptic time and space scale processes affect weather and climate extremes, such as tropical cyclones, El Niño effects, and extra-tropical storms (Gerald et al. 2000).

The changing of the climate components as seen above is followed by the environmental impacts. The consequences are becoming more and more perceptible. Most of the countries in the world are suffering from its devastating effects.

1.2.4 Impacts of climate change

The effects of emissions of CO_2 and other greenhouse gases on the global climate are becoming increasingly visible. The impacts of climate change and adaptation possibilities are examined firstly by synthesizing knowledge from the scientific literature, and secondly thanks to advice and expert report. Thus various impacts of the climate change has then been reported (IPCC 1995; Vellinga et van Verseveld 2000):

1. More Severe or extreme weather events

   Severe weather has always affected human activities and settlements as well as the physical environment. It can damage property, cause loss of life and population displacement, destroy or sharply reduce agricultural crop yields, and temporarily disrupt essential services such as transportation, telecommunications, energy and water supplies.

2. Droughts

   Multiple droughts since 1971 resulted in dry streams, withered and abandoned crops, dead fish, record low rivers and declining ground water levels. Between 2000 and 2005, Washington experienced two drought emergencies, resulting in drought declarations by Governors Locke and Gregoire.

   Droughts cause:

   - Less summer water for farms, cities and forests.
   - Less water for irrigation due to earlier high river flows and decreasing soil moisture.

- Less water for city municipal water sources, affecting industries, businesses and homeowners.
- With a 3.6 degree warming, droughts will occur more frequently: what have been historic 50-year droughts will now occur every 10 years, what have been historic 10-year droughts will now occur about every 2 years.
- Increased forest fires: dry and dying trees are a set-up for forest fires. Large forest fires (more than 500 acres) have increased from an average of 6 per year in the 1970's to 21 per year in the early 21^{st} century. Forest fires release greenhouse gases and destroy the trees that can absorb CO_2 from the air.

3. Floods more extreme and often

   Warmer temperatures result in more winter precipitation falling as rain rather than snow throughout much of the Pacific Northwest. This change will result in:

   - higher winter stream flows with more floods,
   - less winter snow accumulation,
   - earlier spring snowmelt especially in rivers that depend on snowmelt,
   - earlier peak spring stream flow (already 10-30 days earlier than 1948) and
   - lower summer stream flows. These trends have already been observed. In contrast to more rain when we do not need it, there will be less water when we do need it. Substantial reductions in summer stream flow will adversely affect
   - farmers who rely on irrigation,
   - resident and anadromous fish and
   - summertime hydropower production.

     These changes are likely to increase existing conflicts among competing water users, made worse by a regional population increase.

4. More landslides

   Rain-soaked soils are prone to slipping, which results in landslides affecting homes, businesses, power lines and transportation routes. More rain could increase the risk and frequency of landslides.

5. more pollution

More precipitation falling as rain rather than snow quickly runs off the land, especially over paved surfaces, and areas cleared of forest or natural vegetation. In a warmer climate, precipitation falling as rain could increase fall and winter flooding in susceptible river basins.

- As water flows over the land, it carries with it all pollutants left on the ground or flowing off paved surfaces (car oils, antifreeze, brake lining dust, pet and farm waste, fertilizers and pesticides, etc).

6. Earlier river runoff

   As the spring thaws come earlier and faster, the peak period for snow melt could move back weeks or months. This would result in less summer water when it is needed most for crops, fish, cities and hydropower generation. Urban water supply systems that rely on storage of water in mountain snow pack will see less water coming into their reservoirs in late spring/early summer. This will be combined with an increased demand for water caused by higher temperatures. For some systems, these impacts will be substantial.

7. Changing growing season

   With a warming climate, the growing season for some plants may be extended. The last frost would come earlier in the spring and first frost would come later in the fall. However, this advantage can be erased if there is limited water to nourish forests and crops during hot weather. Studies in Washington wine country conclude that more frequent series of extreme hot or cold days can result in damage and loss, even if the rest of the season is more moderate. Warmer winters allow forest and crop pests to reproduce longer and suffer less winter die offs, so pest populations can boom. This is already happening in Canada and even Washington forests where pine bark beetles are rapidly devastating large tracts of forests. Ecosystem changes from shifting seasons can break historic linkages between predator and prey migrations, cause population booms or crashes that affect the rest of the system allow invasive plants animals and insects to move into new territory, stress native species with unusual weather and water conditions.

8. Impacts on Agriculture

   According to Kevin et al. (2000), agricultural crops are mainly sensitive to fluctuations in temperature and precipitation, although solar radiation, wind, and humidity

are also important. In general a crop grows best and produces maximum yield for some optimum value of the relevant climate variable; as conditions depart from the optimum, the plants suffer stress.

9. Multiple emergency response needs

   Extreme weather across the state can

   - overtax the emergency response systems and funding for flood response,
   - result in major storms and power outages,
   - create landslides affecting buildings or transportation routes, and
   - cause drought-related fires.
   - Delayed emergency response can become more common.

The various impacts of the increase of global warming can be summarized as shown the Figure 3 (IPCC 2001a). The five effets (threats to endangered species and unique

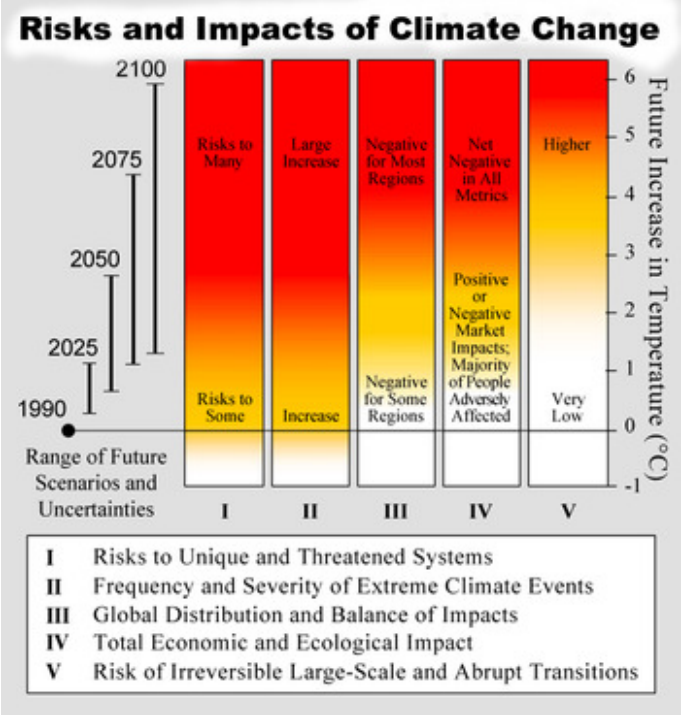

Figure 3: Risks and impacts of climate change ((IPCC 2001a).

systems, damages from extreme climate events, effects that fall most heavily on developing countries and the poor within countries, global aggregate impacts) organized by the IPCC (IPCC 2001b; IPCC 2001c; IPCC 2007a) show increased risks with the increase of global warming.

The poorest countries may be the first victims of climate change impacts. An effective response must pass through both a reduction in emissions of greenhouse gases (to avoid the unmanageable) and by a process of adaptation at the regional, national and local (to manage the inevitable). To that end, we need to know how the climate may change in the future. For this purpose, many models have been developed and experienced. They are the only efficient tools to simulate present weather and extrapolate for representing possible future climate states.

1.3 Modeling the climate

In order to determine how climate may change in the future, we need to know how the concentrations of those atmospheric components which affect the Earth's energy balance may change. Gases such as water vapor, carbon dioxide, methane and nitrous oxide (the greenhouse gases) absorb long-wave (heat) radiation emitted from the Earth's surface and re-emit this energy, ultimately resulting in raised surface temperatures. Whilst these greenhouse gases occur naturally, human activities since the beginning of the industrial revolution have resulted in large increases in the atmospheric concentrations of these gases and it is now widely accepted that this has affected global climate.

It has been only since the early 1990s that climate models have started to be analyzed to study possible changes of future weather and climate extremes (Houghton et al. 1995).

1.3.1 Introduction to climate models

Climate models are the principal tools for investigating potential future climate changes. They attempt to simulate the behavior of the climate system and are based mainly on the laws of physics, but also empirical techniques which use, for example, studies of detailed processes involved in cloud formation. The ultimate objective of climate models is to understand the key physical, chemical and biological processes that govern climate. Through understanding the climate system, it is possible to obtain a clearer picture of past climates by comparison with empirical observation, and predict future climate change. Models can be used to simulate climate on a variety of spatial and temporal scales.

They are global climate models (GCMs) and regional climate models (RCMs) built respectively on global and regional scale. GCMs have coarse spatial resolution between 250km×250km and 600km×600km. RCMs have spatial resolution of about 50km×50km (Karen et al. 2011). An RCM is very similar to a GCM but covers a smaller spatial

domain at a higher resolution, typically for every 3 or 6 hours, at the boundaries of the RCM domain. RCMs provide both better topographical representations than GCMs and better local or regional scale atmospheric dynamics. Because of the relatively coarse spatial resolution of GCM output, many applications of GCMs require processing of the GCM outputs to bring the effective scale of the data to a more local level (Karen et al. 2011). This process that consists in reducing the spatial scale of the GCM outputs is called downscaling. However, all climate models show some limitations:

- processes defining an atmospheric system are very complex and difficult to be modeled entirely and accurately (e.g., the treatment of aerosols by GCMs)

- the process is computationally intensive and there are biases or systematic errors

- More simplifications are done for modeling some complex processes (e.g., oceanic circulation)

- input data at finer spatial resolution are not always available in some areas.

The most sophisticated computer models should simulate the entire climate system. Confidence in models comes from their physical basis, and their skill in representing observed climate and past climate changes (IPCC, Climate Change 2007b).

1.3.2 Climate models classifications

a) Energy Balance Models

Energy balance models (EBMs) simulate the two most fundamental processes governing the state of the climate: - the global radiation balance (i.e. between incoming solar and outgoing terrestrial radiation), and - the latitudinal (equator-to-pole) energy transfer. They balance incoming energy as short wave electromagnetic radiation (visible and ultraviolet) to the earth with outgoing energy as long wave (infrared) electromagnetic radiation from the earth. Any imbalance results in a change in the average temperature of the earth.

b) Radiative-Convective Models

Radiative-convective models (RCMs) are 1-D or 2-D, with height the dimension that is invariably present. RCMs simulate in detail the transfer of energy through the depth of the atmosphere, including: - the radiative transformations that occur as energy is absorbed, emitted and scattered, and - the role of convection, energy transfer via vertical atmospheric motion in maintaining stability.

The simplest case is to consider the two-stream approximation, in which there are vertical fluxes (up-welling and down-welling) of thermal infra-red radiation only. The aim is to deduce the temperature gradient (and thus the temperature at the surface, T_s) for various cases (e.g. levels of insolation, optical thickness, etc).

c) Statistical-Dynamical Models

Statistical-dynamical models (SDMs) are generally 2-D in form, with usually one horizontal and one vertical dimension, though variants with two horizontal dimensions have been developed. Standard SDMs combine the horizontal energy transfer modeled by EBMs with the radiative-convective approach of RCMs. However, the equator-to-pole energy transfer is simulated in a more sophisticated manner, based on theoretical and empirical relationships of the cellular flow between latitudes. Parameters such as wind speed and wind direction are modeled by statistical relations whilst the laws of motion are used to obtain a measure of energy diffusion as in an EBM. Hence the description statistical-dynamical.

d) General Circulation Models

General circulation models (GCMs) use quantitative methods to simulate the interactions of the atmosphere, oceans, land surface, and ice. They are systems of differential equations (Goosse et al. 2010) based on the basic laws of physics, fluid motion, and chemistry ($http://celebrating200years.noaa.gov/breakthroughs/climate\_model/welcome.html$). The fundamental physical quantities calculated by GCMs include Temperature (T), Pressure (P), Winds (East-West = U, North-South = V), and the Specific Humidity (Q). Differential equations are used to relate these fundamental quantities to each other.

The 3-D model formulation is based on the fundamental laws of physics:

- conservation of energy;
- conservation of momentum;
- conservation of mass, and;
- the Ideal Gas Law

The primitive equations are a set of nonlinear differential equations that are used to approximate global atmospheric flow and are used in most atmospheric models. They consist of three main sets of equations:

1. Conservation of momentum: Consisting of a form of the Navier–Stokes equations that describe hydrodynamical flow on the surface of a sphere under the assumption that vertical motion is much smaller than horizontal motion and that the fluid layer depth is small compared to the radius of the sphere

2. A thermal energy equation: Relating the overall temperature of the system to heat sources and sinks

3. A continuity equation: Representing the conservation of mass.

In general, nearly all forms of the primitive equations relate the variables u (velocity in the east/west direction tangent to the sphere called the zonal velocity), v (velocity in the north/south direction tangent to the sphere called the the meridional velocity), ω (the vertical velocity in isobaric coordinates), T (the temperature), P (the pressure), and their evolution over space and time.

GCMs are computationally expensive. They can be considered to simulate reasonably accurately the global and continental-scale climate, but confidence is lacking in the regional detail.

To run a model, scientists divide the planet into a 3-dimensional grid system (WAN et al. 2013) (Figure 4
[$http://celebrating200years.noaa.gov/breakthroughs/climate\_model/modeling\_schematic.html$]
apply the basic equations, and evaluate the results.

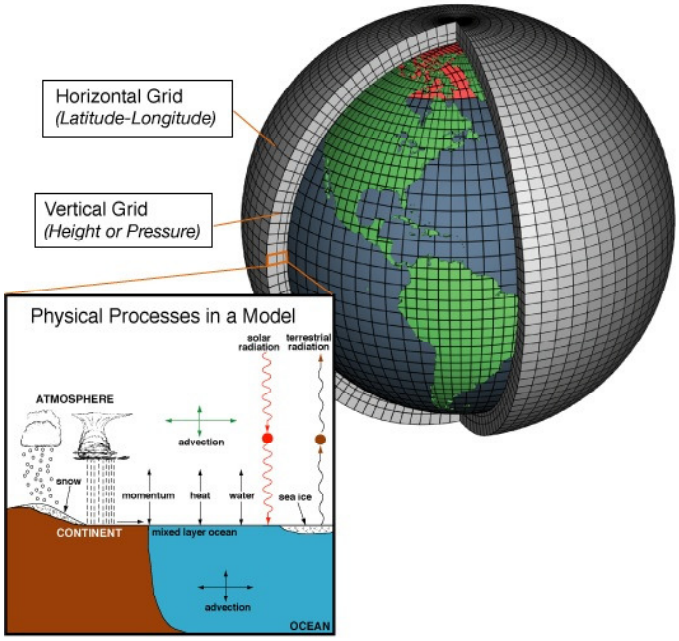

Figure 4: Subdivision of the globe into grid cells.
[$http://celebrating200years.noaa.gov/breakthroughs/climate\_model$
$/modeling\_schematic.html$ (19/11/2013)].

The number of cells in the grid system is known as the "resolution". The more grid cells, the higher the resolution, and the more calculations that must be computed. In general, GCMs are able to represent processes more realistically as they become higher resolution, but the computing time required to do the calculations goes up roughly 10 times for every doubling of the resolution.

The physics equations and parameterizations are then calculated for each cell in the grid over and over again, representing the march forward in time, throughout the simulation.

The coupled atmosphere-ocean general circulation models (AOGCMs) (e.g. MIROC3.2, CSIRO-MK3.0, UKMO-HadCM3, MPI-echam5, MRI-cgcm2.3.2a and BCCR-bcm2.0) represent the most sophisticated model that attempt to simulate the climate system. They combine the two general circulation models, atmospheric and ocean, which are the basis for sophisticated model predictions of future climate, such as are discussed by the IPCC. AOGCMs are complex and represent the only tools that could provide detailed regional predictions of future climate change.

1.3.3 Greenhouse gas emission scenarios for climate model

Given both the natural and anthropogenic emissions of the greenhouse gases, emissions scenarios are estimates of how these greenhouse gas emissions and their accumulation in the atmosphere might unfold over the next century. To make a true prediction of future climate it is necessary to include all the human and natural influences known to affect climate. Because future changes in several external factors, such as solar activity and volcanism, are not known, these must be assumed to be constant until such time as we are able to predict their changes (Kevin et al. 2000). The International Panel on Climate Change (IPCC) has developed a suite of emissions scenarios that are widely used to generate climate projections from GCMs. The first scenarios (IS92) were published in 1992, and a revised version was published in 2000 in the IPCC Special Report on Emissions Scenarios (SRES).

The IS92 emission scenarios

The first scenario developed by the Intergovernmental Panel on Climate Change (IPCC) (IPCC 1992) was IS92a scenario that specifies equivalent greenhouse gas (GHG) concentrations and sulphate aerosol loadings from 1850 to 2100. Climate change simulations based on this scenario have been performed by a number of climate modeling groups who

have contributed to the IPCC Third Assessment Report. The IS92 scenarios reflected the large uncertainty associated with, for example, the evolution of population and economic growth, technological advances, technology transfer and responses to environmental, economic or institutional constraints. There are six families of the IS92 emission scenario: IS92a, IS92b, IS92c, IS92d, IS92e, IS92f.

IS92a: a middle of the range scenario in which population rises to 11.3 billion by 2100, economic growth averages 2.3% year -1 between 1990 and 2100 and a mix of conventional and renewable energy sources are used. Only those emissions controls internationally agreed upon and national policies enacted into law, e.g., London Amendments to the Montreal Protocol, are included.

IS92b: population rises to 11.3 billion by 2100 and the current emissions control policies are enlarged to include stated policies beyond those legally adopted, e.g., the world-wide ratification and compliance of the Montreal Protocol.

IS92c: economic growth averages 1.2% year-1 between 1990 and 2100 and population is forecast to be 6.4 billion by 2100, with population decreasing in the 21st century. As well as assuming lower growth than IS92a and IS92b, low oil and gas resource availability results in higher prices which promote the expansion of nuclear and renewable energy. Lower population growth results in slower deforestation rates.

IS92d: another low scenario, but more optimistic than IS92c. The trend is towards increasing environmental protection but only actions that could be taken due to concerns about local or regional air pollution and waste disposal are included. Population is forecast to be 6.4 billion by 2100 and would be associated with lower natality, falling below the replacement rate late in the 21st century. Low fossil fuel resource availability means that there is greater market penetration of renewable energy and safe nuclear power. A 30% environmental surcharge on fossil energy use is levied to meet the costs of more stringent local pollution controls. Greater well-being is assumed to lead to voluntary actions to halt deforestation, to adopt CFC substitutes with no radiative or other adverse effects and to recover and efficiently use the methane from coal mines and land fills.

IS92e: results in the highest CO_2 emissions. Economic growth averages 3% year-1, between 1990 and 2100 and the population is forecast to reach 11.3 billion by 2100. Fossil resources are plentiful but, due to assumed improvements in living standards, environmental surcharges are imposed on their use. Nuclear energy is phased out by 2075 and, although CFC substitute assumptions are the same as those of IS92d, the plentiful fossil fuel resources discourage the additional used of coal mine methane for energy supply. Deforestation proceeds at the same pace as IS92a.

IS92f: falls below IS92e, has high population growth (17.6 billion by 2100), but lower assumptions of improvements than IS92a. Other assumptions are high fossil fuel resource availability, increasing costs of nuclear power and less improvement in renewable energy technologies and costs.

The SRES emission scenarios

The SRES emission scenarios were developed in 1996 by the IPCC because the IS92 scenarios, have some well-recognized limitations (Wigley 1999). The most marked difference between SRES scenarios and IS92 scenarios are the lower SO2 emissions in the SRES scenarios. The resulting set of 40 scenarios cover a wide range of the main demographic, economic and technological driving forces of future greenhouse gas and sulphur emissions. There are four family of SRES emission scenario: SRES A1, SRES A2, SRES B1, SRES B2 (Wigley 1999).

The A1 scenario family describes a future world of very rapid economic growth, global population that peaks in mid-century and declines thereafter, and the rapid introduction of new and more efficient technologies. Major underlying themes are convergence among regions, capacity building and increased cultural and social interactions, with a substantial reduction in regional differences in per capita income. The A1 scenario family develops into three groups that describe alternative directions of technological change in the energy system. The three A1 groups are distinguished by their technological emphasis: fossil intensive (A1FI), non-fossil energy sources (A1T), or a balance across all sources (A1B) (where balanced is defined as not relying too heavily on one particular energy source, on the assumption that similar improvement rates apply to all energy supply and end-use technologies).

The A2 scenario family describes a very heterogeneous world. The underlying theme is self-reliance and preservation of local identities. Fertility patterns across regions converge very slowly, which results in continuously increasing population. Economic development is primarily regionally oriented and per capita economic growth and technological change more fragmented and slower than other storyline.

The B1 scenario family describes a convergent world with the same global population, that peaks in mid-century and declines thereafter, as in the A1 scenario family, but with rapid change in economic structures toward a service and information economy, with reductions in material intensity and the introduction of clean and resource-efficient technologies. The emphasis is on global solutions to economic, social and environmental

sustainability, including improved equity, but without additional climate initiatives.

The B2 scenario family describes a world in which the emphasis is on local solutions to economic, social and environmental sustainability. It is a world with continuously increasing global population, at a rate lower than A2, intermediate levels of economic development, and less rapid and more diverse technological change than in the A1 and B1. While the scenario is also oriented towards environmental protection and social equity, it focuses on local and regional levels.

Figure 5 shows the specific values of the equivalent CO_2 Concentration according to the three most used scenarios for the period 1900-2100.

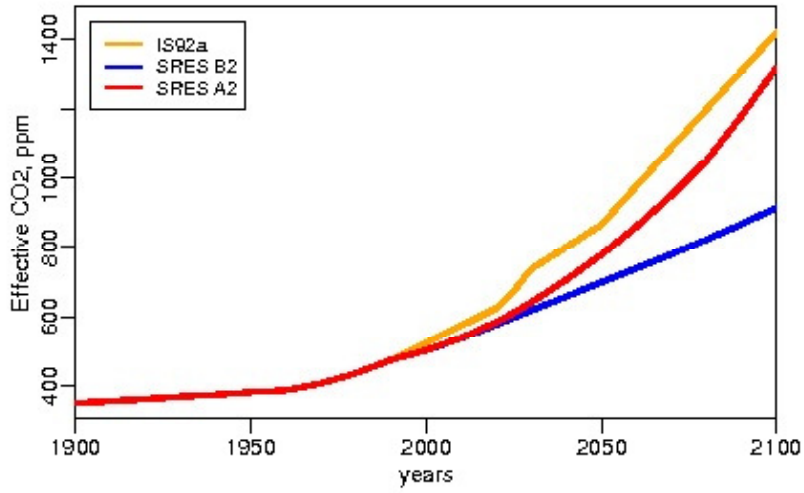

Figure 5: Specific values of the equivalent CO_2 Concentration.
[$http://www.cccma.ec.gc.ca/data/cgcm/cgcm_forcing.shtml$ (19/11/2013)].

Researchers are again working on refining the emissions scenarios to reflect the most up-to-date information. This new set of scenarios will drive the next generation of climate model projections and likely will be included in the next IPCC assessment report.

Projections of the climate takes into account the atmosphere with its constituents affected by human activity (e.g., increased greenhouse gases, sulfate aerosols, etc.). The physical processes of each of the future scenarios of forcing agents (e.g., greenhouse gases and aerosols) are then incorporate in climate models algorithms in order to produce probable results of the climate components during the considered future period.

1.3.4 Evaluating climate models

Forecast verification is the process of assessing the quality of forecasts. In the atmospheric sciences, such an activity is sometimes called validation, or evaluation. Analysis of verification statistics and their components can help in the assessment of specific strengths and

weaknesses of forecasters or forecasting systems. On a fundamental level, forecast verification involves investigation of the properties of the joint distribution of forecasts and observations (Murphy et Winkler 1987). That is, any given verification data set consists of a collection of forecast/observation pairs whose joint behavior can be characterized in terms of the relative frequencies of the possible combinations of forecast/observation outcomes (Daniel 2006).

One way of testing the plausibility of climate model projections is to check their ability to model current mean climate as well as its extremes (Fowler et Hennessy 1995; Gregory et Mitchell 1995; Jones et al. 1997; Frei et al. 1998; Sadiki et Fischer 2005). Kevin et al. (2000) suggested to first run a model for several simulated decades without perturbations to the system. The quality of the simulation can then be assessed by comparing the average, the annual cycle, and the variability statistics on different time scales with observations. If the model seems realistic enough, it can then be run including perturbations such as an increase in greenhouse-gas concentrations. The differences between the climate statistics in the two simulations provide an estimate of the accompanying climate change. These procedures are concerned in our study.

1.3.5 Expected future climates as prospected by climate models

The climate response to an increase in greenhouse gases and sulphate aerosols has been compared with the observed patterns of temperature change by many different research groups. Such studies show a clear similarity between the observed changes and the model calculations.

The results of many models are known and reported to the world community through structures such as the Intergovernmental Panel on Climate Change (IPCC)

Recent climate modeling results indicate that "extreme" weather events may become more common. Rising average temperatures produce a more variable climate system. Localized events could include windstorms, heat waves, droughts, storms with extreme rain or snow, and dust storms.

According to IPCC (1995); IPCC (2007a), climate change is accompanied by:

- a disturbance of the water cycle,
- an increased frequency and intensity of natural disasters related to climate (droughts, floods, storms, cyclones),

- threat of loss of some coastal areas, particularly deltas, mangroves, coral reefs, beaches of Aquitaine, etc..
- a decrease of 17.5 % of land area of Bangladesh, 1 % of that of Egypt,
- an increase risk of malaria, and the extension of infectious diseases such as cholera,
- accelerate the decline of biodiversity: the disappearance of animal and plant species,

For France, the simulations carried out by experts from Meteo France suggest that climate change:

- increase the temperature with an average warming of around 2°C,
- alter precipitation patterns: increase of 20% in winter, decrease of 15% in summer
- could lead to the disappearance of one-third or more of the mass of mountain glaciers over the next hundred years,
- could result in substantially reduced snowpack in the Alps and the Pyrenees,
- could lead to a weakening of the Gulf Stream, resulting in a significant cooling of our ocean frontage (-4°C), bringing average temperatures in France at the level of those achieved during the last glaciation.

Many models project the increase in the precipitation intensity in a future climate with increased greenhouse gases in the atmosphere (Kothavala 1997; Hennessy et al. 1997; Zwiers et Kharin 1998). There are also some indications from observations that such changes of precipitation intensity are already being seen in some regions (Karl et Knight 1998).

Models used in the Fourth Assessment Report (AR4 2007) (IPCC 2007a) for projecting tropical cyclone changes are able to simulate present day frequency and distribution of cyclones, but intensity is less well simulated. Simulation of extreme precipitation is dependent on resolution, parameterization, and the thresholds chosen. In general, models tend to produce too many days with weak precipitation ($<$10 mm day^{-1}) and too little precipitation overall in intense events ($>$10 mm day^{-1}) (IPCC, Climate Change 2007b).

Recent climate modeling results indicate that "extreme" weather events may become more common. Rising average temperatures produce a more variable climate system. Projections of future climate change suggest further global warming, sea level rise, and an increase in the frequency of some extreme weather events (IPCC 2007a).

The models have improved enough over time to at least begin to look at such higher-order features in more detail. This is a product of the rapid development of climate modeling capabilities over the past 10 years, in concert with increased computer resources. The current generation of global coupled climate models have improved resolution (grid points typically every 2.5° of latitude and longitude), more detailed and accurate land surface simulation schemes, and dynamical sea ice formulations (Gerald et al. 2000). However they still have limitations in terms of spatial resolution, simulation errors, and parameterizations that must represent processes that cannot yet be included explicitly in the models, particularly dealing with clouds and precipitation (Gerald et al. 2000).

Summary of the chapter

This chapter has defined many concepts necessary to understand the topic of this work and has presented a review of the literature related to the topic. The next chapter is devoted to the presentation of data used and the methodology of investigation.

Chapter 2

Data used and Methodology of Investigation

2.1 Study domain

a) Brief geographical description

The study domain which encompasses the country of Cameroon is chosen in Equatorial Central Africa and covers the area between 0-14°N and 5-20°E (Figure 6).

The southern part of the country is bordered to the west by the Atlantic Ocean. To the northeast are savannas, which gradually give way to steppes near Lake Chad. There are mangrove swamps along the coast. Countries of the domain have great variety and abundance of wildlife.

b) Climate of the domain

The climate of the area is not uniform, varying from tropical humid in the south to semi-arid and hot in the north. It varies, primarily because of the cooling effect of elevation and the vastly differing amounts of rainfall regionally. The northern part has a dry to arid Sahelian type climate depending on latitude. The southern part is covered by dense rain forest. Annual rainfall decreases from roughly 4060 mm along the coast to less than 510 mm near Lake Chad. Mount Cameroon, with more than 10160 mm annually, is one of the rainiest places in the world. Monthly temperatures throughout most of Cameroon average about 24° to 27° C. Considerably higher averages occur in the far north.

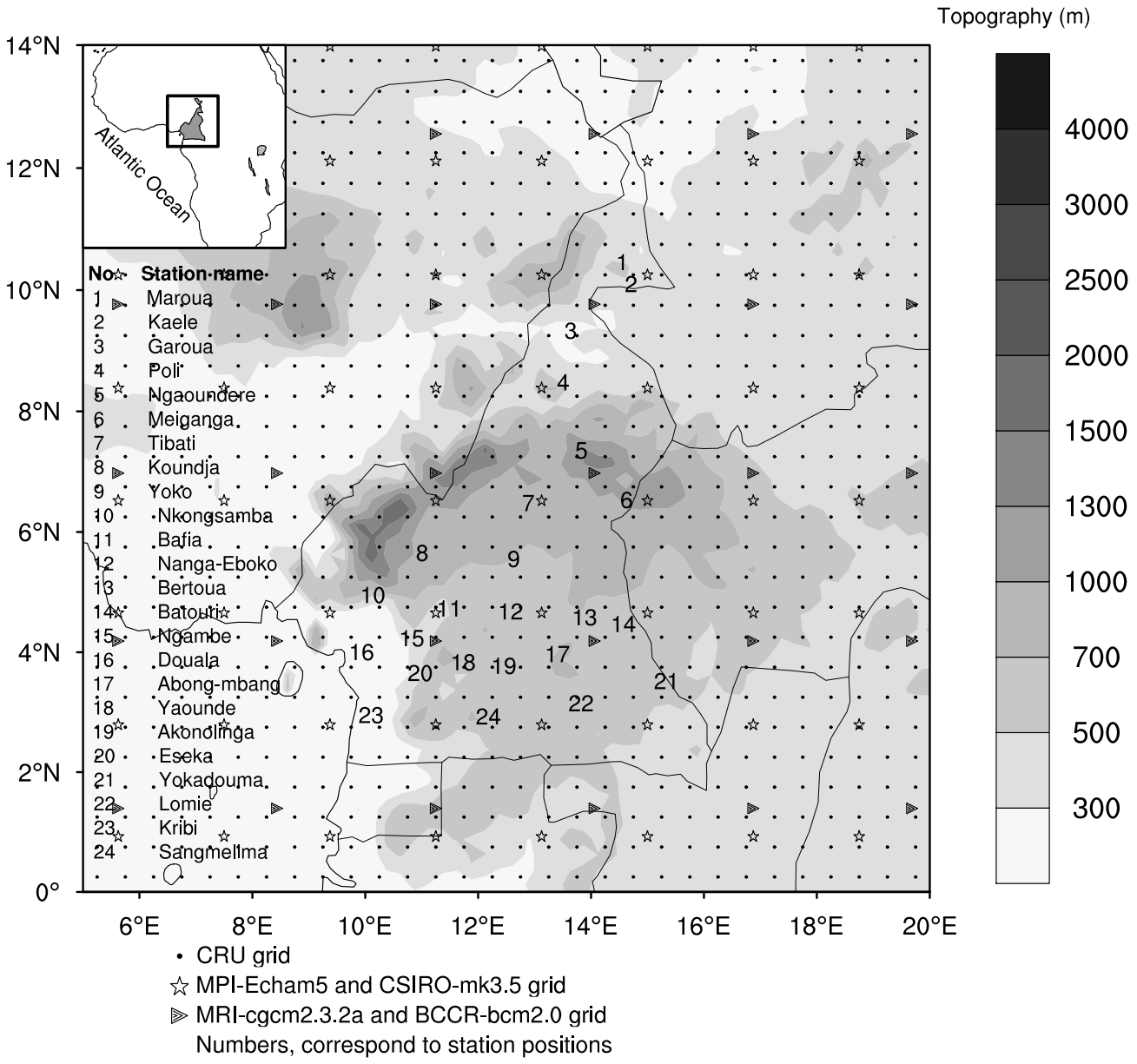

Figure 6: *Study area with the geographical locations of rainfall stations indicated by numbers. Grid positions are shown for CRU data (dots), MRI and BCCR models (triangles) and MPI and CSIRO (stars). Topography is shaded.*

c) Monsoon circulation

Monsoon is a seasonal change in wind direction. This wind shift typically brings about a marked change in local weather. Monsoon describes seasonal changes in atmospheric circulation and precipitation associated with the asymmetric heating of land and sea (Trenberth et al. 2000). In their simplest form, monsoons are caused by differences in solar heating between the oceans and continents, and they are most likely to form where a large continental land mass meets a major ocean basin. The major monsoon systems of the world consist of the West African and Asia-Australian monsoons.

Monsoons are often associated with rainy seasons in the tropics (the areas of Earth within 23.5° latitude of the equator) and the subtropics (areas between 23.5° and about 35° latitude, both north and south). Precipitation is enhanced across interior Africa where warm, dry air from the Sahara intersects relatively moist air from the south (e.g., South Atlantic Ocean) Tropical monsoon climates have monthly mean temperatures above 18°C in every month of the year and feature wet and dry seasons, as Tropical savanna climates do.

The West African monsoon (WAM) is characterized by rainy periods in both the northern and southern hemispheres across interior Africa. It impacts a wide region over the continent from the West African coast right through central Africa to Ethiopia, with a remarkably zonal orientation (Parker et al. 2005). During northern hemisphere summer, this enhanced precipitation is found along the ITCZ, or near 10-15°N, whereas during northern hemisphere winter, this enhanced precipitation is found across south-central Africa. Thus, in some regards, the WAM can be viewed as an enhancement to the ITCZ across Africa during northern and southern hemisphere summer (Parker et al. 2005).

d) The Inter-Tropical Convergence Zone

The Inter-Tropical Convergence Zone (ITCZ) is located just south of the Sahel at about 10°N, dumping rain on the region to the south of the desert. The location of the ITCZ (Inter-Tropical Convergence Zone) varies throughout the year. The Inter-Tropical Convergence Zone is a mobile region characterized by deep moist convection, associated with the zone of maximum heating or thermal equator. Within the ITCZ, areas of convergence and convection grow and decay, and the position and intensity of convergence varies, even on a daily basis. The ITCZ shifts northward and southward on an annual cycle, following the thermal equator, and brings the annual March of rains. There's a diurnal cycle to the precipitation in the ITCZ. Clouds form in the late morning and early afternoon hours

and then by 3 to 4 p.m., the hottest time of the day, convectional thunderstorms form and precipitation begins. These storms are generally short in duration. The position and timing of movement of the ITCZ therefore have major implications for the onset and duration of rains in Africa (especially in the Sahel), South America (the Amazon basin and the Altiplano), Asia (including the monsoon systems of India and Indochina), Indonesia and Australia ($http://www.st-andrews.ac.uk/\ dib2/climate/tropics.html$).

Economic activities in the area are based mostly on agriculture (practiced by about 75% of the population), generally at subsistence levels. Cacao, coffee, bananas, rubber, palm oil, and cotton are the main cash crops grown by farmers. Main food crops are cassava, corn, yams, sweet potatoes, and millet. Logging is another important resource in Cameroon with heavy timber exportation. Most of these activities are rain-fed and the use of irrigation is very marginal.

Electricity is produced at 97.3% by hydroelectric dam. It then depends on rainfall and is most often vulnerable during the dry season.

2.2 Data used

Five data sets were used in this study: daily rainfall data from 24 measuring stations in Cameroon and model simulated daily rainfall from Atmosphere-Ocean General Circulation Model (AOGCM). Observed station rainfall data provided by the National Meteorological Services of Cameroon (NMSC) are the same successfully used by Penlap et al. (2004). They cover a 55-year period and extend from 1951 to 2005. The geographical positions of the stations are shown in Figure 6. Table 1 indicates their names, locations and altitudes.

The percentage of missing values ranges from 0 to 12% and from 0 to 15.9% for monthly and daily precipitation data respectively. Every region of the domain is home of at least one station to ensure a good description of the represented pattern over the country.

Table 1: *Geographical positions and altitudes of the 24 rainfall stations used. Stations are grouped per defined climatic zones. They are also assigned numbers used to represent them in Figure 6. Percentages of missing data are shown for daily and monthly data according to the corresponding study time period.*

						% of missing data	
						(daily)	(monthly)
Region	N°	Station name	Lon (°E)	Lat (°N)	Alt (m)	$1962-93$	$1951-2005$
zone 1	11	Bafia	11.25	4.73	500	12%	10.6%
	12	Nanga-éboko	12.37	4.68	623	12%	9.3%
	13	Bertoua	13.68	4.58	668	3%	2.5%
	14	Batouri	14.37	4.47	650	0.8%	0.6%
	17	Abong-mban	13.20	3.97	693	0%	0%
	18	Yaoundé	11.53	3.83	753	0%	0%
	19	Akonolinga	12.25	3.77	671	6.5%	6%
	20	Eséka	10.77	3.65	228	15.9%	12%
	21	Yokadouma	15.10	3.52	534	3.1%	2.3%
	22	Lomié	13.62	3.15	624	13.5%	10%
	23	Kribi	09.99	2.95	10	3.1%	3.3%
	24	Sangmélima	11.98	2.93	712	0%	0%
zone 2	5	Ngaoundéré	13.57	7.35	1104	3.1%	2.3%
	6	Meiganga	14.0	7.20	1027	0%	0.2%
	7	Tibati	12.63	6.48	873	7.5%	7.9%
	8	Koundja	10.75	5.65	1210	3.1%	2.5%
	9	Yoko	12.37	5.55	1027	6.3%	4.8%
	10	Nkongsamba	09.93	4.95	816	0%	0%
	15	Ngambé	10.62	4.23	610	3.1%	2.7%
	16	Douala	09.73	04.00	5	0%	0.2%
zone 3	1	Maroua	14.26	10.46	423	12.5%	9.3%
	2	Kaélé	14.45	10.10	386	0%	0%
	3	Garoua	13.38	9.33	241	6.2%	5%
	4	Poli	13.25	8.48	436	0.3%	3%
	Mean percentage of missing data					4.7%	4.0%

AOGCM simulated rainfall were obtained from the World Climate Research Program's (WCRP's) Coupled Model Inter-comparison Project phase 3 (CMIP3) multi-model dataset at the Lawrence Livermore National Laboratory (LLNL), USA. These are outputs from the following four AOGCM: MPI-echam5, MRI-cgcm2.3.2a, BCCR-bcm2.0 and

CSIRO-mk3.5. Echam5 is a model of the Max Planck Institute (MPI-echam5) for Meteorology in Germany (Roeckner et al. 1996) while cgcm2.3.2a and mk3.5 are respectively from the Meteorological Research Institute (MRI-cgcm2.3.2a) in Japan (Yukimoto et al. 2006) and the Australian Commonwealth Science and Industrial Research Organization (CSIRO-mk3.5) (Gordon et al. 2002). Model bcm2.0 is from the Bjerknes Centre for Climate Research (BCCR-bcm2.0), University of Bergen, Norway (Furevik et al. 2003). These runs were done for the IPCC 4^{th} Assessment Report (4AR) (Meehl et al. 2007). Grid points for each of the four IPCC 4AR models are shown in Figure 6. Echam5 and Mk3.5 have the same grid spacing of 208 km while Cgcm2.3.2a and Bcm2.0 have spacings of 310 km.

Thirty two years of simulated rainfall data for the current climate (1962-93) and a seventeen years (2082-98) of the future climate projected under the SRES A2 emission scenario were analyzed.

Monthly precipitation data used are computed from daily data of the same 24 measuring stations. The record period now extends from 1951 to 2005 (55 years) with percentage of missing as shown in Table 1.

CRU grid data have $0.25° \times 0.25°$ spatial resolution and are downloadable free of charge from the CRU website (http://badc.nerc.ac.uk/data/cru/).

2.3 Methods of variability studies or change detection

Consistent and comparable methods can be used to detect changes in some parameter relating to climate.

- **The use of anomalies**

  Anomaly is a pattern in the data that does not conform to the expected behavior (mean behavior over a long time period). It also refers to as outliers, exceptions, peculiarities or surprise. Anomalies are computed relative to a fixed reference period. For a given long-term reference period of an atmospheric variable, the mean is taken and the individual value for a date t of the time series of data is compared to that mean. The gap between a single value of data series and the mean corresponds to the anomaly. For example of application of the method, read Douville et Royer (1996) and Angell (1994).

- **The use of trends**

Linear trend coefficients is also a method for detecting changes in variables. But convenient statistical tests need to be applied to the obtained trend at a given confidence level. Trend gives information about a possible increase (positive significant trends) or decrease (negative significant trends) of climatic conditions. Null trends indicate stable climatic conditions. Among studies using these methods there are Salack et al. (2011), Brunetti et al. (2001) and Karl et Knight (1998).

- **The use of SPI (Standardized Precipitation Index)**

  This method is efficient for studying dryness or wetness variability. The Standardized Precipitation Index (SPI) is a probability index that was developed by McKee et al. (1993) to give a better representation of abnormal wetness and dryness. SPI is normally distributed with zero mean and unit standard deviation. This index is negative for drought, and positive for wet conditions. This method was used by Bussay et al. (1998), Szalai et Szinell (2000) and Lloyd-Hughes et Saunders (2002)

- **Comparison between model projection and present time observation**

  Climate models are tools used to reproduce and to predict climate. Climate models have to be validated by efficient mathematical tools in order to determine their efficiency level. When climate models best describe the climate of a reference present period, more confidences are given to their projections. Taking the difference between future and present climatic variables, it may be possible to evaluate their changes. Many studies use climate models for predictions and results are usually represented as patterns of variation in space, time, or both (Mkankam 2000; Emori et al. 2005; Guenang et Mkankam 2012).

2.4 Statistical definitions and formulas

2.4.1 Mean and standard deviation

Given a set of data $(x_1, x_2, x_3, x_4, x_5, ..., x_n)$.

- The mean $\bar{x}$ of these data is calculated by the formula

$$\bar{x} = \frac{1}{n}\sum_{i=1}^{n} x_i \tag{2.1}$$

- The variance s^2 is defined as

$$s^2 = \frac{1}{n-1}\sum_{i=1}^{n}(x_i - \bar{x})^2 \tag{2.2}$$

The square root of the variance, s, is known as the standard deviation.

2.4.2 Pearson correlation

Given two sets of data $(x_1, x_2, x_3, x_4, x_5, ..., x_n)$ and $(y_1, y_2, y_3, y_4, y_5, ..., y_n)$.

The Pearson correlation coefficient r_{xy} between the two sets of data is given by the relation

$$r_{xy} = \frac{1}{n-1} \sum_{i=1}^{n} \left[\frac{x_i - \bar{x}}{s_x} \frac{y_i - \bar{y}}{s_y} \right] \tag{2.3}$$

where s_x and s_y are the respective standard deviations of the variables x and y.

The Pearson correlation has two important properties (Daniel 2006):

- Firstly, it is bounded by -1 and 1; that is, $-1 \leq r_{xy} \leq 1$. If $r_{xy} = -1$ there is a perfect, negative linear association between x and y. That is, the scatter plot of y versus x consists of points all falling along one line, and that line has a negative slope. Similarly if $r_{xy} = 1$, there is a perfect positive linear association. Note that $r_{xy} = 1$ says nothing about the slope of the perfect linear relationship between x and y, except that it is not zero.

- Secondly, the square r_{xy}^2 of the Pearson correlation, specifies the proportion of the variability of one of the two variables that is linearly accounted for, or described, by the other. It is sometimes said that r_{xy}^2 is the proportion of the variance of one variable explained by the other, but this interpretation is at best imprecise and can be misleading.

2.4.3 Some rainfall statistical parameters

There are some statistical parameters useful to understand intensity and frequency of rainfall distribution. In this subsection, we focus on the following parameters and their derivatives:

1. **The annual total amount**

2. **Rain day**

   A rain day is defined as a day when collected precipitation exceed a certain threshold of 1 mm.day^{-1} (Nityanand et Ashwini 2009).

3. **Dry spell**

A day is considered dry if the total precipitation recorded does not exceed the threshold of 1 mm.day^{-1}. Theoretically, let us consider j_1 as the first dry day, j_2, j_3, ..., j_n others consecutive dry days for the same year. When j_{n+1} is not a dry day, then the n consecutive dry days constitute a dry spell (Ratan et Venugopal 2013; Nityanand et Ashwini 2009).

4. **Ninetieth percentile of daily precipitations**

   $Prec_j$ being rainfall corresponding to the j^{th} day of the year. Let $Prec_j$ (j=1, 2, 3, ..., n) being a vector of n elements ranged in ascending order and grouped in 100 classes of equal intervals, with n the total number of rain days for the year. The 90^{th} percentile is defined as the value corresponding to the lower limit of the ninetieth class.

5. **Fraction of rain greater than the 90^{th} percentile**

   For a given year, it is the quotient of the total daily precipitation whose values are greater than the ninetieth percentile of daily precipitation and the total amount of rainfall recorded during the same year.

2.4.4 Statistical distribution functions of data (gamma, exponential, lognormal and weibull functions)

a) The gamma distribution function

The probability density function of the gamma distribution is defined as

$$g(x) = \frac{1}{\beta^{\alpha}\Gamma(\alpha)} x^{\alpha-1} e^{-x/\beta} \qquad for \quad x > 0 \tag{2.4}$$

where $\alpha > 0$ is a shape parameter, $\beta > 0$ is a scale parameter, $x > 0$ is the amount of precipitation and $\Gamma(\alpha)$ is the gamma function (see Lloyd-Hughes et Saunders (2002) and Guttman (1999) for more details).

Parameters α and β of the gamma probability density function are estimated from sample data. This can be done using an approximation for maximum likelihood given by Thom (1958):

$$\hat{\alpha} = \frac{1}{4A}\left(1 + \sqrt{1 + \frac{4A}{3}}\right) \tag{2.5}$$

$$\hat{\beta} = \frac{\bar{x}}{\hat{\alpha}} \tag{2.6}$$

where A is given by

$$A = ln(\bar{x}) - \frac{\sum ln(x)}{n} \tag{2.7}$$

n is the number of observations with actual precipitation and $\bar{x}$ the mean precipitation per event.

Under some conditions, α and β can be better estimated using an iterative procedure suggested by Wilks (1995).

The cumulative probability $G(x)$ of an observed amount of precipitation is expressed after integrating the probability density function (the shape and the scale values α and β are incorporated) with respect to x:

$$G(x) = \int_0^x g(x)\,dx = \frac{1}{\hat{\beta}^{\hat{\alpha}}\,\Gamma(\hat{\alpha})} \int_0^x x^{\hat{\alpha}} e^{-x/\hat{\beta}} dx \tag{2.8}$$

Letting $t = x/\hat{\beta}$, reduce the cumulative probability to the following equation called the incomplete gamma function

$$G(x) = \frac{1}{\Gamma(\hat{\alpha})} \int_0^x t^{\hat{\alpha}-1} e^{-1}\,dt \tag{2.9}$$

When accounting for the fact that the probability of zero precipitation $q = P(x = 0)$ is greater than zero, the cumulative density function takes the form

$$H(x) = q + (1 - q)G(x) \tag{2.10}$$

b) The exponential distribution function

The general formula for the exponential probability distribution function is (Ahmad et Bilal 2010)

$$f(x) = \frac{1}{\beta} e^{-(x-\mu)/\beta} \qquad for \qquad x \geq \mu \qquad and \qquad \beta > 0 \tag{2.11}$$

where μ is the location parameter and β is the scale parameter. The rate parameter λ is sometimes used in place of the scale, with $\lambda = 1/\beta$. β is called the constant failure rate or failures per unit of measurement.

c) The lognormal distribution function

In probability theory, a positive random variable x follows the log-normal (μ, σ^2) distribution if the logarithm of the random variable is normally distributed.

The probability density function of a log-normal distribution is defined as (Bartošová 2006; Diana 2012):

$$f_X(x;\mu,\sigma) = \frac{1}{x\sigma\sqrt{2\pi}}\, e^{-\frac{(\ln x-\mu)^2}{2\sigma^2}}, \quad x>0 \tag{2.12}$$

where $x > 0$, $-\infty < \mu < +\infty$ and $\sigma > 0$.

μ is the scale parameter that stretch or shrink the distribution and σ is the shape parameter that affects the shape of the distribution. They are determined by the maximum likelihood estimators:

$$f_L(x;\mu,\sigma) = \prod_{i=1}^{n}\left(\frac{1}{x_i}\right)\, f_N(\ln x;\mu,\sigma) \tag{2.13}$$

where f_L is the probability density function of the log-normal distribution and f_N that of the normal distribution.

Using the same indexes to denote distributions, we can write the log-likelihood function as

$$\ell_L(\mu,\sigma|x_1,x_2,\ldots,x_n) = -\sum_k \ln x_k + \ell_N(\mu,\sigma|\ln x_1,\ln x_2,\ldots,\ln x_n) \tag{2.14}$$

$$= \text{constant} + \ell_N(\mu,\sigma|\ln x_1,\ln x_2,\ldots,\ln x_n). \tag{2.15}$$

Thus, ℓ_L and ℓ_N are maximized by the same value of their maximum likelihood estimators (MLE) μ and σ. Estimators area

$$\widehat{\mu} = \frac{\sum_k \ln x_k}{n} \tag{2.16}$$

$$\widehat{\sigma}^2 = \frac{\sum_k (\ln x_k - \widehat{\mu})^2}{n}. \tag{2.17}$$

d) The weibull distribution function

The probability density function of a Weibull random positive variable x is (Shuo-Jye 2002; Haniyeh et Saeid 2011) is:

$$f(x;\alpha,\beta) = \alpha\beta x^{\alpha-1}e^{-\beta x^{\alpha}} \tag{2.18}$$

where α and β are the shape and the scale parameters, respectively.

Its complementary cumulative distribution function is a stretched exponential function. The Weibull distribution is related to a number of other probability distributions; in

particular, it interpolates between the exponential distribution ($k = 1$) and the Rayleigh distribution ($k = 2$).

There are no closed-form expressions of the parameters $\widehat{\alpha}$ and $\widehat{\beta}$. So there are estimated by maximizing the log-likelihood expression of equation (2.21) (Haniyeh et Saeid 2011).

2.4.5 Fitting functions to data: the Maximum Likelihood (ML) method of parameter estimation

The maximum-likelihood (ML) method can be used to estimate the parameters of a given statistical function. When applied to a data set, it provides estimates of the function's parameters. It is a versatile and an important alternative that seeks to find values of the distribution parameters that maximize the likelihood function (Wilks 2006). This method indeed maximizes the probability of the observed data under the resulting selected distribution.

To determine the maximum likelihood estimators of a given distribution, suppose a sample of n independent and identically distributed observations x_i ($i = 1, \ldots, n$), coming from a population with an underlying probability density function $f(.|\theta_0)$. θ_0 is the unknown distribution parameter. From the sample of n observation x_i, it is desirable to find an estimator $\hat{\theta}$ which would be as close to the true value θ_0 as possible. Both the observed variables x and the parameter θ_0 can be vectors.

The joint density function for an independent and identically distributed sample, is defined as

$$f(x_1, x_2, \ldots, x_n \mid \theta) = f(x_1|\theta) \times f(x_2|\theta) \times \cdots \times f(x_n|\theta). \tag{2.19}$$

If x_i are fixed parameters of this function and θ the function's variable allowed to vary freely, then the function will be called the likelihood function:

$$\mathcal{L}(\theta \,|\, x_1, \ldots, x_n) = f(x_1, x_2, \ldots, x_n \mid \theta) = \prod_{i=1}^{n} f(x_i|\theta). \tag{2.20}$$

In practice, the log-likelihood is more convenient. It is the logarithm of the likelihood function so that

$$\ln \mathcal{L}(\theta \,|\, x_1, \ldots, x_n) = \sum_{i=1}^{n} \ln f(x_i|\theta), \tag{2.21}$$

The average log-likelihood can also be used:

$$\hat{\ell} = \frac{1}{n} \ln \mathcal{L}. \tag{2.22}$$

The hat over ℓ indicates that it an estimator. $\hat{\ell}$ estimates the expected log-likelihood of a single observation in the model.

The maximum likelihood method estimates θ_0 by finding a value of θ that maximizes $\hat{\ell}(\theta|x)$. It defines a maximum-likelihood estimator (MLE) of θ_0 as

$$\{\hat{\theta}_{\text{mle}}\} \subseteq \{\arg\max_{\theta \in \Theta} \hat{\ell}(\theta \,|\, x_1, \ldots, x_n)\}. \tag{2.23}$$

2.4.6 Linear regression

Regression is most easily understood in the case of simple linear regression, which describes the linear relationship between two variables, say x and y. Conventionally the symbol x is used for the independent, or predictor variable, and the symbol y is used for the dependent variable, or predictand.

Essentially, simple linear regression seeks to summarize the relationship between two variables, shown graphically in their scatter-plot, by a single straight line. The regression procedure chooses the line producing the least error for predictions of y given observations of x.

Given a data set of (x, y) pairs, the problem is to find the particular straight line,

$$Y = a + bX \tag{2.24}$$

minimizing the squared vertical distances (thin lines) between it and the data points. The vertical distances between the data points and the line (Figure 7) are also called errors or residuals.

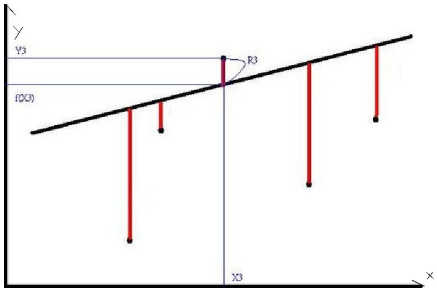

Figure 7: *Illustration of the simple linear regression method.*

The residuals are given by

$$e_i = y_i - Y(x_i). \tag{2.25}$$

There is a separate residual e_i for each data pair (x_i, y_i).

Combining Equations 2.24 and 2.25 for each data i, yields the regression equation,

$$y_i = Y(x_i) + e_i = a + bx_i + e_i \tag{2.26}$$

In order to minimize the sum of squared residuals,

$$\sum_{i=1}^{n}(e_i)^2 = \sum_{i=1}^{n}(y_i - Y_i)^2 = \sum_{i=1}^{n}(y_i - [a + bx_i])^2 \tag{2.27}$$

it is only necessary to set the derivatives of Equation (2.27) with respect to the parameters a and b to zero and solve. The solutions are

$$\hat{b} = \frac{\sum_{i=1}^{n}(x_i - \bar{x})(y_i - \bar{y})}{\sum_{i=1}^{n}(x_i - \bar{x})^2} \tag{2.28}$$

and

$$\hat{a} = \bar{y} - b\bar{x} \tag{2.29}$$

Thus, the calculated $\hat{a}$ and $\hat{b}$ are the ML estimators of a an b (Bretscher 1995). The parameter $\hat{b}$ quantifies the difference between variables.

2.4.7 Statistical significance or Confidence test

There is an interest of measuring the absolute quality of a climate model forecast. Scientists collect data in order to learn about the processes and systems the data represent. Often they have prior ideas, called hypotheses, of how the systems behave (Helsel et Hirsch 2002). One of the primary purposes of collecting data (e.g the precipitation data) is to test whether those hypotheses can be substantiated, with evidence provided by the data. Statistical tests are the most quantitative ways to determine whether hypotheses can be substantiated, or whether they must be modified or rejected outright.

a) Statistical hypothesis testing

A statistical hypothesis test is a method of making decisions using data from a scientific study. In statistics, a result is called statistically significant if it has been predicted as unlikely to have occurred by chance alone, according to a pre-determined threshold probability, the significance level. The tests of significance are used in determining what outcomes of a study would lead to a rejection of the predefined null hypothesis (called H0) for a pre-specified level of significance (called α); this can help to decide whether results contain enough information to cast doubt on conventional wisdom establishing the null hypothesis. The critical region of a hypothesis test is the set of all outcomes which cause the null hypothesis to be rejected in favor of the alternative hypothesis.

A confidence interval gives an estimated range of values which is likely to include an unknown population parameter, the estimated range being calculated from a given set of sample data. If independent samples are taken repeatedly from the same population, and a confidence interval calculated for each sample, then a certain percentage (confidence level) of the intervals will include the unknown population parameter. Confidence intervals $(1 - \alpha)$ are usually calculated so that this percentage is 90%, 95%, 99.9% (or whatever) confidence intervals for the unknown parameter. White area below the curve in Figure 8 represent a confidence interval in the case where data follow a normal distribution.

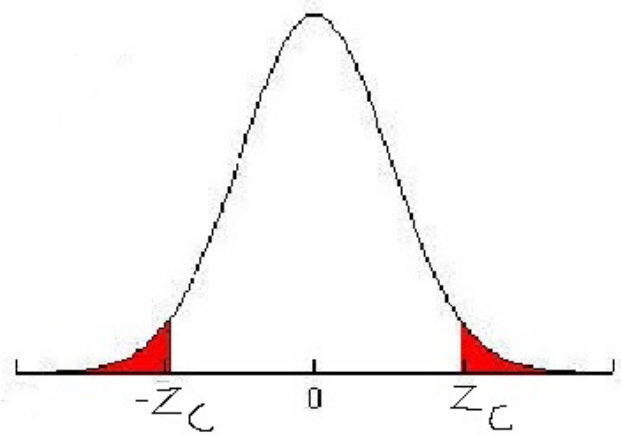

Figure 8: *Illustration of a confidence interval for normal distribution. White area below the curve represent the confidence interval and shaded area the critical region. Z_c is the critical value of the variable Z from which chosen hypothesis is rejected.*

The width of the confidence interval gives some idea about how uncertain we are about the unknown parameter (precision). A very wide interval may indicate that more data should be collected before anything very definite can be said about the parameter.

Confidence intervals are more informative than the simple results of hypothesis tests

(where we decide "reject H0" or "don't reject H0") since they provide a range of plausible values for the unknown parameter.

b) Procedure Used to test for Significance

The following steps are necessary to Test for Significance (Lehmann et Romano 2005):

- define an initial research hypothesis of which the truth is unknown.

- state the relevant null and alternative hypotheses.

- consider the statistical assumptions being made about the sample in doing the test; for example, assumptions about the statistical independence or about the form of the distributions of the observations.

- Decide which test is appropriate, and state the relevant test statistic T.

- Derive the distribution of the test statistic under the null hypothesis from the assumptions. In standard cases this will be a well-known result. For example the test statistic may follow a Student's t distribution or a normal distribution.

- Select a significance level (α) defining a probability threshold below which the null hypothesis will be rejected. Common values are 5% and 1%.

- The distribution of the test statistic under the null hypothesis partitions the possible values of T into those for which the null-hypothesis is rejected, the so called critical region, and those for which it is not. The probability of the critical region is α.

- Compute from the observations the observed value t_{obs} of the test statistic T.

- Decide to either reject the null hypothesis in favor of the alternative or not reject it. The decision rule is to reject the null hypothesis H0 if the observed value t_{obs} is in the critical region, and to accept or "fail to reject" the hypothesis otherwise.

c) Evaluation of the test Statistic

In statistical significance testing, the p-value is the probability of obtaining a test statistic at least as extreme as the one that was actually observed, assuming that the null hypothesis is true.

If the p-value is less than the required significance level (equivalently, if the observed test statistic is in the critical region), then we say the null hypothesis is rejected at the given level of significance (Goodman 1999). Rejection of the null hypothesis is a conclusion.

If the p-value is not less than the required significance level (equivalently, if the observed test statistic is outside the critical region), then the test has no result. The evidence

is insufficient to support a conclusion.

2.4.8 Some useful statistical test applied in this study

a) Non-parametric Mann-Kendall test for linear correlation

Non-parametric tests are generally distribution-free, thus do not depend on the underlying distribution. They detect trend or change, but do not quantify the size of the trend or change. They are very useful because most hydrological time series data are not normally distributed, especially when the period range is short (Daniel 2006).

The Mann-Kendall test (Mann 1945) can be stated as a test for whether values Y (precipitation series for example) tend to monotonically increase or decrease with time represented by the variable X.

To perform the test, Kendall's S statistic is computed (Alan et Justin 2003; Helsel et Hirsch 2002) as:

$$S = \sum_{j=1}^{n-1} \sum_{i=j+1}^{n} sgn(Y_i - Y_j) \tag{2.30}$$

where sgn is the sign (positive, negative, zero) of the expression $(Y_i - Y_j)$ and n the total number of elements in X vector array (number of time). To test the significance, a statistic closely approximated by the standard normal distribution is developed:

$$Z_S = \begin{cases} \frac{S-1}{\sigma_S} & if \quad S > 0 \\ 0 & if \quad S = 0 \\ \frac{S+1}{\sigma_S} & if \quad S < 0 \end{cases} \tag{2.31}$$

σ_S is the standard deviation on S defined by the expression

$$\sigma_S = \left[\frac{n(n-1)(2n+5)}{18} - \frac{1}{18} \sum_{j=1}^{q} m_j(m_j - 1)(2m_j + 5) \right]^{\frac{1}{2}} \tag{2.32}$$

where q is the number of tied groups and m_j is the number of observation in the j^{th} group.

The test statistic S following a Student-t distribution with n-2 degrees of freedom under the null hypothesis is defined as

$$S = b/\sigma \tag{2.33}$$

where

$$\sigma = \sqrt{\frac{12\sum_{i=1}^{n}(Y_i - a - bX_i)}{n(n-2)(n^2-1)}} \tag{2.34}$$

b) The Anderson-Darling statistical test

The Anderson-Darling statistic measures how well a given data sample Y_i $(i = 1, \ldots, n)$ follow a particular distribution function F. For a given data set and distribution, the better the distribution fits the data, the smaller this statistic will be.

The Anderson-Darling statistic (A^2) is defined as follows (Anderson et Darling 1952; Anderson et Darling 1954):

$$A^2 = -n - \frac{1}{n}\sum_{i=1}^{n}(2i-1)[ln(F(Y_i)) + ln(1 - F(Y_{n+1-i}))] \tag{2.35}$$

The hypothesis regarding the distributional form is rejected at the chosen significance level (α) if the test statistic, A^2 is greater than the critical value obtained from a table. In this case no parameters are estimated in relation to the distribution function F.

c) The Kolmogorov-Smirnov statistical test

- **Definition**

  The Kolmogorov–Smirnov test (K–S test) is a nonparametric test for the equality of continuous, one-dimensional probability distributions that can be used to compare a sample with a reference probability distribution (one-sample K–S test), or to compare two samples (two-sample K–S test). It quantifies a distance between the empirical distribution function of the sample and the cumulative distribution function of the reference distribution, or between the empirical distribution functions of two samples (Figure 9).

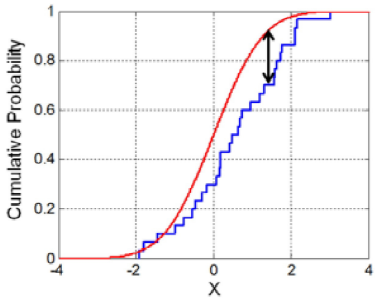

Figure 9: *Illustration of the Kolmogorov-Smirnoff statistic. Red line is cumulative density function (CDF), blue line is an empirical cumulative density function (ECDF), and the black arrow is the K-S statistic.*

The null distribution of this statistic is calculated under the null hypothesis that the samples are drawn from the same distribution (in the two-sample case) or that the sample is drawn from the reference distribution (in the one-sample case). In each case, the distributions considered under the null hypothesis are continuous distributions but are otherwise unrestricted.

The Kolmogorov–Smirnov test can be modified to serve as a goodness of fit test. In the special case of testing for normality of the distribution, samples are standardized and compared with a standard normal distribution. This is equivalent to setting the mean and variance of the reference distribution equal to the sample estimates.

The Kolmogorov–Smirnov statistic for a given cumulative distribution function $F(x)$ is defined as

$$D_n = sup_x|F_n(x) - F(x)| \tag{2.36}$$

where n is the number of observations in the population x and sup_x is the supremum of the set of distances between the empirical cumulative distribution function $F_n(x)$ and the theoretical cumulative distribution function $F(x)$.

D_n converges to 0 almost surely, when the sample comes from distribution $F(x)$.

- **Hypothesis Testing and interpretation**

  The null and the alternative hypotheses are:

  H_0: the data follow the specified distribution;

  H_A: the data do not follow the specified distribution.

  The hypothesis regarding the distributional form is rejected at the chosen significance level (α) if the test statistic, D, is greater than the critical value obtained from a table. The fixed values of (0.01, 0.05 etc.) are generally used to evaluate the null hypothesis (H_0) at various significance levels. A value of 0.05 is typically used for most applications, however, in some critical industries, a lower value may be applied. The standard tables of critical values used for this test are only valid when testing whether a data set is from a completely specified distribution. If one or more distribution parameters are estimated, the results will be conservative: the actual significance level will be smaller than that given by the standard tables, and the probability that the fit will be rejected in error will be lower.

The P-value (which is another parameter yielded by the test), in contrast to fixed values, is calculated based on the test statistic, and denotes the threshold value of the significance level in the sense that the null hypothesis (H_0) will be accepted for all values of less than the P-value. For example, if P-value=0.025, the null hypothesis will be accepted at all significance levels less than P-value (i.e. 0.01 and 0.02), and rejected at higher levels, including 0.05 and 0.1.

The P-value can be useful, in particular, when the null hypothesis is rejected at all predefined significance levels, and we need to know at which level it could be accepted.

2.5 Determination of onset, retreat and length of the rainy season

Various methods have been developed to determine onset and retreat dates of the rainy season. Odekunle (2006) classified these methods into five main categories: 1) Inter-tropical Discontinuity (ITD)-rainfall model (Ilesanmi 1972a), 2) rainfall-evapotranspiration relation model (Benoit 1977), 3) percentage cumulative mean rainfall model, based on rainfall data alone (Ilesanmi 1972b; Adejuwon et al. 1990; Adejuwon 2006), 4) wind shear model (Omotosho 1990a; Omotosho 1990b), 5) the theta-E technique (Omotosho 2002). The percentage cumulative mean rainfall is the most used method. It has the advantage of depending only on rainfall data that are readily available from direct measurements rather than other rainfall-associated factors (Odekunle et al. 2005). This method was used by Olaniran (1983a) to study the onset of rains and the start of the growing season in Nigeria. The results revealed that there is no significant difference between the mean onset date obtained and the mean start of the growing season.

The method adopted in this study for the determination of onset and retreat dates was the cumulative percentage mean rainfall amount (Ilesanmi 1972a). Daily rainfall data for each year were grouped into 5-day means (pentads). This grouping was performed on non-overlapping 5-day means starting at pentad 1 (1-5 January) and ending at pentad 73 (27-31 December). In the first step of the method, the percentage of mean annual rainfall was determined at 5-day intervals. Next, cumulative percentages were calculated for the full year. Finally, the mean timings of the accumulation of 7 to 8 percent and of 90 percent of the annual rainfall were taken as onset and retreat of rains respectively. The length of the rainy season was defined simply as the period between onset and retreat

dates. According to the method adopted here, the monsoon rainy season, between onset and retreat accounts for 83.5% of annual rainfall.

In the first part of the analysis, the temporal mean onset and retreat dates of the rainy season were first calculated for each station of the domain. Secondly, the following criteria were used to divide the study domain into sub-domains or zones: stations where both onset and retreat dates are different by 4 pentads at most were assigned to a common climatic zone. The 4 pentad interval appeared to be the one giving reasonable separate zones (stations spatially grouped) as compared to interval of 1, 2 or 3 pentads (Figures shown in appendices). For model outputs, zone definitions were extended to neighboring areas of Cameroon in order to increase the number of grid points used. Some studies on domains comprising our study area (Olaniran 1989; Olaniran 1983b) can justify this extension. Next, observed and simulated data were analyzed in every zone by calculating for each year and at each station (grid point) onset and retreat dates and length of the rainy season. Annual results were averaged for stations (grid points) within each zone giving a 32-year time series per zone for both observations and model outputs. Finally, means, standard deviations and inter-annual variability were analyzed and compared. Statistics on how each model reproduces the observed parameters (onset and retreat dates and duration of the rainy season) were estimated as the ratio of the observed number of parameters simulated correctly to the total number of cases.

Climate change evaluations were based on comparisons between current climate and future SRES A2 scenario perturbed climate. The A2 scenario recognized as the most severe (Cook et Vizy 2006) assumes strong CO2, CH4, and SO2 increases throughout the twenty-first century (except for SO2, which declines after 2030) (IPCC 2001a). Knowledge about how models respond to these changes are useful for predictions of economic impacts.

2.6 Analysis of rainfall statistical parameters

We also examined the ability of the models to simulate spatial distributions and inter-annual trends of current climate at daily, intra-annual and annual time scales using various rainfall statistical parameters: total amounts, annual number of rain days, ratio of the 90^{th} percentile of daily to mean daily precipitation, fraction of annual total contributed by daily events above the 90^{th} percentile value and maximum length of dry spells. Spatial distribution and inter-annual trends of observed and modeled parameters were analyzed. A day with precipitation less than 1 mm was considered to be dried.

In order to compare the spatial representation of observed and modeled data, the

station precipitations were specialized using standard gridding methods (kriging). This led to highly smoothed observed fields. Given that the annual total amounts of MPI-echam5 and CSIRO-mk3.5 seemed complementary, they were averaged to form a 2 member ensemble for some of the analysis.

For trend study, a parametric (student's t-statistic) and a non-parametric (Mann-Kendall statistic) test were used for the detection of significant trend in time series. Trend magnitudes were also estimated and model results were compared to observation.

The null hypothesis H_0 is that there is no trend.

For the Mann-Kendall statistic, we reject the H_0 hypothesis at significance level $\alpha = 0.05$ if $|Z_S| > Z_{\frac{\alpha}{2}}$, where $Z_{\frac{\alpha}{2}}$ is the critical value from standard normal distribution.

The t-student statistic is also used at 0.05 significant level and the results are compared to those from the Mann-Kendall statistic. According to Woodward et Gray (1993), the goal is to test whether $H_0 : b = 0$ based on the fact that $b/SE(b)$ is distributed as Student's t with (n-2) degrees of freedom when H_0 is true. b (the magnitude of the trend) is the slope of the linear regression model defined as in Equation (2.28) and a, the intercept is estimated as in Equation (2.29) so that the linear equation can be stated by

$$Y = bX + a + \varepsilon \tag{2.37}$$

where ε is the residual.

The linear regression test assumes that the data are normally distributed and that the errors (deviations from the trend) are independent and follows the same normal distribution with zero mean.

For projected future climate, it was found useful to calculate the ratio for a given rainfall statistical parameter of the mean future climate to the mean present climate. C_P being some rainfall statistical parameter under the present climate and C_F its value in the future climate, its relative change is $\frac{C_F - C_P}{C_P} = r - 1$, where r is ratio of C_F over C_P.

2.7 The Standardized Precipitation Index (SPI)

2.7.1 Calculation procedure

The method used for SPI computation was developed by McKee et al. (1993) and Edwards et McKee (1997) to study relative departures of precipitation from normality. It has been widely applied in many studies (Vicente-Serrano 2006; Sergio et al. 2009). It uses monthly precipitation aggregates at various time scales (e.g. 1-, 3-, 6-, 12-, 18-, 24-month,

etc). As an illustration of the procedure, for 3-month time scale, precipitation accumulation from the $j-2$ to the j months are summed up and attributed to the j month. At this time scale, the first two months of data time series are missing. Similar treatment were applied on data over other time scale. Next follows the normalization procedure, where the long-term time series of aggregated precipitation are first fitted with an appropriate probability distribution function (gamma, exponential, weibull and lognormal). Then the chosen distribution is used to calculate the cumulative probabilities of the data points, which are finally transformed into standardized normal variates. This is repeated for all needed time scales. Because the processes generating rainfall in our study domain vary in time and in space, many distributions may be needed. The maximum likelihood estimation method (MLE) was used to fit four probability density functions (i.e. gamma, exponential, weibull and lognormal) to the data. This method is widely used to estimate the parameters of statistical distributions. It is the most popular method to estimate the distribution parameters from an empirical sample. It finds the model parameters that maximize the likelihood of the observed data with respect to the theoretical model. The distribution with the lowest value of the Anderson-Darling goodness of fit test statistic (Anderson et Darling 1952; Anderson et Darling 1954) was retained as best suited to represent the underlying distribution of the data. Finally, the appropriate probability distribution function was used to fit the corresponding long-term time series of precipitation accumulation and the results were transformed into a normal distribution given the SPI so that the mean SPI for a given station and for the considered period is zero.

Using the approximate conversion provided by Abramowitz et Stegun (1965), the normal variable Z in the case where gamma is used to fit distribution, is expressed by the formula

$$Z = SPI = -\left(t - \frac{c_0 + c_1 t + c_2 t^2}{1 + d_1 t + d_2 t^2 + d_3 t^3}\right) \qquad for \qquad 0 < H(x) \leq 0.5 \tag{2.38}$$

$$Z = SPI = +\left(t - \frac{c_0 + c_1 t + c_2 t^2}{1 + d_1 t + d_2 t^2 + d_3 t^3}\right) \qquad for \qquad 0.5 < H(x) < 1 \tag{2.39}$$

where

$H(x) = q + (1-q)G(x)$ (Equation 2.10) is the cumulative density function

$$t = \sqrt{ln\left[\frac{1}{(H(x))^2}\right]} \qquad for \qquad 0 < H(x) \leq 0.5 \tag{2.40}$$

$$t = \sqrt{ln\left[\frac{1}{(1-H(x))^2}\right]} \qquad for \qquad 0.5 < H(x) < 1 \tag{2.41}$$

and c_0, c_1, c_2, d_1, d_2 and d_3 the constants such that

$$\begin{aligned} c_0 &= 2.515517 \qquad c_1 = 0.802853 \qquad c_2 = 0.010328 \\ d_1 &= 1.432788 \qquad d_2 = 0.189269 \qquad d_3 = 0.001308 \end{aligned} \tag{2.42}$$

2.7.2 SPI interpretation and operational drought definition

The SPI, often called the z-score is the number of standard deviations from the mean at which an event occurs. Generally speaking, high, medium and low SPI values represent high, normal (medium) and low precipitation events respectively. Thus, the 3-month SPI value provides a comparison of accumulated precipitation over that specific 3-month period concerned, with the mean precipitation total for the same 3-month time period, calculated over the full study period. This applies to any n-month SPI value, where n, the number of months of accumulation, is the time scale. Short time scales of the order of three months may be important for agricultural applications, whereas long time scales of up to many years are of more interest in water supply management (Guttman 1998).

Many classification of dryness and wetness events based on SPI exist in the literature, an example is shown in Table 2 (Lloyd-Hughes et Saunders 2002).

Table 2: *Drought classification by SPI value (Lloyd-Hughes et Saunders 2002).*

SPI value	Class
2.00 or more	Extremely wet
1.50 to 1.99	Severely wet
1.00 to 1.49	Moderately wet
0 to 0.99	Mildly wet
0 to -0.99	Mild drought
-1.00 to -1.49	Moderate drought
-1.50 to -1.99	Severe drought
-2 or less	Extreme drought

To use indices such as SPI for operational monitoring, it is necessary to define drought levels for various preventive or corrective actions. Goodrich et Ellis (2006) proposed using preselected percentiles of the drought index to determine thresholds, based on the fitted parametric statistical distribution. Contrary to Goodrich et Ellis (2006) who simply used empirical distributions, Quiring (2009) used percentiles values from the best of four tested distributions to define more objective drought levels. Table 3 shows the five-category drought definition from the U.S. Drought Monitor (USDM), with their description and corresponding percentiles (Svoboda et al. 2002).

Table 3: *USDM drought definitions (Svoboda et al. 2002).*

Category	Description	Percentile
D0	Abnormally dry	21% - 30%
D1	Moderate drought	11% - 20%
D2	Severe drought	6% - 10%
D3	Extreme drought	3% - 5%
D4	Exceptional drought	$< 2\%$

After Calculating SPI for all stations, the results were submitted to the Kolmogorov-Smirnov test of normality at 5% significant level. Similar study was done using CRU precipitation at grid points nearest the station locations and results were compared to observations.

Operational drought thresholds were also calculated in the similar way as in Quiring (2009):

- fitting the five PDF (gamma, weibull, exponential, lognormal and normal) to SPI data.
- Applying the Kolmogorov-Smirnov (KS) test to select the appropriate PDF fitting the SPI. The PDF with the lowest KS value was chosen as the appropriate.
- Using preselected percentiles as defined by Svoboda et al. (2002) (Table 3) and applying them to the SPI (normalized with the appropriate PDF) to determine drought thresholds.

Analyses of some SPI time series focused on four stations (Kaele, Ngaoundere, Bertoua and Kribi), representing the four different observed climatic zones of the study domain. These stations are distant and content less missing data than others of the same zone.

The station of Kaele is located north of the domain in the Sahelian zone, Ngaoundere in the Adamawa plateau, the middle part of the domain, Bertoua in the eastern part in dense forest and Kribi in the south-western part closest to the Atlantic Ocean. .

2.8 Data processing aspects

Such a tedious study cannot be completed without a high level of computational algorithm and plotting method. Computation of each parameter requires a considerable time as it has to be done for (each station)×(total number of stations) and for (each grid point)×(total number of grid points)×(number of models) multiplied by the number of years according to the period considered.

Softwares used to perform algorithms and to draw plots are Fortran 90, Surfer 7.0, NCL (The NCAR Command Language) and R command language. NCL is a product of the Computational and Information Systems Laboratory at the National Center for Atmospheric Research (NCAR) and sponsored by the National Science Foundation. It is a free interpreted language designed specifically for scientific data processing and visualization. NCL has robust file input and output. It can read and write netCDF-3, netCDF-4 classic, HDF4, binary, and ASCII data, and read HDF-EOS2, GRIB1, GRIB2, and OGR files (shapefile, MapInfo, GMT, TIGER). The graphics are world class and highly customizable. The R software were particularly used for statistical aspect of the study.

Summary of the chapter

This chapter has given a description of the study domain and the data used for the study. It has also presented mathematical tools, defined calculated indices and described the methodology. The next chapter (Chapter 3) shows results of our investigation and related analysis and discussion.

Chapter 3

Results and Discussions

3.1 Validation of model rainfall outputs in the present time climatology (1962-1993)

3.1.1 Onset, retreat and length of the rainy season for the period 1962-1993

a) The cumulative percentage of mean rainfall amount

The cumulative percentage of mean rainfall amounts for each year and for each dataset was calculated and the results were shown in Figure 10.

The onset and retreat of the rainy season are the dates corresponding to the intersection between the patterns and the horizontal lines at 7-8% and 90% respectively. Results for all stations were then used for the classification.

b) Classification of rainfall stations in climatic zones

A total of 3 zones were defined in the study domain (Figure 11) using the criteria presented in chapter 2, section 2.5. These zones are similar to those defined using other criteria (Olaniran 1989; Olaniran 1983b). Thus we can consider:

1. The equatorial forest zone (zone 1) mostly covered by dense forests and having two rainy seasons;

2. The Midland zone (zone 2) which predominantly covers highlands where topography effectively extends the length of the humid period, due to localized convection and orographic effects (Olaniran 1983b);

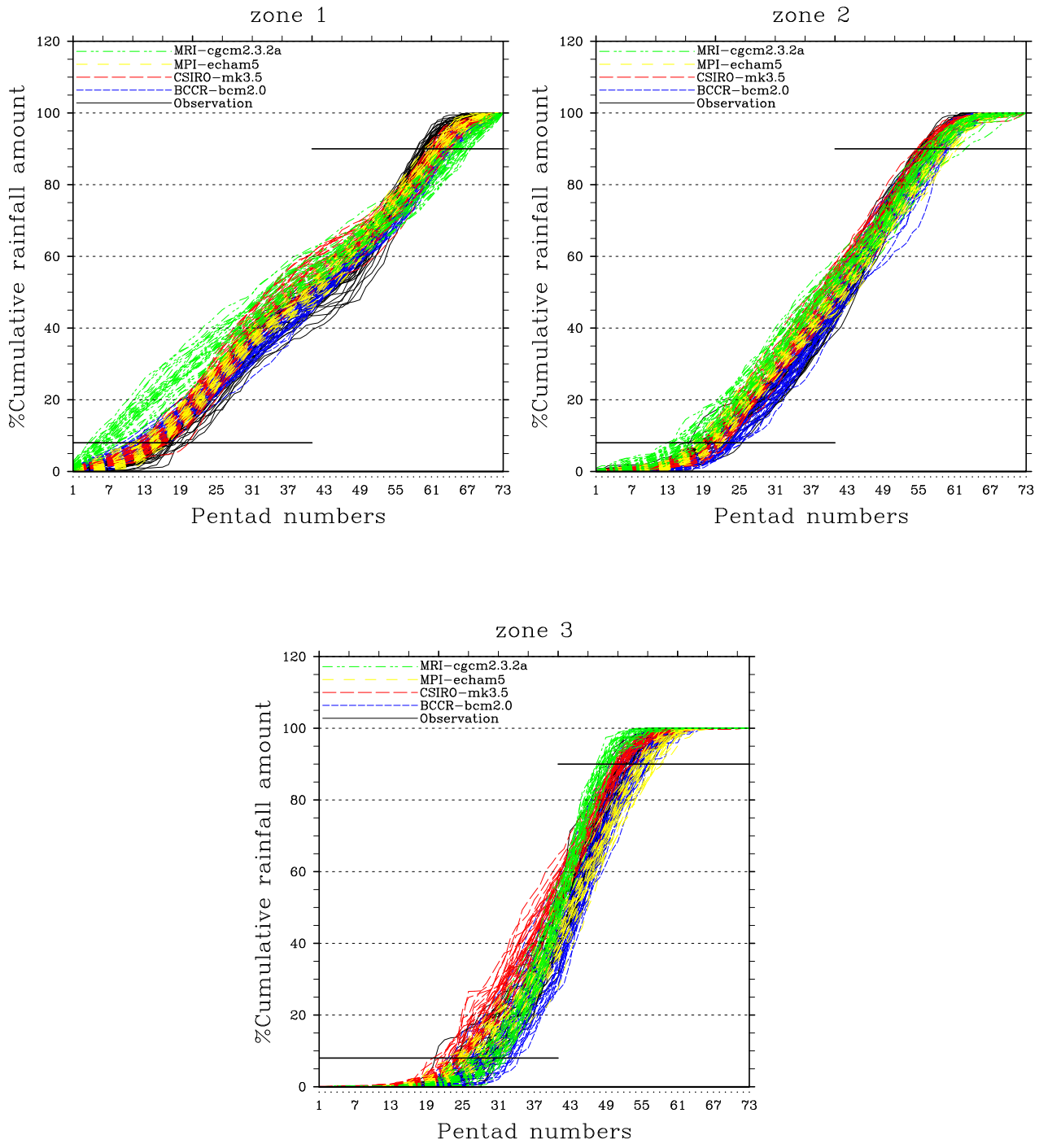

Figure 10: *Cumulative percentage of rainfall amounts for the full year and for zones 1, 2 and 3 respectively.*

3. The Sahelian zone (zone 3), where the tropical continental air mass predominates, except during the Monsoon season when the tropical maritime air mass covers the area for 3 to 5 months at most (Olaniran 1983b).

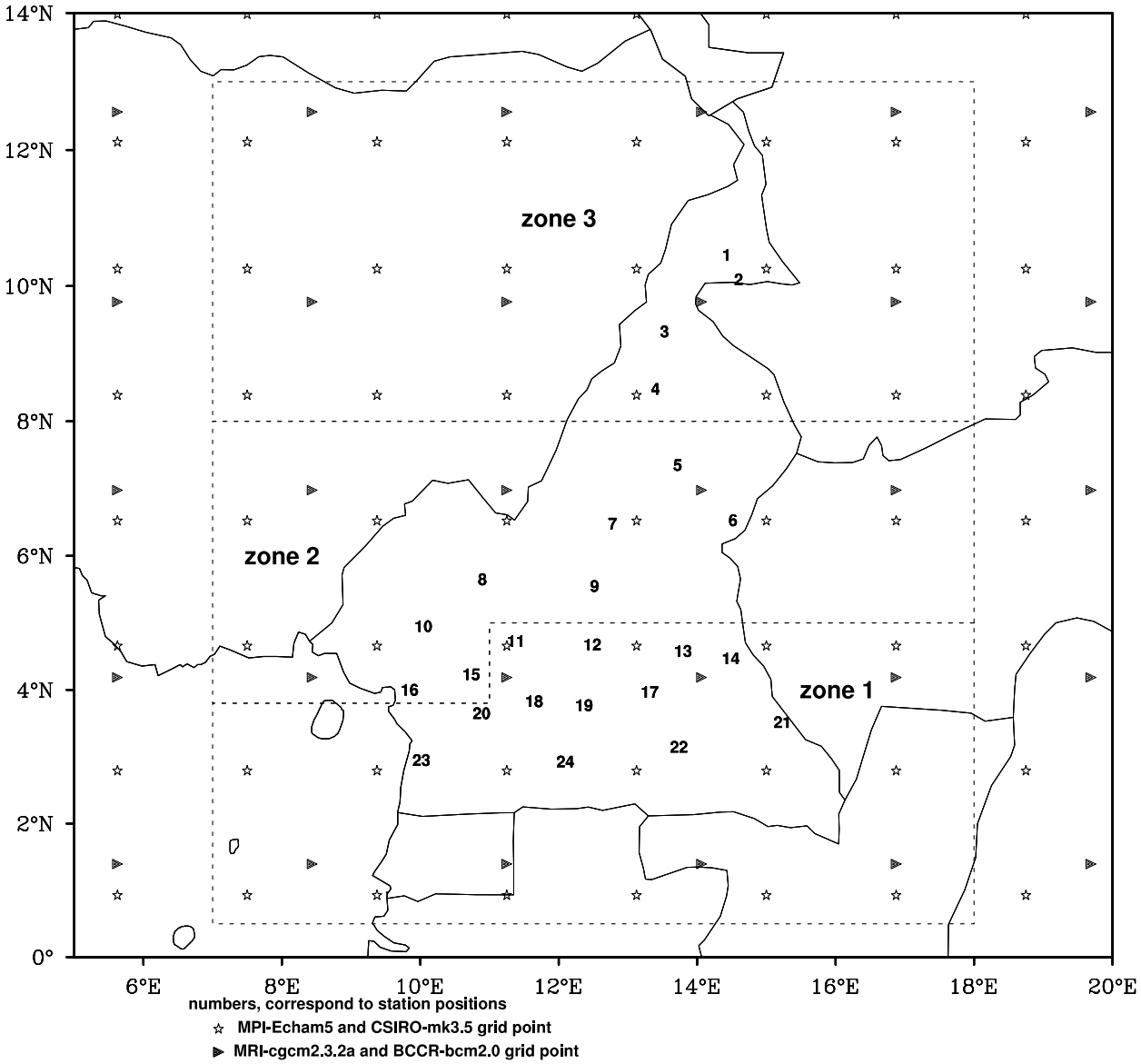

Figure 11: *Study area with the geographical locations of rainfall stations (indicated by numbers. See Table 1 for the names, longitudes and latitudes of stations corresponding to numbers) and of climate models grid points (BCCR-bcm2.0, CSIRO-mk3.5, MPI-echam5 and MRI-cgcm2.3.2a). Grid point locations for each model are indicated by a specific marker. Dashed lines show delimited zones.*

Table 4 shows the range of mean onset and mean retreat dates for each zone. These ranges were obtained by averaging on yearly mean onset and retreat dates per zone de-

duced from the Figure 10. The standard deviations to the various averages were also calculated.

Table 4: *Range of mean onset and retreat dates of the rainy season for each zone. Results are given in pentad number and the corresponding calendar dates are in parentheses. The first pentad is the period from Jan 1 to Jan 5.*

Sub-domain	Onset date range	Retreat date range
zone 1	15^{th}-17^{th}Pentad (12 Mar-26 Mar)	60^{th}-62^{nd}Pentad (23 Oct-6 Nov)
zone 2	19^{th}-21^{st}Pentad (1 Apr-15 Apr)	55^{th}-59^{th}Pentad (22 Sep-22 Oct)
zone 3	25^{th}-29^{th}Pentad (1 May-25 May)	52^{nd}-54^{th}Pentad (13 Sep-27 Sep)

c) Mean onset and retreat dates and lengths of the rainy season

Mean onset and retreat dates and lengths of the rainy season as well as associated standard deviations for each zone are shown in Table 5 for observed and simulated data.

As expected, rainfall onset and retreat follow the northward move of the ITD during the months of March to August and its southward retreat between September and October, respectively. Similar spatial migrations of onset and retreat dates were observed in many African countries, for example in Nigeria, Senegal and western Kenya (Odekunle 2004; Mugalavai et al. 2008; Salack et al. 2011). Retreat is more abrupt as it takes only 8 pentads compared to 12 for onset. This rapid retreat was also observed in neighboring Nigeria (Ayoade 1974; Odekunle 2006). Earliest onset is in zone 1, south of the study domain, on the 16^{th} pentad of the year ($17^{th} - 21^{st}$ March), followed by zone 2 four pentads (20 days) later, and latest onset, close to 2 months (11 pentads) after zone 1, is in the northernmost stations (Table 5 (a)). Retreat starts in the North and moves South (Table 5 (b)) and time lags between zones are less than for onset dates. Uncertainties are higher (higher standard deviations) on onset than on retreat dates. The length of the rainy season (Table 5 (c)) decreases from South to North: 25 consecutive pentads (4 months) in zone 3, 37 (6 months) in zone 2 and 45 (7.5 months) in zone 1. This is in agreement with annual rainfall amounts observed in theses areas. The spatial variation in duration affects the choice of crop types and farming techniques, depending on zones in order to avoid losses due to insufficient number of rainy days. That is why in Kenya where the maximum length of the growing season is about 4 months, irrigation is recommended during the short rainy season as a way of supplementing the limited rainfall (Mugalavai

Table 5: *Mean onset and retreat dates and lengths of the rainy season for the period 1962-93 in the three zones. Onset and retreat dates are in pentads number ± standard deviation. The corresponding calendar range of dates are in brackets without the standard deviations. Lengths of the rainy season are in pentads and the equivalent number of days are indicated in parentheses.*

	(a) Onset date			(b) Retreat date			(c) Length (*retreat* − *onset*)		
Data	zone 1	zone 2	zone 3	zone 1	zone 2	zone 3	zone 1	zone 2	zone 3
0bservation	16^{th}Pentad±2 (17-21 Mar)	20^{th}Pentad±2 (6-10 Apr)	28^{th}Pentad±3 (16-20 May)	61^{st}Pentad±1 (22 Oct-1 Nov)	57^{th}Pentad±1 (8-12 Oct)	53^{rd}Pentad±2 (18-22 Sep)	45 Pentads±2 (225 days)	37 Pentads±3 (185 days)	25 Pentads±3 (125 days)
BCCR-bcm2.0	12^{th}Pentad±2 (25 Fev-1 Mar)	22^{nd}Pentad±2 (16-20 Apr)	29^{th}Pentad±3 (21-25 May)	64^{th}Pentad±1 (12-16 Nov)	59^{th}Pentad±1 (18-22 Oct)	54^{th}Pentad±2 (23-27 Sep)	52 Pentads±2 (260 days)	36 Pentads±2 (180 days)	25 Pentads±4 (125 days)
CSIRO-mk3.5	14^{th}Pentad±2 (7-11 Mar)	20^{th}Pentad±2 (6-10 Apr)	24^{th}Pentad±2 (26-30 Apr)	63^{rd}Pentad±1 (7-11 Nov)	57^{th}Pentad±1 (8-12 Oct)	52^{nd}Pentad±1 (13-17 Sep)	49 Pentads±2 (245 days)	37 Pentads±2 (185 days)	28 Pentads±2 (140 days)
MPI-echam5	14^{th}Pentad±2 (7-11 Mar)	19^{th}Pentad±2 (1-5 Apr)	26^{th}Pentad±2 (6-10 May)	63^{rd}Pentad±1 (7-11 Nov)	60^{th}Pentad±1 (23-27 Oct)	56^{th}Pentad±1 (3-7 Oct)	49 Pentads±2 (245 days)	40 Pentads±2 (200 days)	30 Pentads±2 (150 days)
MRI-cgcm2.3.2a	6^{th}Pentad±2 (26-30 Jan)	16^{th}Pentad±2 (17-21 Mar)	29^{th}Pentad±2 (21-25 May)	66^{th}Pentad±1 (22-26 Nov)	58^{th}Pentad±1 (13-17 Oct)	49^{th}Pentad±1 (29 Aou-2 Sep)	60 Pentads±2 (300 days)	42 Pentads±2 (210 days)	20 Pentads±2 (100 days)

et al. 2008). The increase in the length of the rainy season from zone 3 to zone 1 may be explained by the annual migration of the ITD, which controls the Monsoon influx of humid maritime air into the continent. This favorable rainfall-producing factor has the least residence period over zone 3.

Of the four general circulation models, only MPI-echam5 has an onset date within one standard deviation of observations in all the three zones. A similar analysis shows that CSIRO-mk3.5 gives good onset in zones 1 and 2, while BCCR-bcm2.0 and MRI-cgcm2.3.2a succeed in only one zone. Based on this criterion, three models have the right simulation in zone 3 and two in the other zones. Because there is less dispersion on retreat dates (standard deviation of 1), no model is on target in zone 1, one is in zone 2 and two are in zone 3. For both onset and retreat, boxplot diagrams (Figure 12 (a) and (b)) indicate that dispersion between models is low, the models tending to agree more among them than with observations. Their poor performance on retreat dates translates into poor results for the length of the season (Figure 12 (c)) which are mostly off target in zone 1 but slightly better in zones 2 and 3. It is also to be noted that MRI-cgcm2.3.2a is often even out of the range of extreme observations.

A quantitative verification of the model simulations is needed in order to objectively analyze and compare their performances. In Figure 12, numbers expressed in percentages and represented below each model boxplots are statistical probabilities for models to capture the observed parameters (onset and retreat dates and length of the rainy season).

In zone 1, CSIRO-mk3.5 and MPI-echam5 show better results than the other two models. While their statistical probabilities for predicting onset date are greater than 50% (61% for CSIRO-mk3.5 and 58% for MPI-echam5), they give poor results for retreat date and duration (less than 10%). In zone 2, CSIRO-mk3.5 shows best results and also has the greatest statistical probability (100% for both onset date and duration, 81% for retreat date). The second best performance is by MPI-echam5 for onset (94% of statistical probability for prediction) and by BCCR-bcm2.0 for duration (85%). Other models show poorer results (less than 50%). In zone 3, the best statistical probability for prediction is by MPI-echam5 for onset date (74%), CSIRO-mk3.5 for retreat date (75%) and BCCR-bcm2.0 for duration of the rainy season (78%). For onset and retreat dates, the second best is BCCR-bcm2.0. Overall, CSIRO-mk3.5 shows highest combined statistical probability for prediction of onset and retreat dates and duration of the rainy season, followed by MPI-echam5. MRI-cgcm2.3.2a shows lowest statistical probability.

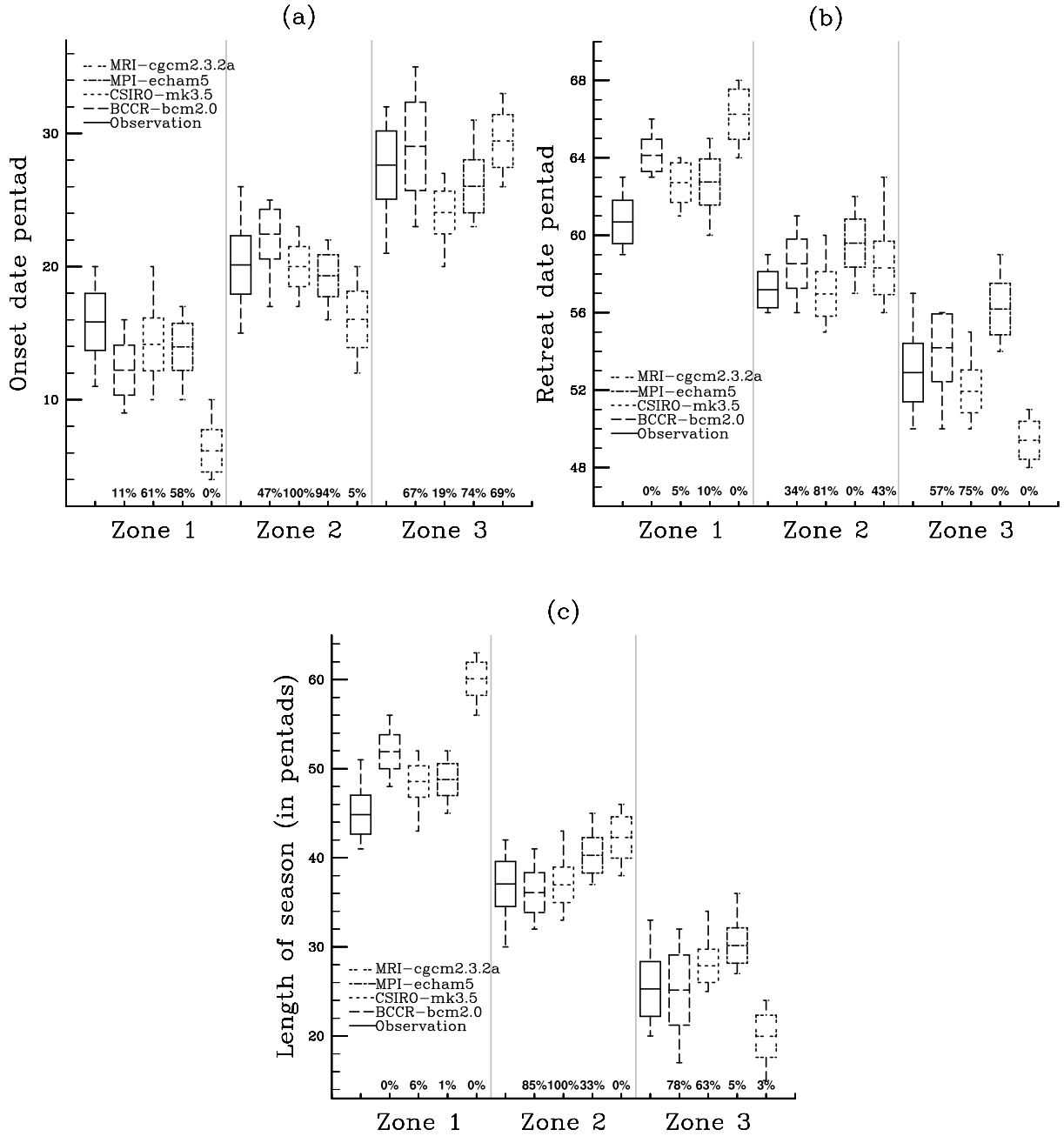

Figure 12: *Onset date, retreat date and duration of the rainy season for observation and models simulations. Numbers expressed in percentage and presented below each model boxplot represent the statistical probability for each model to forecast the observed onset date (a), retreat date (b) and duration of the rainy season (c).*

Table 6: *Correlation coefficients of models to simulate observed interannual variabilities of onset and retreat dates of the rainy season for the current climate (1962-93).*

	Onset date			Retreat date		
Data	zone 1	zone 2	zone 3	zone 1	zone 2	zone 3
BCCR-bcm2.0	0.12	-0.11	-0.17	-0.44	-0.22	-0.20
CSIRO-mk3.5	-0.09	0.18	0.05	0.12	0.10	0.25
MPI-echam5	0.17	-0.19	-0.12	0.13	0.24	-0.41
MRI-cgcm2.3.2a	0.25	0.05	0.20	-0.12	0.03	-0.13

d) Interannual variability

The value of standard deviation of a time series can be used to elucidate temporal variability (Syed et al. 2010). For onset date, observed standard deviations of 2 pentads in zone 1 and 3 pentads in zones 2 and 3 indicate that interannual variability of this parameter is lower in the Equatorial forest zone. Retreat dates and lengths of the rainy season in all the three zones show lower amplitudes of fluctuations than onset dates (Figure 13). These amplitudes decrease from zone 3 in the Sahelian zone to zone 1 south of domain.

Figure 13 below indicates the interannual variabilities of onset and retreat dates of the rainy season for zone 1, 2 and 3 respectively.

Extreme values (minima and maxima) observed in the interannual variability of onset dates are much farther from their means, compared to retreat and duration of the rainy season. Table 6 shows correlation coefficients between models and observation for onset and retreat dates of the rainy season. In general, correlation coefficients are low and those of the onset date of the rainy season are lower. Models outputs poorly reproduce these interannual variations (correlation coefficient $|r| < 0.5$) (Table 6). However MPI-echam5 in most cases do the best job.

e) Interannual trends

Regression lines of the interannual trends of onset and retreat dates of the rainy season for the period 1962-93 are shaded on Figure 13. Their slopes are recapitulated on Tables 7 and 8 for onset and retreat dates respectively.

Onset date of the rainy season has known a slight positive tendency (slope of the regression line greater than zero) in all zones (Table 7). Observed trends in yearly onset dates are higher in the Sahelian zone and decreases southwards. All models fail to represent these trends, but signs are well simulated in zone 1 by BCCR-bcm2.0 and MPI-echam5,

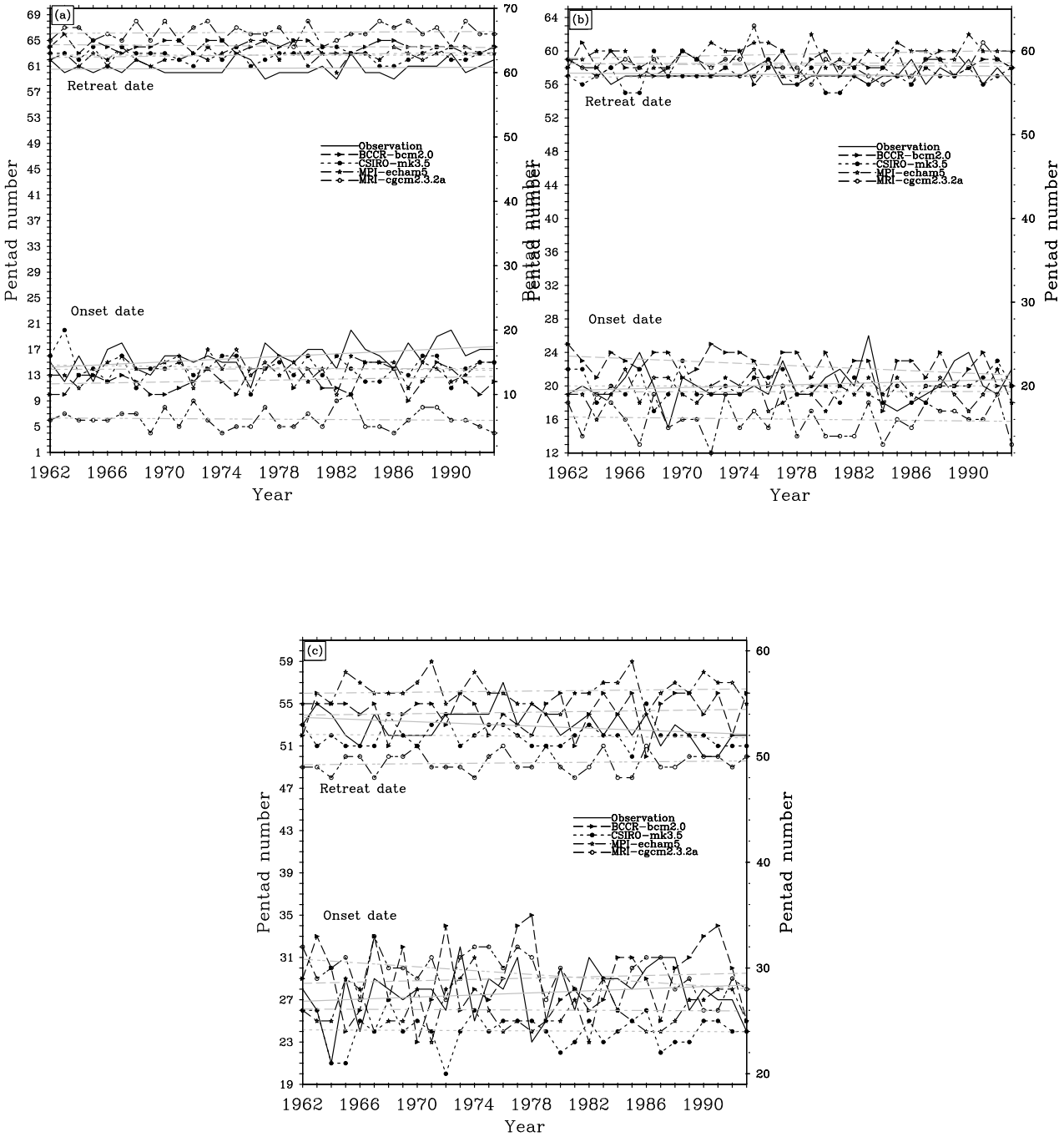

Figure 13: *Interannual variabilities of onset and retreat dates of the rainy season for observation and models in zone 1 (Figure (a)), zone 2 (Figure (b)) and zone 3 (Figure (c)). Regression line for each curve is shaded.*

in zone 2 by MPI-echam5 and in zone 3 by BCCR-bcm2.0 and CSIRO-mk3.5.

Table 7: *Slope of the regression line of inter-annual trend of onset date for the period 1962-93 and for the three zones.*

	Slope for Onset date (mm/year). t-value in brackets.				
Region	0bservation	BCCR-bcm2.0	CSIRO-mk3.5	MPI-echam5	MRI-cgcm2.3.2a
zone 1	0.52 (tv=2.83)	0.04 (tv=0.34)	-0.07 (tv=-0.40)	0.01 (tv=0.07)	-0.10 (tv=-0.65)
zone 2	0.24 (tv=1.18)	-0.37 (tv=-2.35)	-0.00 (tv=-0.02)	0.05 (tv=0.37)	-0.32 (tv=-1.78)
zone 3	0.02 (tv=0.08)	0.13 (tv=0.44)	0.052 (tv=0.36)	-0.12 (tv=-0.61)	-0.32 (tv=-1.61)

Table 8: *Slope of the regression line of inter-annual trend of retreat date for the period 1962-93 and for the three zones.*

	Slope for Retreat date (mm/year). t-value in brackets.				
Region	0bservation	BCCR-bcm2.0	CSIRO-mk3.5	MPI-echam5	MRI-cgcm2.3.2a
zone 1	0.01 (tv=0.13)	-0.09 (tv=-1.16)	-0.11 (tv=-1.18)	0.13 (tv=1.22)	0.06 (tv=0.61)
zone 2	-0.04 (tv=-0.39)	-0.12 (tv=-0.97)	0.03 (tv=0.34)	0.11 (tv=1.06)	-0.01 (tv=-0.07)
zone 3	-0.40 (tv=-1.42)	-0.01 (tv=-0.07)	0.07 (tv=0.69)	0.07 (tv=0.54)	0.08 (tv=0.86)

As for retreat date, observed trends are weaker compared to onset date. Positive trend is observed in zone 1 while negative trends are observed in zones 2 and 3, with the amplitude increasing southwards (table 8). All models well capture the observed low trends. Right signs of slopes are well simulated in zone 1 by MPI-echam5 and MRI-cgcm2.3.2a, in zone 2 by BCCR-bcm2.0 and MRI-cgcm2.3.2a and in zone 3 only by BCCR-bcm2.0. But, they all fail to represent amplitudes of tendencies.

3.1.2 Spatial distribution and tendencies of rainfall statistical parameters for the period 1962-1993

a) Spatial distribution

Here we focus on the spatial patterns of rainfall statistical parameters.

Mean annual total amounts

Mean annual precipitation for the period under study (1962-1993) ranges from 3600 mm on the South Western Atlantic coast to 800 mm in the Northernmost region (Figure

14 (a)). This range of values comprises a strong West-East gradient near the coastal region and a generally South-North negative gradient over the rest of the country, with a vast area extending from 2° to 9°N, where annual precipitation varies little between 1600 and 1100 mm. This is followed in the Sahel region by a faster decrease to values of 800 mm at 10°N (i.e. 200 mm/degree latitude). MPI-echam5 (Figure 14 (b)) reproduces observed pattern and the different gradients, except around the coastal atlantic area where it slightly underestimates rainfall intensities. As for MRI-cgcm2.3.2a (Figure 14 (d)), the only right patterns are in the northern part of the country particularly above 8° of latitude and intensities are strongly underestimated around the coastal Atlantic area. The model BCCR-bcm2.0 (Figure 14 (e)) represents patterns and intensities above 8°N and fails below it by underestimating rainfall intensities around the coastal Atlantic area and by not showing the west-east gradient. CSIRO-mk3.5 (Figure 14 (c)) well represents pattern and intensity in the southern part of the country (below 8°N) and fails in the northern part by overestimating rainfall intensities. In general, some models underestimate rainfall intensities while others overestimate on the same areas. This suggest that ensemble means of model outputs may give better overall results. The mean annual total amounts of combined outputs of CSIRO-mk3.5 and MPI-echam5 (Figure 14 (f)) shows improved results in pattern and intensities while other combinations such as Mk3.5-Cgcm2.3.2a, Echam5-Cgcm2.3.2a and Mk3.5-Echam5-Cgcm2.3.2a (Figures not shown) do not suit as well for annual total amounts.

A seasonal analysis (not shown) reveals that MPI-echam5 has best results in the March-April-May (MAM) and JJA seasons, but underestimates September-October-December (SON) total amounts in the coastal Atlantic area by a factor of about 2. This failure is compensated in the DJF season by an overestimation of same proportion. CSIRO-mk3.5 and MRI-cgcm2.3.2a give good spatial representation in the MAM and SON seasons, but both fail to simulate the right JJA seasonal amount and overestimate DJF as compensation especially south of 7°N of the latitude.

The mean annual cycle is represented (Figure 15) for 3 zones representing 3 different climate regimes: the Sahelian zone (zone 3) from 8°N to 13°N where the annual precipitation cycle is unimodal, the equatorial forest zone (zone 1) from 1°N to 5°N (the annual precipitation cycle is bimodal) and the intermediate zone (zone 2) characterized by high lands and bimodal annual precipitation cycle. All models more or less represent the shape of the mean annual cycle and best results are obtained for the Sahelian zone (Figure 15 (a)). MPI-echam5 and MRI-cgcm2.3.2a show worst results by underestimating rainfall intensities during rainy periods (August-November) in all zones. The two other

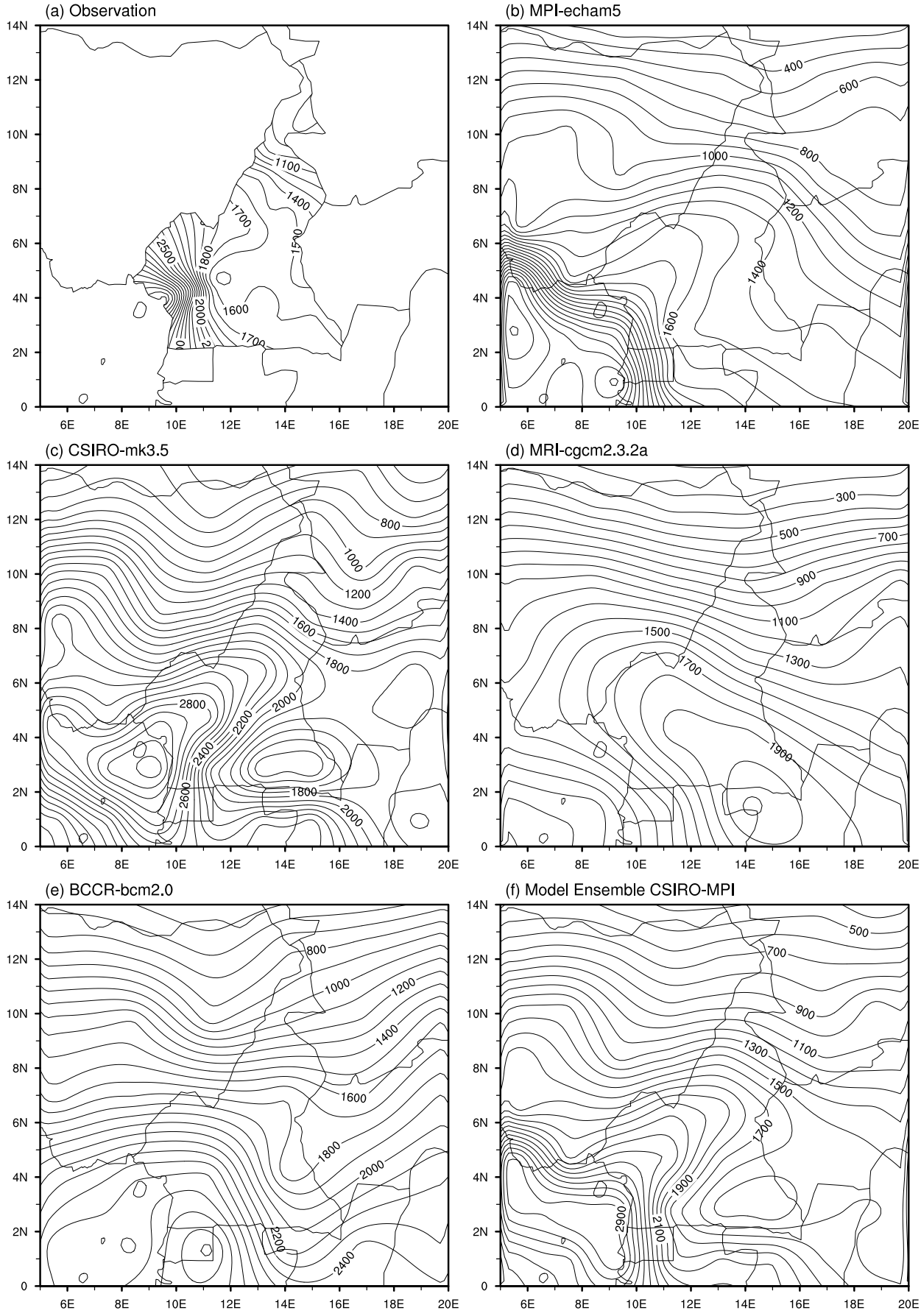

Figure 14: *Mean annual total amounts for current climate. (a) observation, (b) MPI-echam5, (c) CSIRO-mk3.5, (d) MRI-cgcm2.3.2a, (e) BCCR-bcm2.0., (f) model ensemble CSIRO-MPI*

models (BCCR-bcm2.0 and CSIRO-mk3.5) overestimate rainfall intensities in zones 1 and 2 during the rainy periods. Dry periods are well simulated by all models.

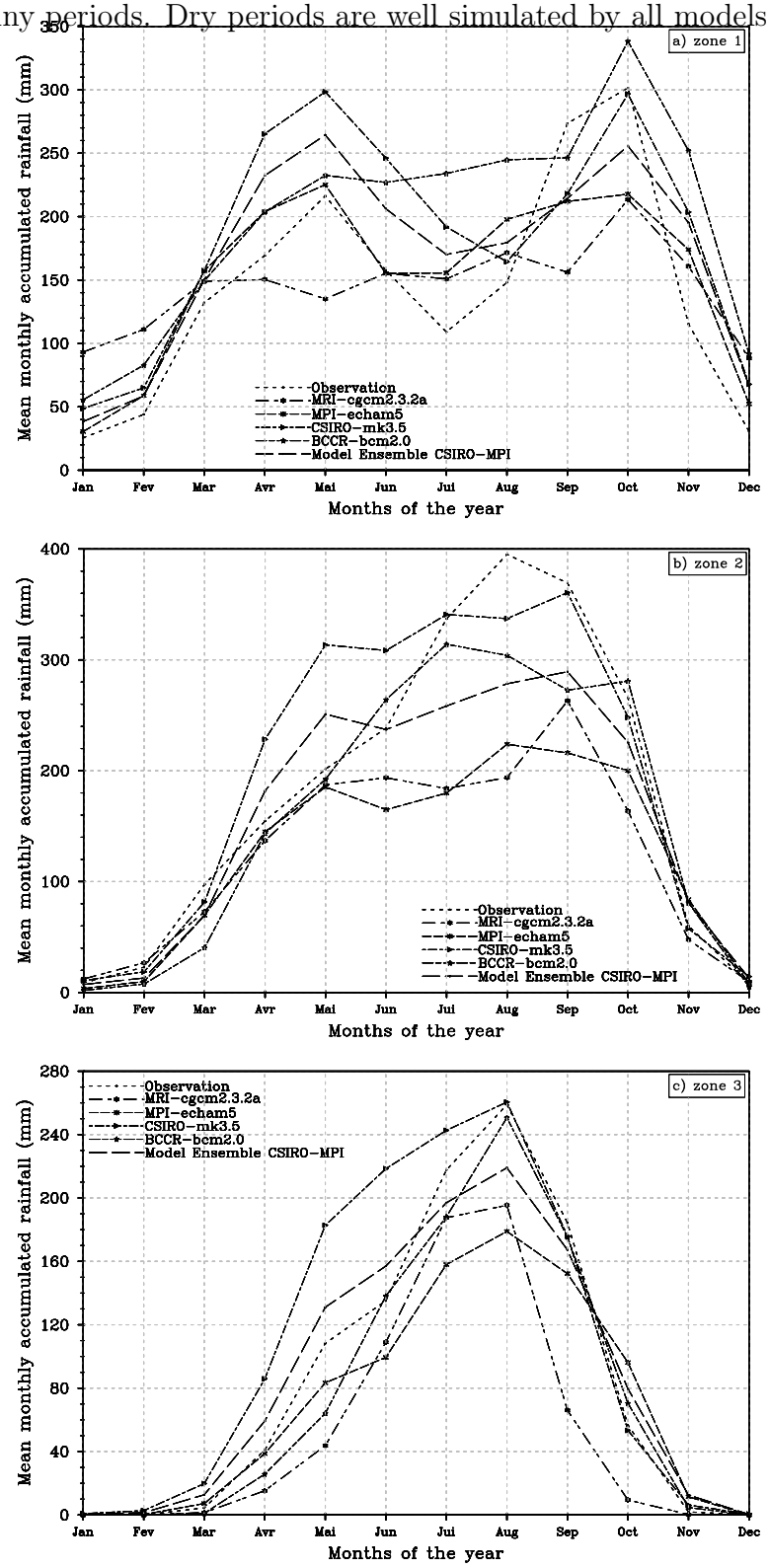

Figure 15: *Mean annual cycle per zone.*

Mean annual number of rain day.

A day is considered rainy if the measured precipitation is 1 mm or more. The spatial pattern of the mean annual number of rain days (Figure 16) is similar to that of mean annual totals, for both observed (Figure 16 (a)) and simulated precipitation (Figure 16 (b), (c), (d) and (e)). MPI-echam5 overestimates this parameter by a factor of 2 above 10°N and slightly less than 2 elsewhere. CSIRO-mk3.5 simulated spatial patterns and intensity are close to those of MPI-echam5 while MRI-cgcm2.3.2a patterns are similar to BCCR-bcm2.0. The later two both overestimate mean annual number of rain days by a factor of about 2 in the southern part of the domain and of 1 in the Sahelian zone. The model ensemble CSIRO-MPI (Figure 16 (f)) better represents observed pattern of the parameter than individual model, but estimations are overestimated by a factor of 2.

Maximum length of dry spells.

Mean maximum length of dry spells increases with latitude (positive South-North gradient) giving zonally oriented patterns (Figure 17 (a)). Extreme Southern area is the least dry with an average annual maximum dry spell of 20 days, while the Sudano Sahelian area is the driest (95 consecutive dry days per year). Seasonal analysis reveals that the annual lengths of dry spell coincide with the dry season (DJF). The four CMIP3 dataset represent well the spatial pattern of this parameter (Figures 17 (b), (c), (d) and (e)). CSIRO-mk3.5 and MPI-echam5 furthermore give the right intensities over the entire domain while other models only succeed below 8°N and overestimate elsewhere. The model ensemble CSIRO-MPI (Figure 17 (f)) shows improved results but slightly fails to reproduce patterns south of domain.

Ninetieth percentile of daily precipitations

This parameter is an indicator of extremes and can also inform on the shape of the distribution of daily precipitations. Figure 18 represents the ratio of the 90^{th} percentile of daily precipitations to the mean daily precipitation. The isolines of Figure 18 (a) are very close in orientations to those of Figure 14 (a). South of 8° North, the gradient of this parameter has a sign opposite to that of mean precipitation, but it is sufficiently weak for the entire area to be considered homogeneous. Above 8° North, the values of the parameter fall off from 3.4 to 2.6. When looking at the fraction of annual precipitation contributed by events above the 90^{th} percentile (Figure 19 (a)), we also note that the Southern part of the domain is homogeneous with values around 0.7, whereas in the North we have

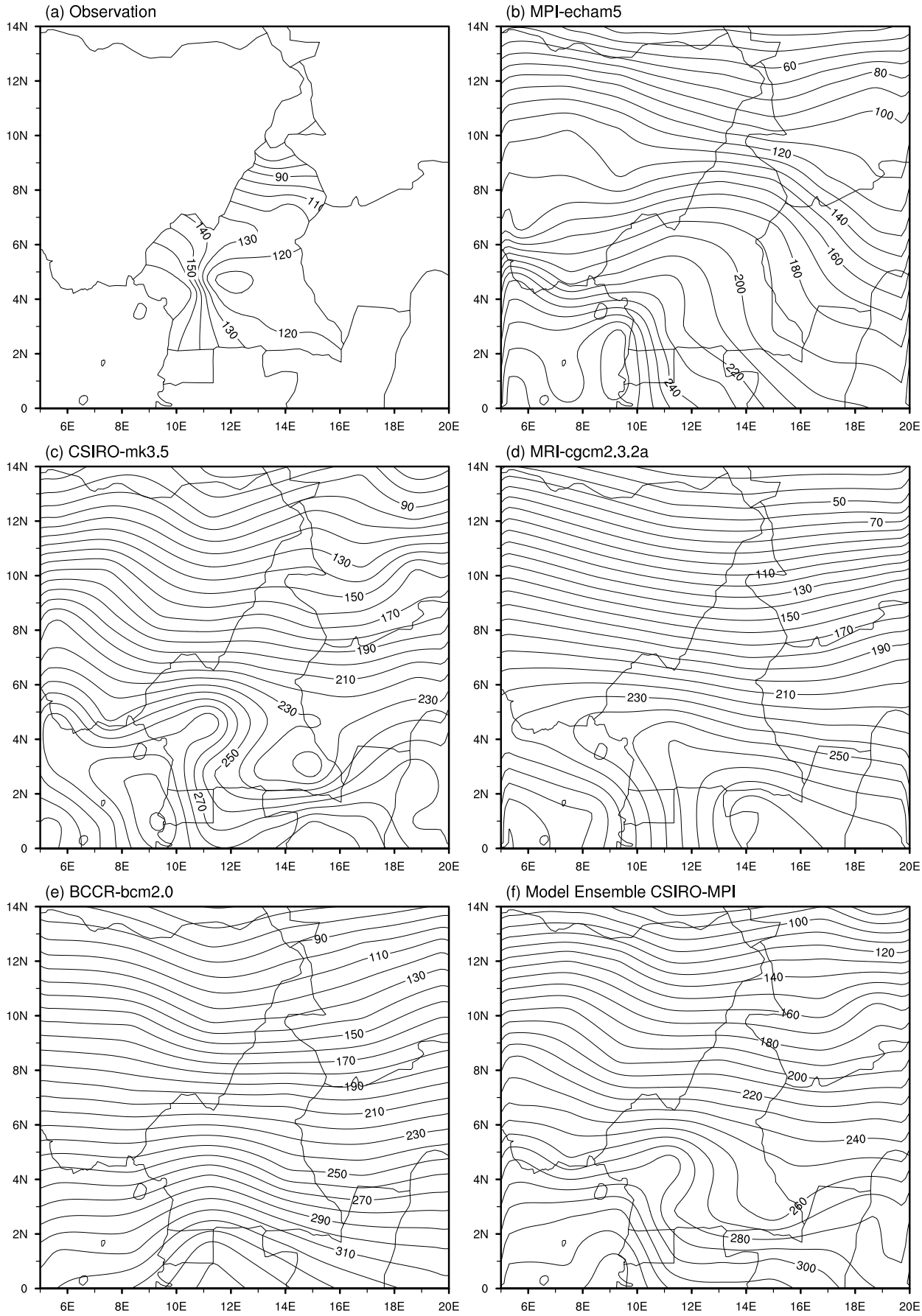

Figure 16: *Mean annual number of rainy day for current climate. (a) observation, (b) MPI-echam5, (c) CSIRO-mk3.5, (d) MRI-cgcm2.3.2a, (e) BCCR-bcm2.0 and (f) model ensemble CSIRO-MPI.*

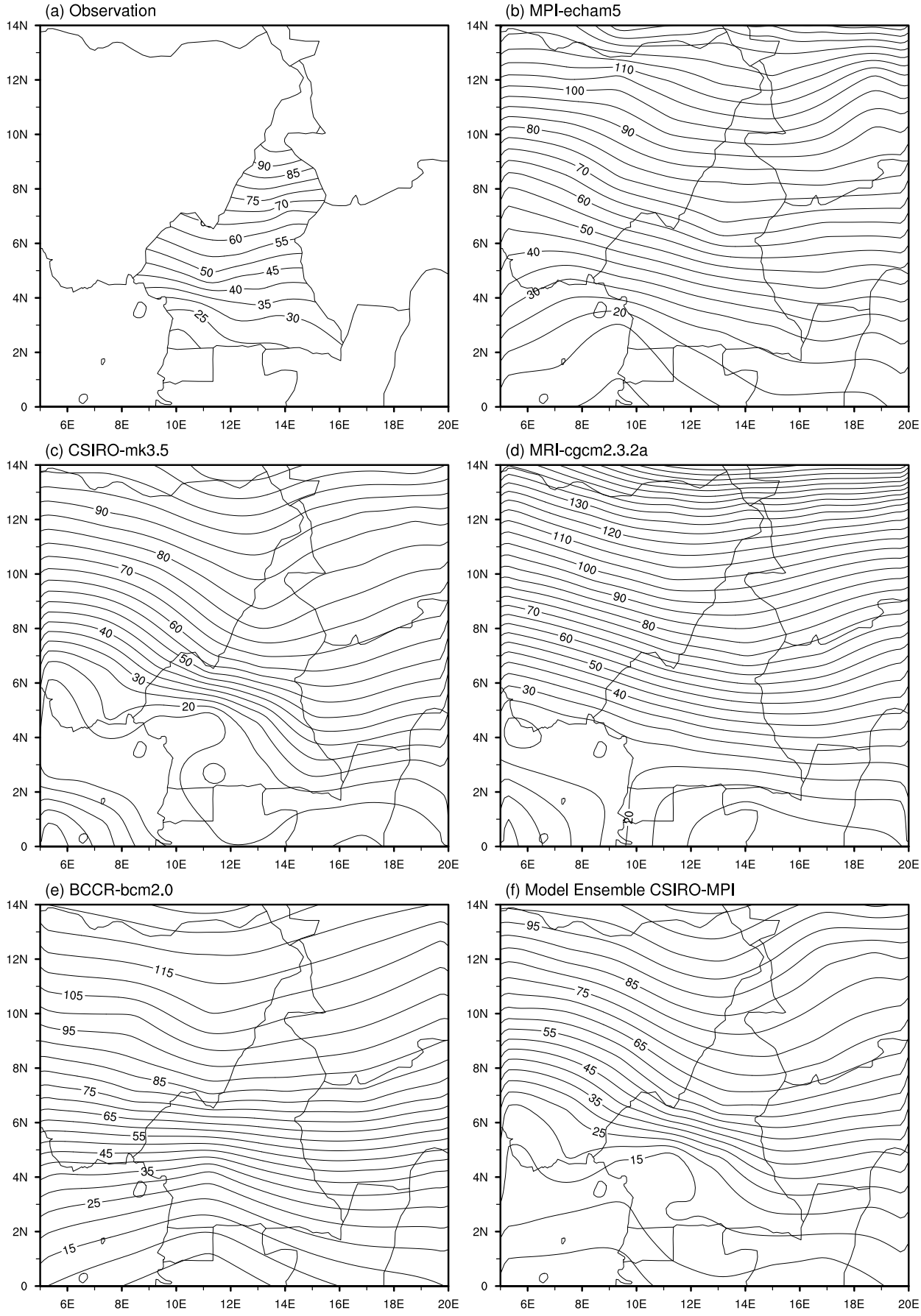

Figure 17: *Maximum length of dry spells. (a) observation, (b) MPI-echam5, (c) CSIRO-mk3.5, (d) MRI-cgcm2.3.2a, (e) BCCR-bcm2.0 and (f) model ensemble CSIRO-MPI.*

a positive gradient and higher values (0.9). These patterns indicate that there are two different rainfall regimes. In the Northern Sahelian region, annual rainfall are contributed by very few intense events (related to the passage of African Easterly Waves). In the Southern regions, the intensity of convective activities has a wider spectrum.

Modeled spatial pattern from MPI-echam5 and CSIRO-mk3.5 are similar to observed showing two gradients with different directions, latitudinal in the north and zonal in the south (Figures 18 (b) and (c)). But the amplitudes of the 90^{th} percentile related parameters are not well captured. Spatial pattern for BCCR-bcm2.0 and MRI-cgcm2.3.2a both show a single south-north gradient. MPI-echam5, BCCR-bcm2.0 and CSIRO-mk3.5 show wrong signs of gradient for the northern part of the country for the ratio of the 90^{th} percentile of daily precipitations to the mean daily precipitation (Figures 18 (b), (c) and (e)) and right signs for the fractions of annual precipitations contributed by daily events above the 90^{th} percentile of daily values (Figures 19 (b), (c) and (e)). MRI-cgcm2.3.2a shows the right signs for the two extreme parameters. For the ratio of the 90^{th} percentile of daily precipitations to the mean daily precipitation, all models underestimate values bellow 8° and overestimate them above. They also all underestimate over the entire domain the fraction of annual precipitations contributed by daily events above the 90^{th} percentile of daily values. Overall, the models tend to underestimate amplitudes of the ratio of the 90^{th} percentile of daily precipitation to the mean daily precipitation and of the fraction of annual precipitation contributed by events above the 90^{th} percentile.

The model ensemble CSIRO-MPI generally fails to represent gradients and patterns south of domain.

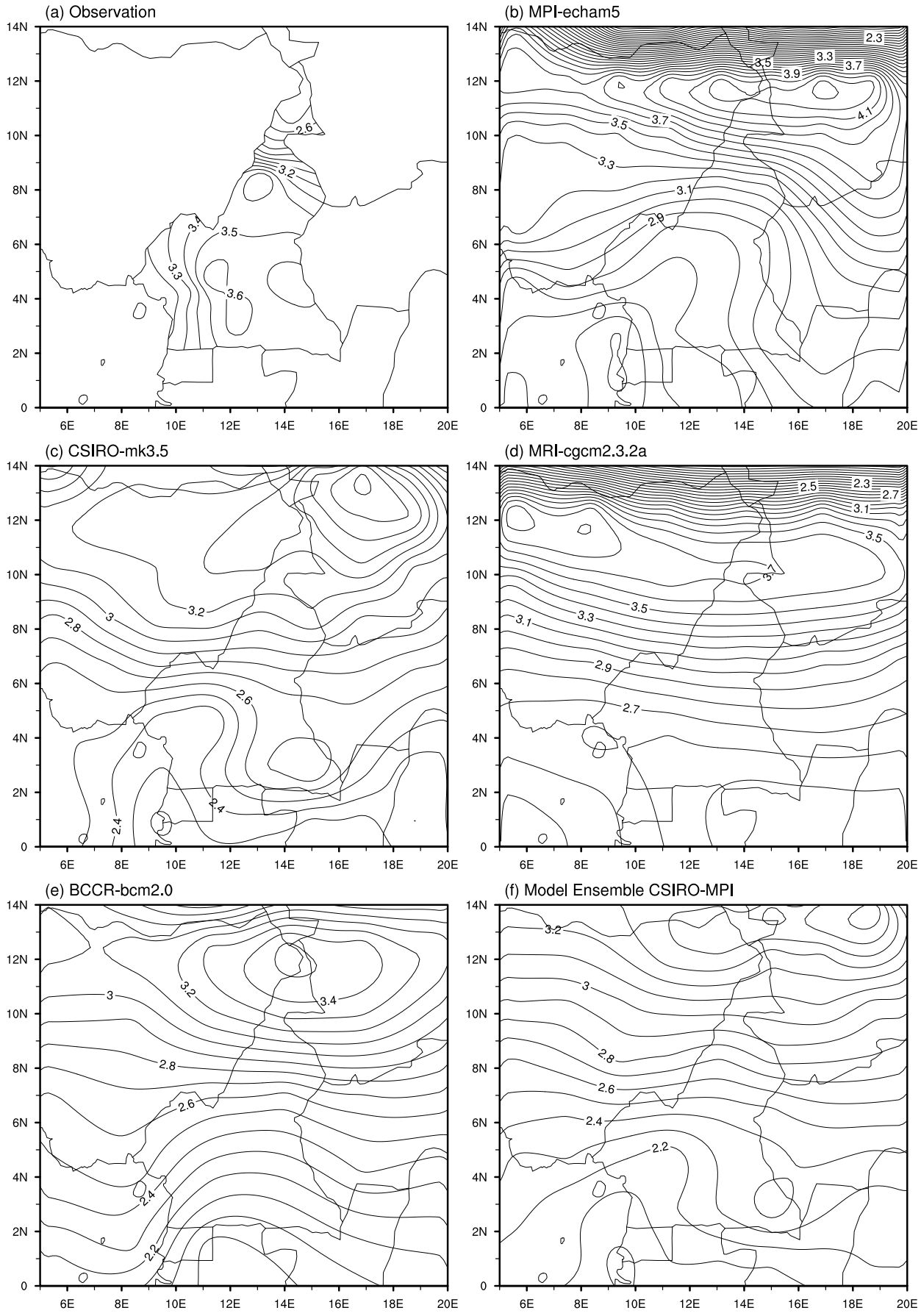

Figure 18: *Ratio of the 90^{th} percentile of daily precipitations to the mean daily precipitation. (a) observation, (b) MPI-echam5, (c) CSIRO-mk3.5, (d) MRI-cgcm2.3.2a, (e) BCCR-bcm2.0 and (f) model ensemble CSIRO-MPI.*

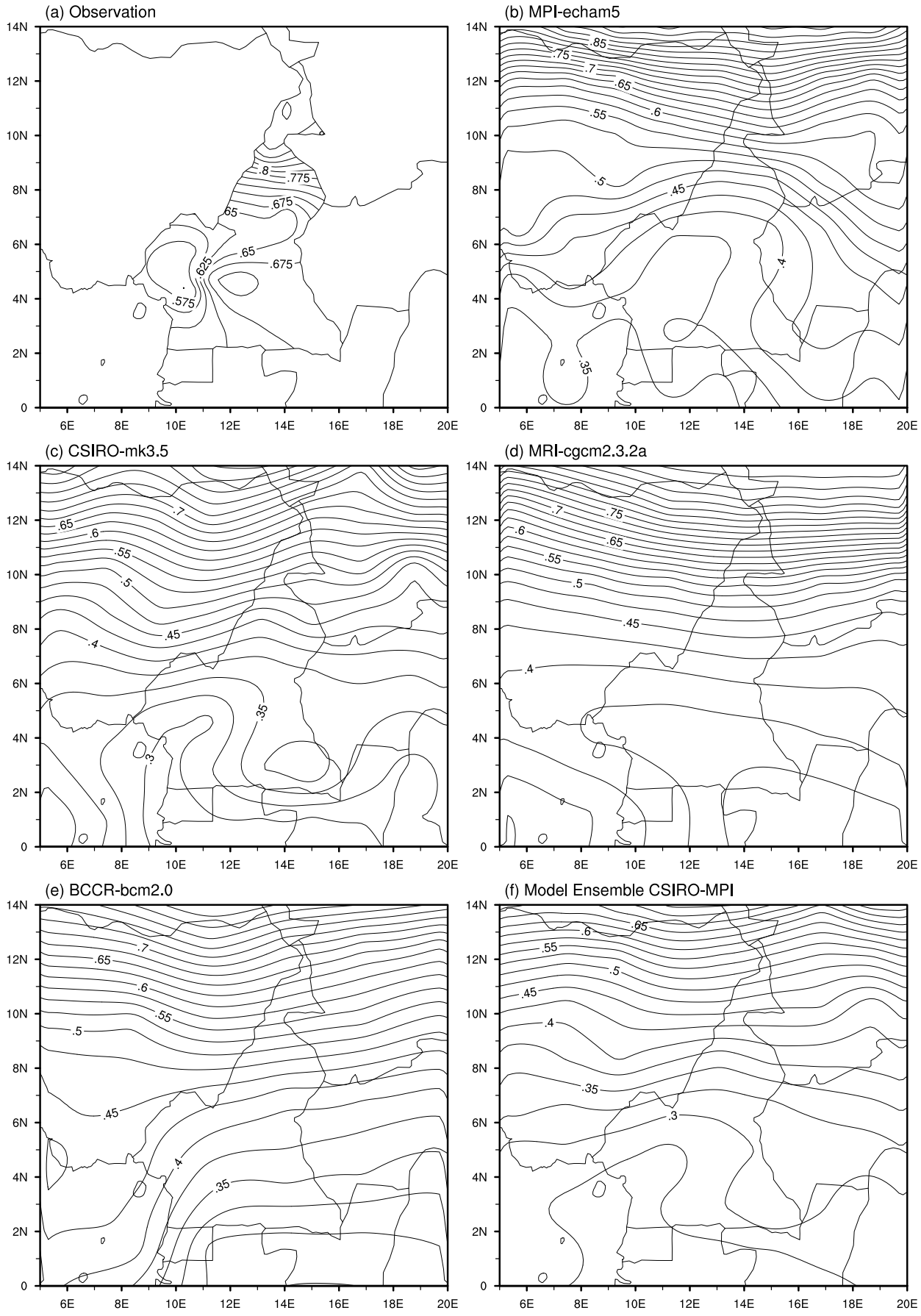

Figure 19: *Fraction of annual precipitations contributed by daily events above the* 90^{th} *Percentile of daily values. (a) observation, (b) MPI-echam5, (c) CSIRO-mk3.5, (d) MRI-cgcm2.3.2a, (e) BCCR-bcm2.0 and (f) model ensemble CSIRO-MPI.*

b) Trends in observed and simulated current climate

Temporal variability in observed data was first studied for each station. Trends for the 1962-93 period, represented by the slope of their linear regression against time were calculated for each rainfall statistical parameter. This study were done for the three different zones defined in section 3.1.1: the Equatorial forested region (zone 1), the Sahelian region (zone 3) and a transition zone (zone 2) from around 5° to 8°N. Trends were tested for significance using student's t-test at 95% confidence level. The results are summarized in Figure 20. Non-significant trends were not represented. The two tests (student's t-statistic and Mann-Kendall) are discordant on very few cases (21 out of 90). In these cases, the considered trends are from the statistic for which more stations (higher percentage) have contributed to the trend.

In all zones, negative trends for annual total amounts are observed (Figure 20 (a_i)) and annual number of rain day (Figure 20 (b_i)) and positive trends for the fraction of annual precipitations contributed by daily events above the 90^{th} percentile of daily values (Figure 20 (d_i)). So over the entire domain, precipitation frequency and intensity decreased while heavy rainfall increased, i.e precipitation became rare but heavier when they did occur. The ratio of the 90^{th} percentile of daily precipitation to the mean daily precipitation (Figures 20 (c_1) and (c_3)) showed negatives trends in all zones and the maximum length of dry spells (Figures 20 (e_1) and (e_3)) showed positive trends in zones 1 and 2. These last results showed that dried periods increased in Sahelian and transition zones (zones 1 and 2) during the 20^{th} century. On the other hand, intense precipitation decreased in the same zones. The transition zone is then influenced by the increase of dried periods of the Equatorial forest zone (zone 1) and by the decrease of intense rains of the Sahelian zone (zone 3).

BCCR-bcm2.0 and CSIRO-mk3.5 simulation showed the right trend in all three zones for the fraction of annual precipitations contributed by daily events above the 90^{th} percentile of daily values and only BCCR-bcm2.0 does well for annual numbers of rain days in the three zones. For other rainfall statistical parameters, very few models showed consistent results in all three zones, succeeding at best in one zone. Therefore we undertake a simple statistical count of the successes and failures of each model to simulate trends of considered rainfall parameters. Results are summarized in table 9. BCCR-bcm2.0 shows best score while MPI-echam5 has the worst score.

Table 9: *statistical count of the model performance to simulate signs of trends of the five rainfall statistical parameters. Deduced from Figure 20.*

Region	Number of succeeded simulated trend over number of parameters			
	BCCR-bcm2.0	CSIRO-mk3.5	MRI-cgcm2.3.2a	MPI-echam5
zone 1	3/5	5/5	0/5	1/5
zone 2	5/5	3/5	1/5	2/5
zone 3	4/5	3/5	4/5	1/5
total	12/15	11/15	5/15	4/15

Trend magnitudes were estimated as the slope of the linear regression line. They were tested at 90% confidence level using student t statistic. The models evaluated in this part are BCCR-bcm2.0 and CSIRO-mk3.5 because they show best results in the trend detection, especially for mean annual total amounts and fraction of annual precipitations contributed by daily events above the 90^{th} percentile of daily values. Interannual variability associated with regression line for chosen models and rainfall statistical parameters (Figures shown in annexe) leads to establish Tables 10 and 11 of trend magnitude respectively for mean annual total amounts and fraction of annual precipitations contributed by daily events above the 90^{th} percentile. Observed trend magnitudes for annual total amounts (Table 10) show a slight decrease in zone 3 (-2.46 mm/year) and larger decrease in zone 2 (-8.31 mm/year) and 1 (-9.03 mm/year). The two models underestimate these magnitudes with largest values below -4 mm/year. The fraction of annual precipitations contributed by daily events above the 90^{th} percentile of daily values (Table 11) has positive but negligible trends of the order of 10^{-3} mm/year. We can thus consider that no

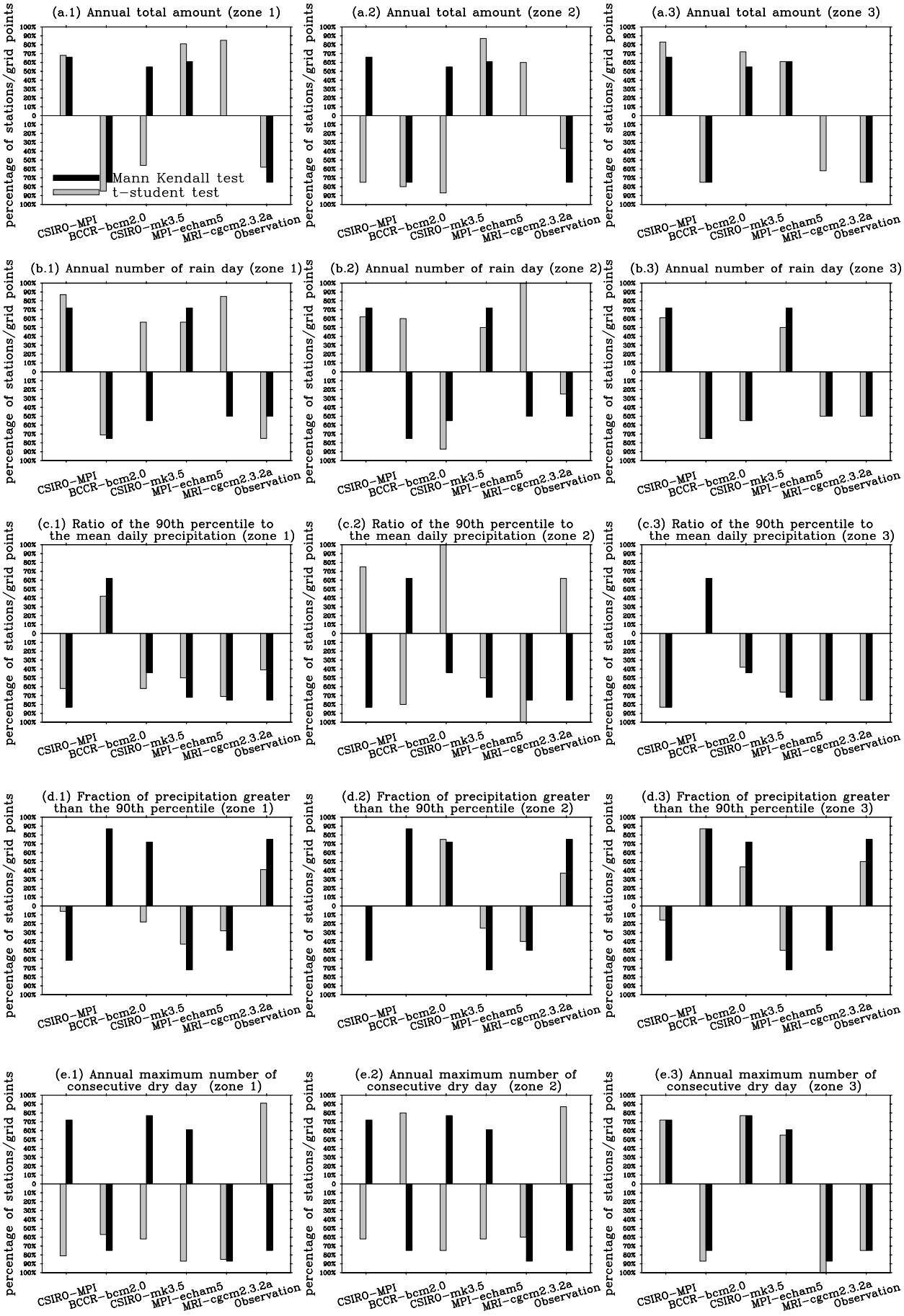

Figure 20: *Recapitulated tendencies of rainfall statistical parameters, according to student's t-statistic and Mann Kendall statistic. The H0 hypothesis has been rejected at 0.05 significant level. Non-significant trends are not represented.*

significant trend was found in this parameter.

Table 10: *Interannual trend magnitudes of mean annual total amounts for the period 1962-93 (in mm/year).*

zone	Observed	CSIRO-mk3.5	BCCR-bcm2.0
1	-9.03	-0.34	-2.76
2	-8.31	-2.50	-0.37
3	-2.46	0.92	-3.63

Table 11: *Interannual trend magnitudes of fraction of annual precipitations contributed by daily events above the 90^{th} percentile for the period 1962-93 (in mm/year).*

zone	Observed	CSIRO-mk3.5	BCCR-bcm2.0
1	0.00	-0.00	5.90
2	0.00	0.00	0.00
3	0.00	0.00	0.00

3.2 Projections of models rainfall outputs under a perturbed climate (2082-2098)

3.2.1 Future onset, retreat and length of the rainy season for the period 2082-2098

Projected mean onset and retreat dates and length of the rainy season

To assess the effect of increased greenhouse gas (GHG) concentration in the atmosphere on onset and retreat dates and length of the rainy season, projected dates for the period 2082-98 were analyzed. These were determined from the outputs of GCM simulations using the same methodology presented earlier.

Results under the perturbed climate of a given GCM were compared to its own simulation of current climate. Differences in onset and retreat dates of the rainy season and in duration between future and present climates are shown in Figures 21 (a), (b) and (c) respectively.

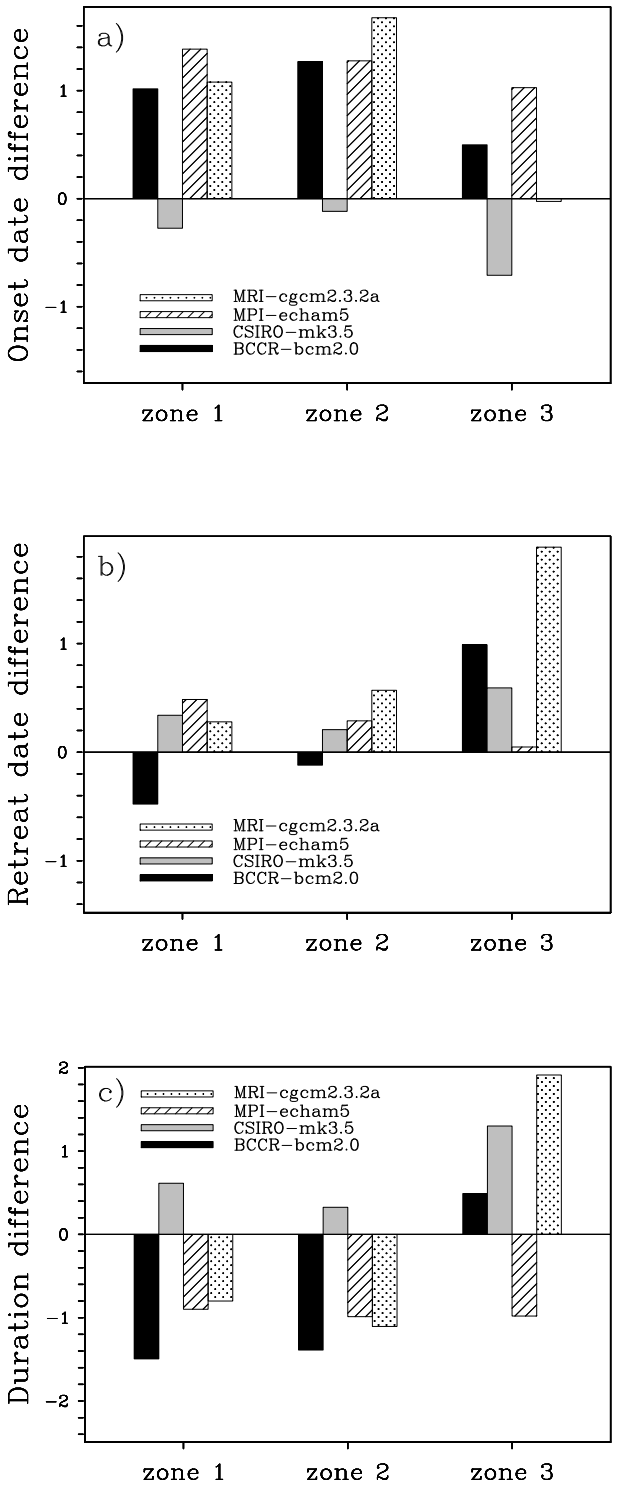

Figure 21: *Gap between mean future and mean current climate dates for onset (a)), retreat (b)) and differences in the duration (c)) of the rainy season. Vertical axis are graduated in pentads.*

Surprisingly there are no great changes in either onset or retreat dates. Three of the models (MPI-echam5, BCCR-bcm2.0 and MRI-cgcm2.3.2a) show late onset of one pentad in all zones, while CSIRO-mk3.5 has approximately normal start in zones 1 and 2 and early start of about one pentad in zone 3. Retreat occurs mostly earlier, but by less than one pentad, except for MRI-cgcm2.3.2a in zone 3 where it is almost 2 pentads earlier. Rainy seasons are shorter by approximately one pentad in zones 1 and 2 and longer in zone 3 by up to 2 pentads. These changes are all within the range of variability of current climate simulated by each model and could not be considered significant. This result corroborates that of Mkankam (2000) given the strong relationship between onset and rainfall attributes (Stewart 1991; Ati et al. 2002). The shortening of the rainy season is one of the most feared result of anthropogenic climate change. But projections under the SRES A2 scenario by the four models used here indicate that to the end of the 21^{st} century, no major perturbations of the seasons are expected, and it will be possible to continue growing the same crops as at present time in Cameroon.

Projected interannual variability

Figures 22 shows models projections of rainfall onset and retreat dates variabilities over the period 2082-98. Comparing to the present time simulation, it is expected lower fluctuations in onset and retreat date. There will likely be a lot of inconsistencies between the two models in zones 1 and 2. Most of the models project for all the three zones no tendency in the future interannual retreat date and a slight positive trend in onset date. In many cases, CSIRO-mk3.5 is not part of the consensus.

3.2.2 Future spatial distribution of rainfall statistical parameters for the period 2082-2098

The perturbed climate is represented by projections for the period 2082-2098 under IPCC SRES A2 emission scenario from four IPCC AR4 AOGCM. SRES A2 (Special Report on Emissions Scenarios A2) (IPCC, Climate Change 2007a; IPCC, Climate Change 2007c) assumes a strong, but regionally oriented economic growth and fragmented technological change with an emphasis on human wealth. It projects slightly lower GHG emissions than the IS92a scenario (IPCC 1992), but also slightly lower aerosol loadings, thus the warming response differs little from that of IS92a. For each model the projected climate is compared with the base climate simulated by the same model for the period 1962 to 1993. Only models and parameters they represented well in current climate are used.

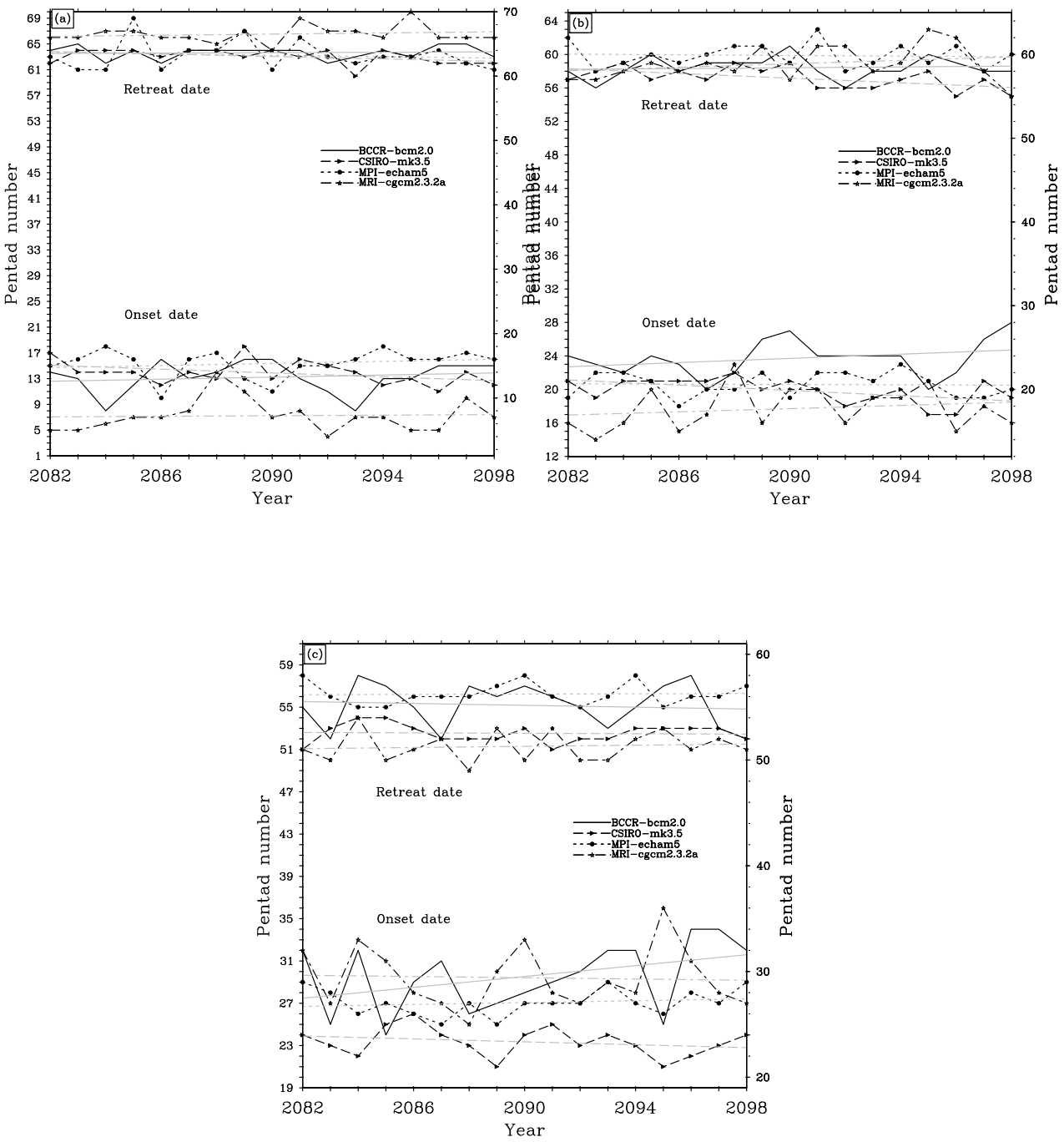

Figure 22: *Projected interannual variabilities (2082-2098) of onset and retreat dates of the rainy season for observation and models in zone 1 (Figure (a)), zone 2 (Figure (b)) and zone 3 (Figure (c)). Regression line for each curve is shadded.*

Thus, MPI-echam5 and CSIRO-mk3.5 are considered for mean annual total amounts, mean annual number of rain days, the maximum length of dry spells and the fraction of annual precipitations contributed by daily events above the 90^{th} percentile of daily values. Figure 23 shows the spatial patterns of the ratio of the mean future climate to the mean current climate for above parameters. More confidence is given to projections for which the two models show similar results.

For the *annual total amounts* (Figure 23 (a)), the two models CSIRO-mk3.5 and MPI-echam5 project positive gradients from the border of domain to its center. CSIRO-mk3.5 shows a belt of ratio 1 arount Adamowa and East part of domain. It is projected a ratio of 1.16 inner this belt and 0.98 outer. Therefore, according to CSIRO-mk3.5, annual total amounts is expected to increase from 16% $(1.16 - 1)$ East of domain, constant around Adamawa Plateau and Centre-East while a decrease of 2% $(0.98 - 1)$ is expected elsewhere. As for MPI-echam5, the increase of this parameter concerns a wider area with a rate ranging from 4% $(1.04 - 1)$ and 16% $(1.16 - 1)$ around the limites of the Cameroon territory to the heard of the country and a decrease of 2% in a smaller area (Western part of the northernmost of domain).

For the *annual number of rain days* (Figure 23 (b)), CSIRO-mk3.5 projects patterns and values similar to that of annual total amounts. This model shows a direct link between annual total amounts and annual number of rain days. The model MPI-echam5 for which projections are reduced to the North-East area of domain agrees with CSIRO-mk3.5, but the belt of ratio 1 where no change is expected is slightly displaced of about 1° towards the North-East.

The *maximum length of dry spells* is shown in Figure 23 (c). The two models show patterns with similar orientations. Furthermore, they show two negative gradients South-North and North-South. They project an increase around 8% $(1 - 1.08)$ and 16% $(1.16 - 1)$ in the southern part of domain, especially below 5°N and no change above. In the intermediate zone (5°N-10°N), the two models are discordant, CSIRO-mk3.5 projecting a decrease of about 2% $(0.98 - 1)$ and MPI-echam5 an increase of 2% $(1.08 - 1)$.

The projected spatial patterns for the *fraction of annual precipitations contributed by daily events above the 90^{th} percentile of daily values* (Figure 23 (d)) are not regular. CSIRO-mk3.5 projects a decrease of 2% $(0.98 - 1)$ in the South-Eastern part of domain and an increase of 8% $(1.08 - 1)$ elsewhere. However, there exist a line of direction (North-West)-(South-East) with the label 1 (no change expected) crossing the domain. MPI-echam5 projects an increase on the entire domain with a rate ranging from 8% right of 12°E to 16% on the left.

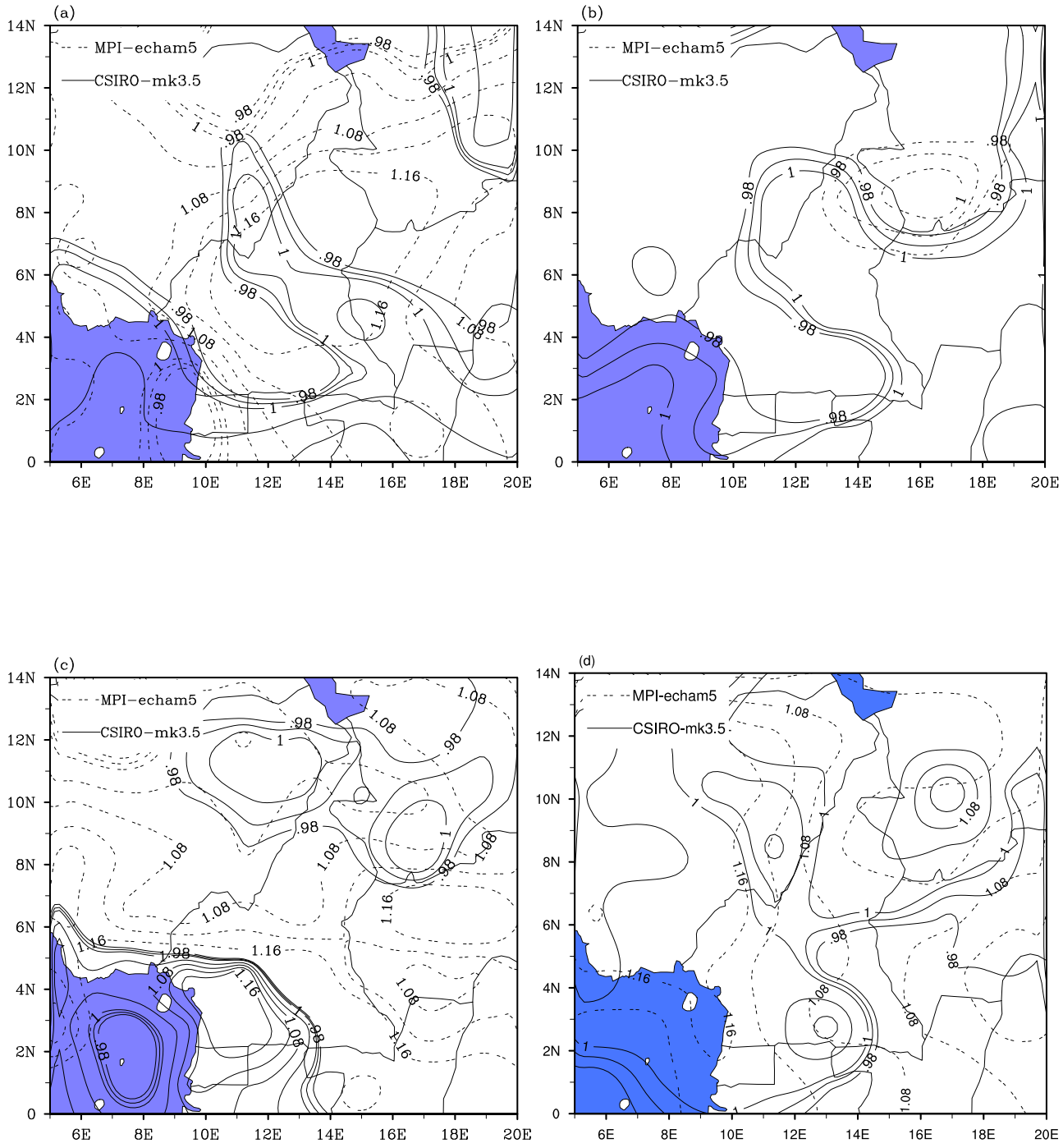

Figure 23: *Ratio of the mean future climate (2082-2098) to the mean present climate (1962-1993). (a) Annual total amounts. (b) Annual number of rainy days. (c) Maximum length of dry spells. (d) Fraction of annual precipitations contributed by daily events above the* 90^{th} *percentile of daily values.*

3.3 Computation of the Standardized Precipitation Index (SPI) and its use to assess drought occurrences in Cameroon over recent decades.

3.3.1 Suitable distribution functions for precipitation data

Distribution functions for station precipitation

Four statistical distribution functions (gamma, exponential, weibull and lognormal) were fitted to station precipitation data aggregated at various time scales. Figures 24 and 25 show results of the cumulative density function for empirical precipitation and for each of the trial distribution functions. Figures were shown for four stations (Kaele, Ngaoundere, Bertoua and Kribi), at 3-month and 12-month time scales.

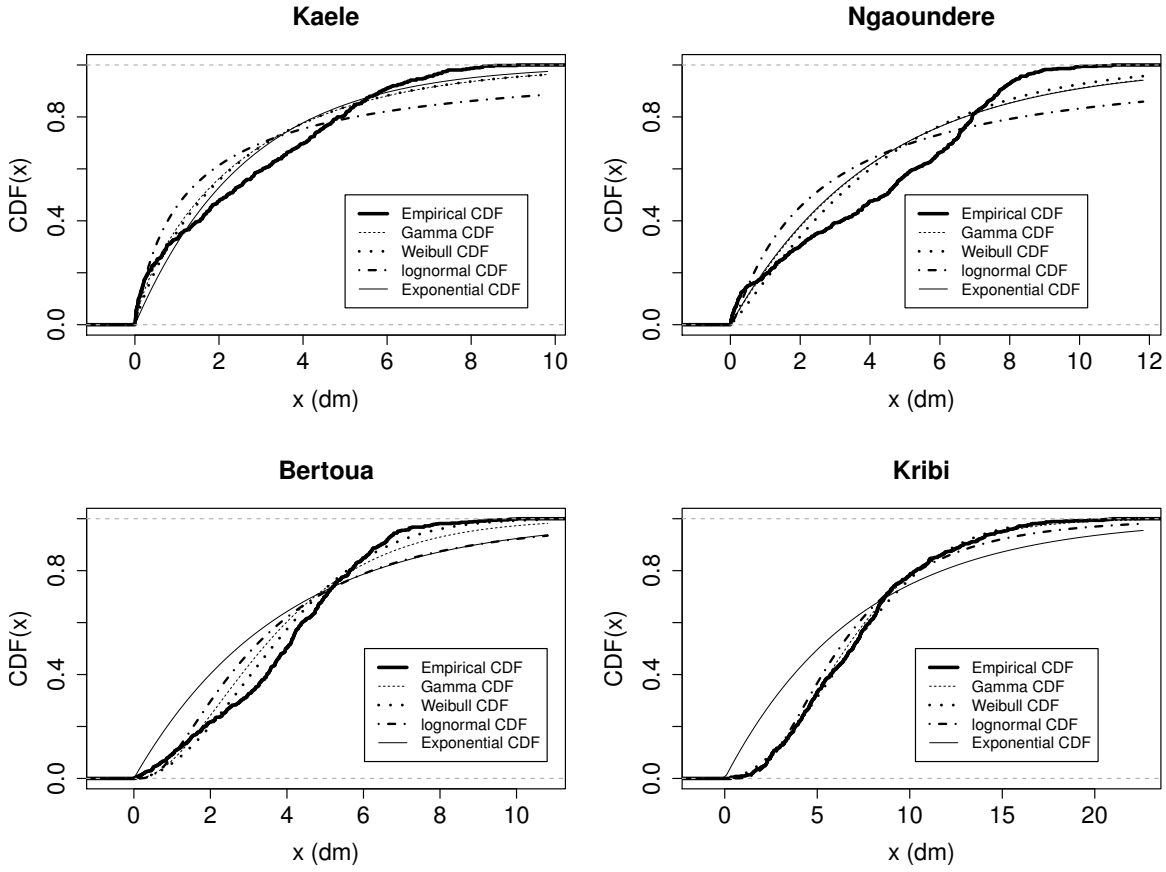

Figure 24: *Cumulative distribution functions for 3-month aggregated precipitation showing the empirical cumulative distribution function (ECDF) and gamma, weibull, lognormal, and exponential distributions fitted to the data. x represents precipitation values.*

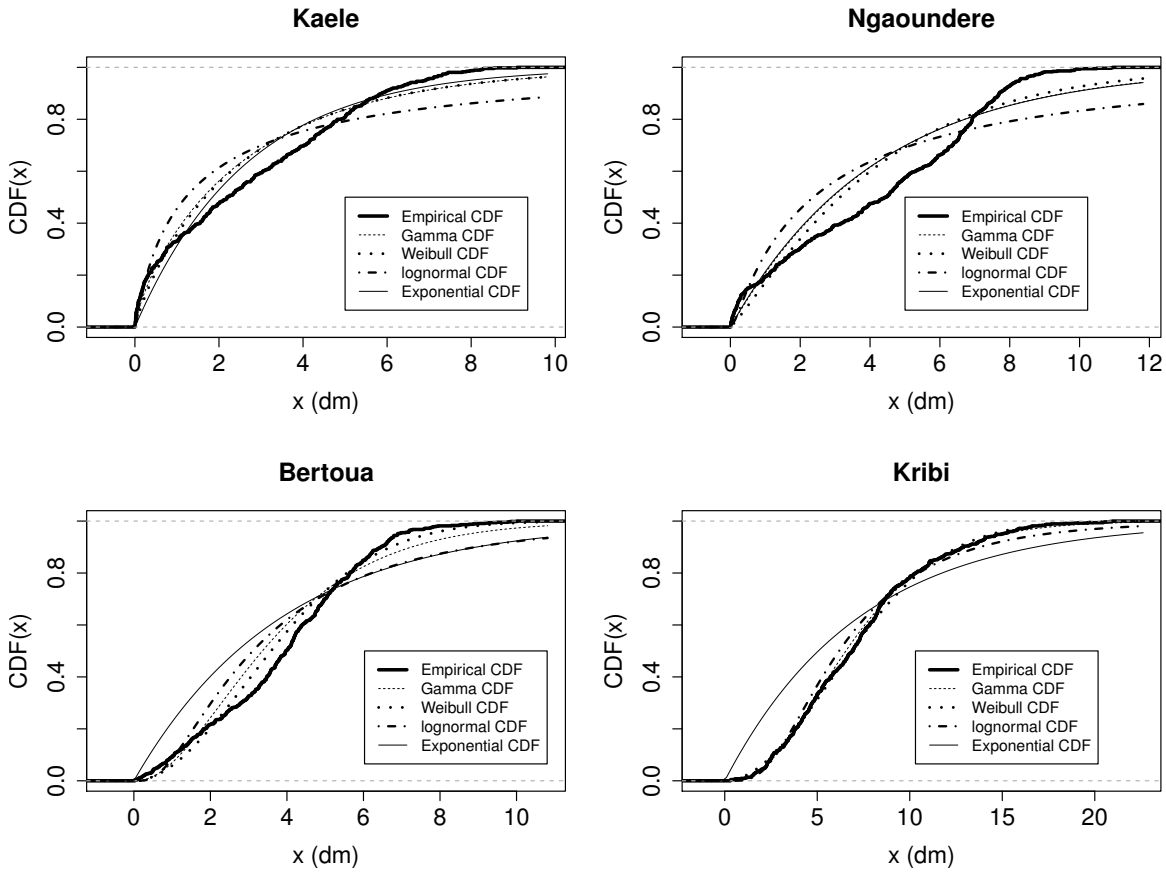

Figure 25: *Cumulative distribution functions for 12-month aggregated precipitation showing the empirical cumulative distribution function (ECDF) and gamma, weibull, lognormal, and exponential distributions fitted to the data. x represents precipitation values.*

The choice of the suitable distribution function describing precipitation data in each case was based on the minimum value of the Anderson-Darling statistic, as illustrated in Table 12 for 1-month and 12-month time scale. The exponential function shows worst results as the number of months in time scale increase.

Table 12: *Anderson-Darling statistic for all stations at 95% confidence level. The letters g, w, e and ln indicate the distribution functions gamma, weibull, exponential and lognormal respectively. Bold characters indicate the smallest values of the statistic and then the the corresponding distribution functions are selected as the best.*

		Distribution function							
		For 3-month time scale				For 12-month time scale			
No	Station	g	w	e	ln	g	w	e	ln
1	Maroua	**8.12**	9.24	11.16	18.72	1.48	9.45	184	**1.13**
2	Kaele	**8.91**	10.20	13.36	21.50	**2.03**	3.84	171	2.22
3	Garoua	13.10	**12.19**	14.08	25.52	1.58	9.31	195.8	**1.04**
4	Poli	18.88	**18.35**	18.58	35.65	**1.08**	3.46	207.7	1.59
5	Ngaoundere	24.21	**23.20**	24.43	41.22	4.84	**1.36**	218	6.76
6	Meiganga	17.36	**16.08**	18.51	34.30	1.03	6.96	223.9	**0.91**
7	Tibati	19.37	**17.15**	21.09	37.43	**0.72**	3.88	199.8	1.24
8	Koundja	16.22	**12.87**	22.70	35.21	**0.90**	4.35	223.8	1.12
9	Yoko	16.40	**13.01**	23.83	30.83	1.08	5.10	167.9	**0.91**
10	Nkongsamba	8.15	**7.099**	14.15	19.84	**1.20**	3.60	229	1.89
11	Bafia	20.55	**13.62**	45.14	36.81	**1.81**	5.99	200	2.24
12	Nanga-eboko	12.36	**6.65**	43.15	26.78	4.97	**0.72**	179	6.91
13	Bertoua	15.19	**7.65**	58.47	30.30	**0.47**	5.41	210.8	0.53
14	Batouri	11.48	**6.02**	49.79	21.08	**1.21**	2.68	165.9	1.57
15	Ngambe	5.50	**4.18**	12.81	14.85	**2.35**	3.09	172	2.59
16	Douala	4.62	**4.32**	14.37	10.63	**3.58**	4.15	213	3.9
17	Abong-mbang	10.99	**5.02**	54.07	22.15	**1.46**	5.78	183	2.03
18	Yaounde	11.41	**5.69**	58.96	22.46	**0.51**	4.24	217.7	0.96
19	Akonolinga	10.98	**5.58**	56.85	21.06	2.30	**1.43**	186	3.12
20	Eseka	11.61	**5.37**	58.21	22.31	0.81	7.75	183.7	**0.48**
21	Yokadouma	11.51	**5.61**	61.34	20.96	**2.50**	5.82	187	3.67
22	Lomie	8.04	**3.12**	58.36	15.48	**1.03**	8.48	161.7	1.05
23	Kribi	**0.70**	0.84	61.56	4.77	**0.94**	4.24	200	1.15
24	Sangmelima	6.25	**1.63**	70.84	13.34	0.86	10.6	184	**0.56**

Table 13 recapitulates the choices extended to all stations and for various time scales.

Table 13: *Suitable distribution functions of station precipitation data for various time scales (g=gamma; w=weibull; e=exponential and ln=logormal). The selected distribution functions are those minimizing the Anderson-Darling statistic.*

		Best distribution for n-month time scale						Number of CRU
No	Station	n=1	n=3	n=6	n=12	n=18	n=24	agreement out of 6
1	Maroua	g	g	g	ln	w	g	3
2	Kaele	g	g	w	g	g	ln	5
3	Garoua	w	w	w	ln	w	g	4
4	Poli	w	w	w	g	g	w	4
5	Ngaoundere	w	w	w	w	g	w	3
6	Meiganga	w	w	w	ln	g	ln	1
7	Tibati	w	w	w	g	g	w	5
8	Koundja	w	w	w	g	g	g	3
9	Yoko	w	w	w	ln	g	ln	3
10	Nkongsamba	w	w	w	g	g	g	4
11	Bafia	w	w	w	g	g	g	5
12	Nanga-eboko	w	w	w	w	w	w	3
13	Bertoua	w	w	w	g	g	w	5
14	Batouri	w	w	w	g	g	ln	6
15	Ngambe	e	w	w	g	g	w	4
16	Douala	w	w	w	g	g	ln	5
17	Abong-mbang	w	w	g	g	g	w	4
18	Yaounde	w	w	g	g	g	g	2
19	Akonolinga	w	w	g	w	g	g	4
20	Eseka	w	w	g	ln	ln	ln	2
21	Yokadouma	w	w	w	g	g	g	6
22	Lomie	w	w	g	g	g	g	5
23	Kribi	w	g	ln	g	ln	ln	3
24	Sangmelima	w	w	g	ln	ln	ln	3

It appears that for time scales equal to 6 months and less, distribution of station precipitation show bias to the weibull function which are suitable for the highest number of station (21 for both 1- and 3-month time scale and 16 for 6-month time scale) out of the 24 studied stations. The gamma function outperforming in very few cases. One exceptional case of exponential and lognormal are observed for 1-month and 6-month time scale respectively. Above 6-month time scale, the number of station precipitation best fitted by the weibull function decreases falling to 3 and 7 in the benefit of the gamma function that is suitable for up to 18 stations at 18-month time scale. The number of station precipitation following the lognormal function also increases with the number of months in time scale, reaching 8 station out of 24.

Figure 26 shows the spatial pattern of the suitable distribution functions over the

domain of study, for 3-month (Figure 26a), 6- and 12-month (Figure 26b) and 18- and 24-month time scales (Figure 26c).

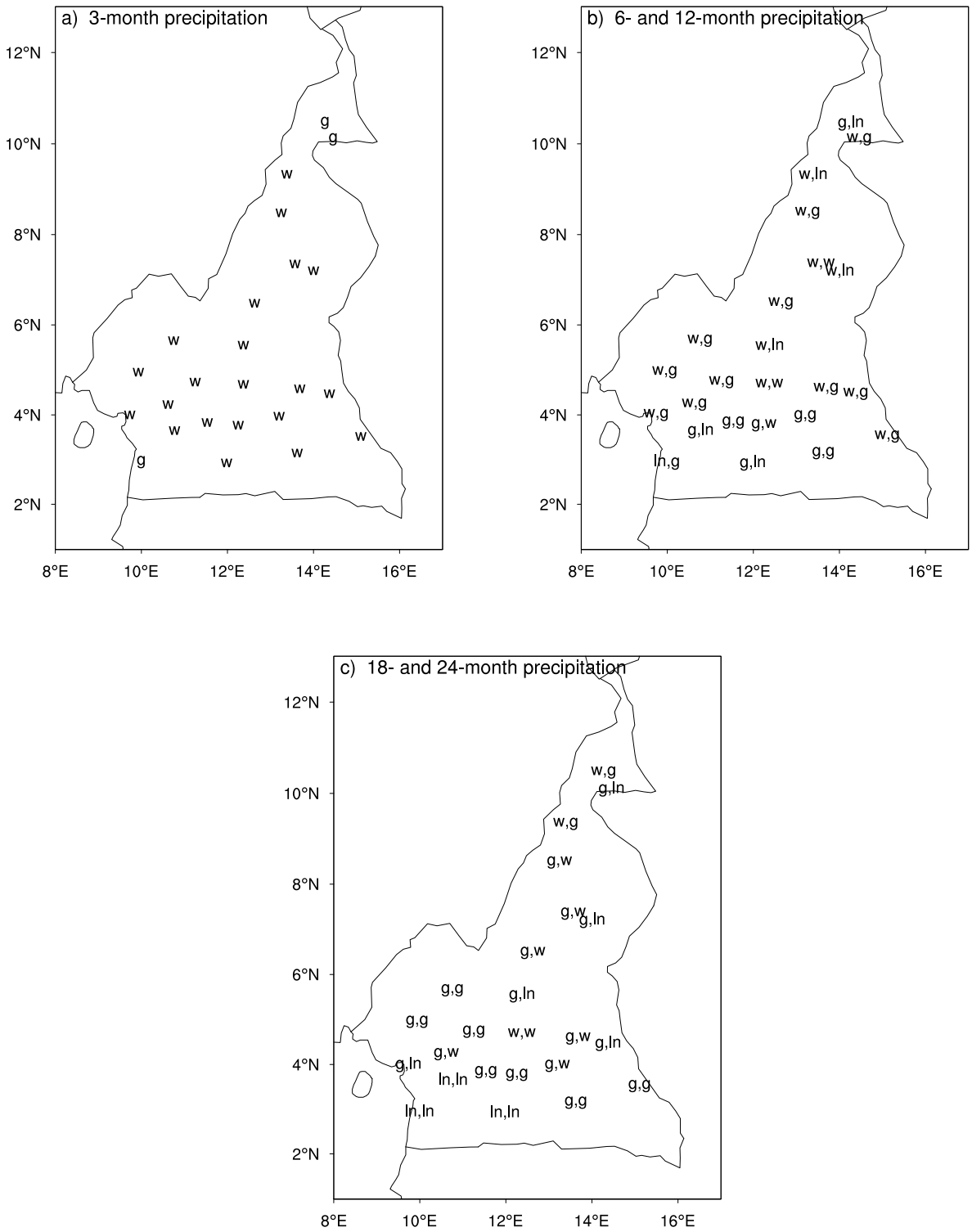

Figure 26: *Appropriate station distribution function for different time scales (g=gamma; w=weibull; e=exponential and ln=logormal). In b) and c), the first letter refers to the first time scales and the second letter to the second time scale.*

For not more than 3-month time scale (illustration for 3-month in Figure 26a)), the gamma distribution function is suitable north of the domain (Sahelian region), particularly above 10°N while below, the weibull function is the best fit, except a single case at the boundary of the Atlantic Ocean, showing bias to gamma. The weibull function remains the most suitable at 6-month time scale between 4 and 10°N which represent the transition zone between the Sahelian and the equatorial forest zone. However, stations of the equatorial forest zone, covering southern plateau (below 4°N) mostly show bias to gamma. At 12-month time scale and more, there is a mixture of gamma, lognormal and weibull distributions in different zones leading to no apparent spatial organized pattern (Figures 26b and 26c). Pattern for 18-month time scale looks more like that of 6-month with gamma in place of weibull function. An almost equal number of gamma (9), lognormal (8) and weibull (7) functions fit the 24-month time scale, with no particular spatial organization. These apparent inconsistencies are due to the fact that in most cases, more than one distribution were adequate and the Anderson-Darling statistics may not have been significantly different. Between 18- and 24-month time scale, the number of station data showing bias to lognormal function increases up to 8 in the South-Western part of the domain (right of the Atlantic Ocean).

Distribution functions for CRU precipitation

Similar study with CRU precipitation data on the same time scale and at the grid points nearest the stations show many cases of similarity. Results are recapitulated in Table 13 in which the last column indicates the number of cases out of the 6 various time scales analyzed, where the same distribution functions fitted station and CRU data. The highest number of agreements (no failure) across time scales between the two datasets is obtained in the South-Eastern part of the domain (Batouri and Yokadouma stations). In 3 instances there was agreement on less than 3 time scales, i.e. Yaounde and Eseka in the South and Ngaoundere on the Adamawa Plateau. Overall, stations and CRU gridded precipitations are mostly fitted by the same functions.

3.3.2 Analysis of the Standardized Precipitation Index (SPI) for different time scales

Operational drought thresholds

The operational drought thresholds as described in section 2.7.2 were calculated for all stations and for the five UDSM categories of Table 3 (column 3 to 5) and for 3- and 12-month time scales. They are useful for defining drought levels for various preventive or corrective actions.

SPI data calculated for all stations were fit using gamma, weibulll, exponential, log-normal and normal distributions (Figure 27 for illustration).

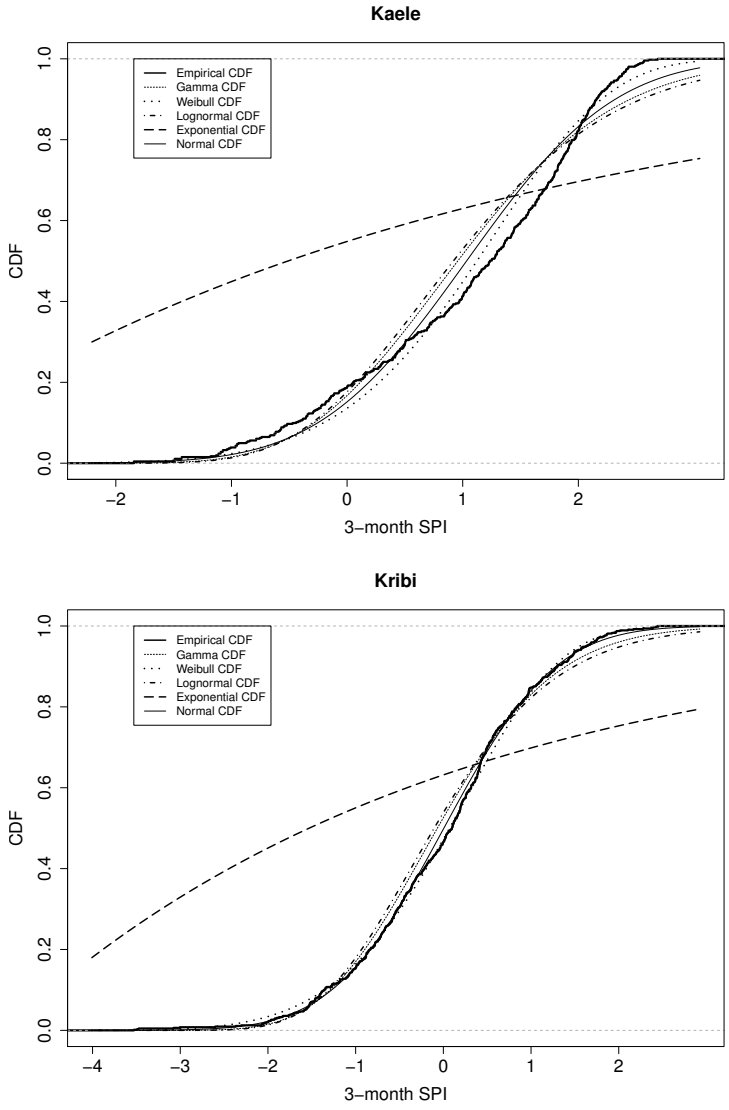

Figure 27: *Cumulative probability distribution for 3-month SPI showing the empirical distribution (EDF) and gamma, weibull, lognormal, exponential and normal distributions that were fit to the data.*

Tables 14 and 15 show results of the KS statistic that was applied to evaluate how well these distributions fit the SPI data.

Table 14: *KS statistic for 3-month SPI after being fit using various PDF (gamma, weibulll, exponential, lognormal and normal). Bold characters indicate the minimum values.*

No	Station name	gamma	weibulll	exponential	lognormal	normal
1	Maroua	0.11	**0.09**	0.43	0.11	0.10
2	Kaele	0.11	**0.08**	0.42	0.12	0.09
3	Garoua	0.14	**0.09**	0.41	0.15	0.11
4	Poli	0.16	**0.12**	0.39	0.17	0.13
5	Ngaoundere	0.16	**0.12**	0.39	0.16	0.14
6	Meiganga	0.13	**0.10**	0.40	0.14	0.11
7	Tibati	0.14	**0.10**	0.40	0.15	0.12
8	Koundja	0.12	**0.08**	0.41	0.14	0.09
9	Yoko	0.16	**0.10**	0.40	0.17	0.13
10	Nkongsamba	0.08	**0.05**	0.43	0.09	0.06
11	Bafia	0.15	**0.09**	0.40	0.17	0.12
12	Nanga-eboko	0.11	**0.06**	0.42	0.13	0.08
13	Bertoua	0.12	**0.06**	0.42	0.14	0.09
14	Batouri	0.11	**0.06**	0.42	0.13	0.09
15	Ngambe	0.09	**0.046**	0.43	0.10	0.054
16	Douala	0.07	**0.05**	0.45	0.08	0.06
17	Abong-mbang	0.10	**0.05**	0.42	0.12	0.08
18	Yaounde	0.11	**0.05**	0.42	0.13	0.08
19	Akonolinga	0.11	**0.06**	0.42	0.12	0.09
20	Eseka	0.11	**0.05**	0.41	0.12	0.08
21	Yokadouma	0.11	**0.06**	0.42	0.13	0.09
22	Lomie	0.10	**0.05**	0.43	0.12	0.08
23	Kribi	0.06	**0.035**	0.45	0.08	0.038
24	Sangmelima	0.09	**0.04**	0.43	0.10	0.06

Table 15: *KS statistic for 12-month SPI after being fit using various PDF (gamma, weibulll, exponential, lognormal and normal). Bold characters indicate the minimum value.*

No	Station name	gamma	weibulll	exponential	lognormal	normal
1	Maroua	0.05	0.06	0.47	0.06	**0.04**
2	Kaele	0.07	0.07	0.48	0.08	**0.06**
3	Garoua	**0.03**	0.08	0.47	0.04	0.05
4	Poli	0.06	0.05	0.47	0.08	**0.04**
5	Ngaoundere	**0.03**	0.06	0.49	0.04	0.04
6	Meiganga	0.05	0.05	0.49	0.06	**0.04**
7	Tibati	0.05	0.039	0.46	0.06	**0.035**
8	Koundja	0.06	**0.038**	0.48	0.07	0.042
9	Yoko	0.04405	0.06	0.48	0.05	**0.04397**
10	Nkongsamba	0.07	**0.03**	0.46	0.08	0.04
11	Bafia	0.07	0.07	**0.46**	0.09	0.05
12	Nanga-eboko	0.05	0.05	0.49	0.06	**0.04**
13	Bertoua	0.04	0.06	0.48	0.05	**0.03**
14	Batouri	0.07	**0.04**	0.48	0.08	0.05
15	Ngambe	0.08	**0.06**	0.47	0.08	0.07
16	Douala	0.09	**0.07**	0.47	0.09	0.08
17	Abong-mbang	0.06	0.07	0.48	0.08	**0.04**
18	Yaounde	0.05	0.034	0.47	0.06	**0.027**
19	Akonolinga	0.0373	0.07	0.50	**0.0372**	0.05
20	Eseka	**0.0254**	0.06	0.48	0.035	0.0317
21	Yokadouma	0.11	0.07	0.50	0.15	**0.06**
22	Lomie	0.05	0.07	0.48	0.06	**0.04**
23	Kribi	0.04	0.04	0.49	0.05	**0.03**
24	Sangmelima	**0.02781**	0.06	0.48	0.04	0.02784

It appears that the weibull distribution fits the 3-month SPI well for all stations while the 12-month SPI is well fitted with the normal distribution in most station and with other distributions in very few cases. These SPI data fitted with The appropriate distribution functions were used to determine the drought thresholds across Cameroon, especially in the stations for which data were available for this study. All the values are shown in Table

16 for 3- and 12-month time scales.

Table 16: *Operational drought thresholds for various time period and for all stations, calculated using 3- and 12-month SPI.*

No	Station name	Drought category for 3-month time scale					Drought category for 12-month time scale				
		D4	D3	D2	D1	D0	D4	D3	D2	D1	D0
1	Maroua	-2.03	-1.74	-1.5	-1.02	-0.59	-1.64	-1.47	-1.32	-0.94	-0.71
2	Kaele	-2.08	-1.86	-1.47	-1.04	-0.62	-1.64	-1.47	-1.32	-0.94	-0.71
3	Garoua	-2.25	-1.92	-1.49	-1.09	-0.51	-2.28	-1.61	-1.19	-0.74	-0.48
4	Poli	-2.49	-2.21	-1.58	-0.91	-0.55	-1.64	-1.47	-1.32	-0.94	-0.71
5	Ngaoundere	-2.55	-2.05	-1.69	-0.93	-0.49	-2.05	-1.63	-1.2	-0.73	-0.47
6	Meiganga	-2.35	-1.9	-1.56	-0.99	-0.54	-1.64	-1.47	-1.32	-0.94	-0.71
7	Tibati	-2.66	-1.99	-1.54	-0.9	-0.47	-1.64	-1.47	-1.32	-0.94	-0.71
8	Koundja	-2.55	-1.83	-1.49	-0.9	-0.45	-1.57	-1.4	-1.24	-0.83	-0.61
9	Yoko	-2.44	-1.91	-1.48	-0.91	-0.45	-1.64	-1.47	-1.32	-0.94	-0.71
10	Nkongsamba	-1.97	-1.64	-1.45	-1.01	-0.55	-1.79	-1.57	-1.17	-0.83	-0.51
11	Bafia	-2.36	-1.94	-1.44	-0.99	-0.32	-1.64	-1.47	-1.32	-0.94	-0.71
12	NangaEboko	-2.27	-1.74	-1.38	-0.9	-0.45	-1.64	-1.47	-1.32	-0.94	-0.71
13	Bertoua	-2.31	-1.77	-1.42	-0.9	-0.41	-1.64	-1.47	-1.32	-0.94	-0.71
14	Batouri	-2.2	-1.74	-1.45	-0.88	-0.5	-1.64	-1.45	-1.28	-0.92	-0.6
15	Ngambe	-1.98	-1.67	-1.37	-1	-0.54	-1.75	-1.61	-1.29	-0.85	-0.59
16	Douala	-1.73	-1.5	-1.31	-0.97	-0.62	-1.76	-1.5	-1.19	-0.9	-0.63
17	AbongMbang	-2.18	-1.71	-1.38	-0.84	-0.48	-1.64	-1.47	-1.32	-0.94	-0.71
18	Yaounde	-2.16	-1.74	-1.45	-0.88	-0.49	-1.64	-1.47	-1.32	-0.94	-0.71
19	Akonolinga	-2.13	-1.7	-1.4	-0.94	-0.47	-1.93	-1.7	-1.44	-0.88	-0.46
20	Eseka	-2.06	-1.78	-1.46	-0.81	-0.46	-2.09	-1.65	-1.32	-0.85	-0.54
21	Yokadouma	-1.97	-1.71	-1.41	-0.91	-0.46	-1.64	-1.47	-1.32	-0.94	-0.71
22	Lomie	-1.94	-1.62	-1.32	-0.9	-0.51	-1.64	-1.47	-1.32	-0.94	-0.71
23	Kribi	-1.82	-1.46	-1.27	-0.83	-0.55	-1.64	-1.47	-1.32	-0.94	-0.71
24	Sangmelima	-1.85	-1.6	-1.24	-0.85	-0.52	-2.05	-1.58	-1.32	-0.85	-0.47

Considering the extreme drought category D4 for 3-month timescale, it is seen that range from a maximum of -1.73 in the coastal city of Douala, to a minimum of -2.66 in Tibati on the Adamawa Plateau. The spatial distribution of D4 thresholds is quite coherent, with values lower than -2.40 on the high grounds of the Adamawa Plateau. Continental stations located between latitudes 2° and 7° north have thresholds between -2.10 and -2.40. In the southern part of the domain and on the coastal area in the south-west, values are higher than -2.0. Values for the three sahelian stations of Kaele, Maroua and Garoua are respectively $-2.08, -2.03$ and -2.25. At this scale, extreme drought category D3 follows the general pattern of D4. For 12-month SPI, most of the stations have D4 threshold of -1.64, with only three stations below -2.0. From the spatial analysis of the drought category D4, there is no strong dependence on topography although most stations have very similar thresholds (-1.64) at 12-month time scale.

Frequency of drought events

Objective drought thresholds were also used to examine frequency in SPI time series. In Figure 28, appropriate D4 category threshold values are represented by dashed horizontal lines and exceedances corresponding to drought occurrences.

For 3-month SPI (left column in Figure 28), each station had at lest one event of value lower than -3. For the first 25 years of the study period, the four stations differ markedly in D4 category drought frequency: 10 in Kaele, 6 in Kribi, only 2 in Ngaoundere and none in Bertoua. Whereas in the second half of the period, these episodes are more frequent, two stations had 13 events each and the two other had 8 events each. For 12-month SPI (Figure 28 right), all categories of drought events are frequent, especially from the mid-sisties. The dramatic drought episodes of the seventies and the eighties are clearly visible, with each station recording at least one D4 event. Table 17 summarizes drought occurrences in all categories, with the number of events and its percentage with respect to the total number of time steps in the data.

Table 17: *Number of drought events from 1951 to 2005 and for the five drought categories (D0, D1, D2, D3 and D4). Results in brackets represent the percentage of realization of the event over the considered time period.*

	Number of events for 3-month time scale				Number of events for 12-month time scale			
	Kaele	Ngaoundere	Bertoua	Kribi	Kaele	Ngaoundere	Bertoua	Kribi
D4	21 (4%)	11 (1%)	14 (2%)	23 (3%)	9 (1%)	2 (0%)	3 (0%)	8 (1%)
D3	26 (5%)	32 (5%)	32 (4%)	36 (5%)	10 (1%)	3 (0%)	2 (0%)	14 (2%)
D2	39 (8%)	53 (9%)	41 (6%)	45 (6%)	13 (2%)	6 (0%)	7 (1%)	20 (3%)
D1	59 (12%)	76 (13%)	53 (8%)	55 (8%)	16 (2%)	21 (3%)	24 (3%)	21 (3%)
D0	81 (17%)	90(15%)	62 (9%)	66 (10%)	21 (3%)	32 (5%)	33 (5%)	27 (4%)

For 3-month time scale, this percentage is 1% to 2% for exceptional droughts, around 5% for extreme droughts. For 12-month scale, the percentage remains low for all categories, ranging from 1% fo D4 to 5% for D0 events.

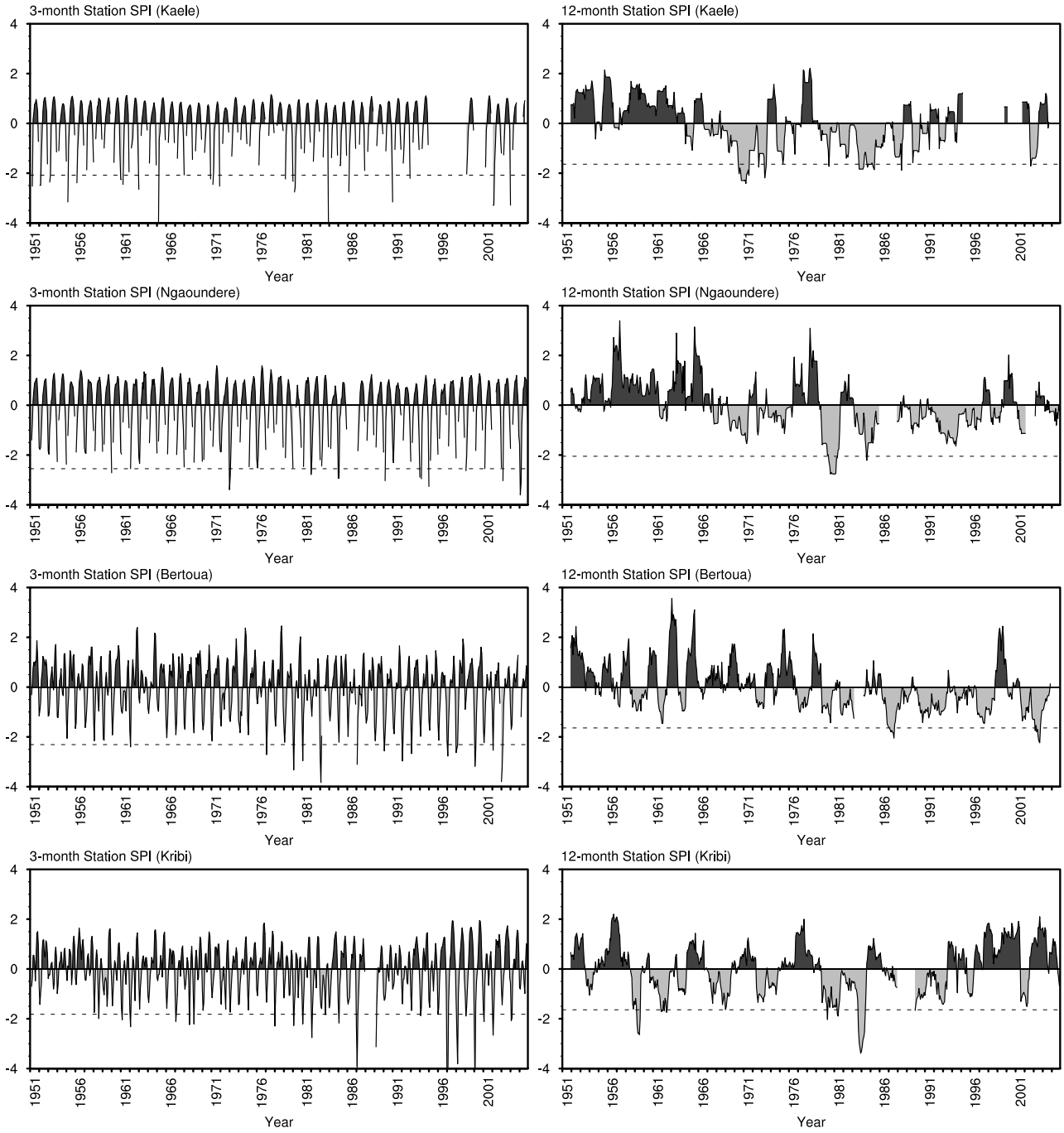

Figure 28: *Station SPI time series for 3- and 12-month time scales. The horizontal dashed lines indicate operational drought thresholds for exceptional drought category (D4).*

Station versus CRU SPI

Figure 29 presents 3- and 12-month scale SPI time series from CRU gridpoint nearest each of the four observations stations of Figure 5. This choice is justified by the fact that the angular distance weighted (ADW) interpolation technique used to construct the CRU set gives more weight to the station nearest the gridpoint, thus making it the best representative of the station. In the present analysis, we compare these time series to those of the stations in Figure 28, in order to access how well the gridded data reproduce drought characteristics obtained from station observations. For 3-month scale SPI, the two time series agree overall, with some discrepancies occurring at dates that differ from station to station: in Kaele in early 1950s, in the 1970s and late 1980s; in Bertoua in late 1990s and in Kribi in late 1990s, except for the drought of 1997. Most strong events present in at least three stations are reproduced in the gridded data, noticeably in 1962, 67, 83, 87, 97 and in 2004. Of more concern are the results of Kaele, where station data show high year to year variability of drought intensities, with 6 events with SPI $<$ -3, when CRU has an excessively large number of events of magnitude -2. At the same station, three strong events of early 1950s are much weaker on the gridded data, whereas weak ones in the 1970s are amplified. In the other stations, CRU tends to show more severe droughts. Thus for events with SPI values less than -3, there are 12 against 5 in Bertoua, 11 against 7 in Ngaoundere but only 3 against 5 in Kribi. This reverse situation in Kribi is due to the underestimation of strong drought events between 1997 and 2000. For 12-month scale SPI, the main wet (1950s and late 1990s) and dry (1970s and 1980s) periods show up in both time series. Most drought events last many years, and CRU indicates more extreme values than do stations. The discrepancies noted at shorter time scales tend to be amplified at this and higher scales. Thus in Kaele gridded data shows wet (against dry) episode the mid-1960s and early 2000s, and the reverse in 1994. This phase opposition between the two data sets is also found in late 1960s in Ngaoundere, early 1970s and 1990s in Bertoua.

Amplification of disagreement between station and CRU data are better seen in Figure 30 (gray color indicates that data are missing at the corresponding area. This is always the case at the beginning of the time series because the first $(n-1)$ months are considered missing, but have been used to calculate the first SPI value given that the precipitation aggregated must be taken on the first n consecutive months) showing multi-time scales SPI (The SPI calculated were submitted to the Kolmogorov-Smirnov test in other to check and define their significant level. Many stations show normally distributed SPIs at 5%

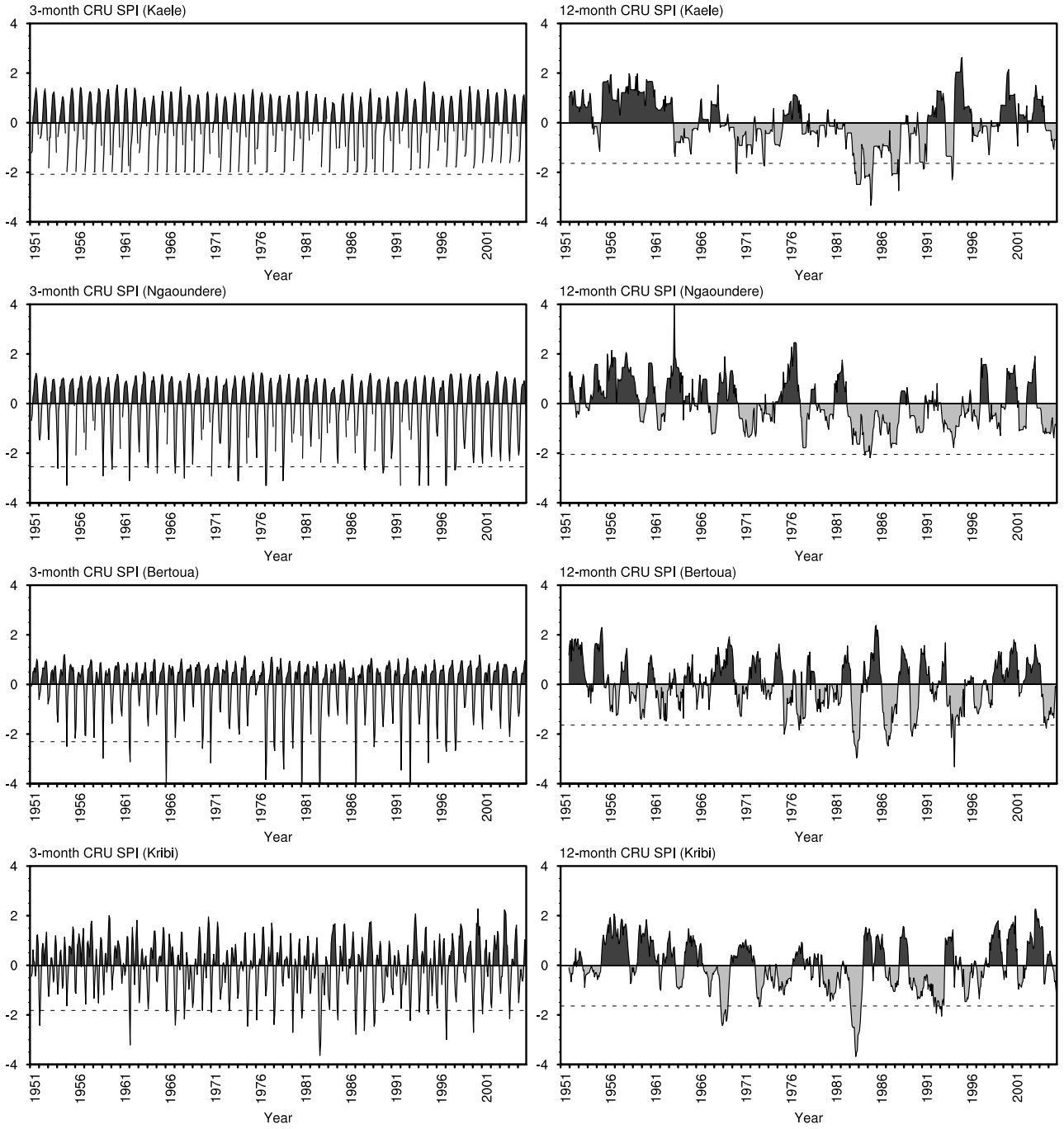

Figure 29: *3- and 12-month scales SPI time series from CRU gridpoint nearest each of the four chosen stations. The horizontal dashed lines indicate operational drought thresholds for exceptional drought category (D4).*

significant level (Annexe C)). A case in point is the 1996 to 2000 period in Kribi. On the 3-month scale (Figure 6), the 4 years of severe droughts indicated by the station are underestimated by CRU. At the 12-month scale, the period is wet for both, and more so for the station. This reversal is due to the strong wet peaks occurring in the same period at the station, but not on the CRU grid, and that contributes to the longer scale SPI. Overall, the CRU gridded data give a fair representation of drought events in the study area, and can be used where no local station observations are available. The absence of missing data points is an additional advantage. It may however be of interest to evaluate the merits of using more than one grid point at a given site.

Figure 30 shows many additional information. For example, from the east (Bertoua station) to the Sahelian zone (Kaele) and to the neighboring Atlantic Ocean (Kribi), drought spells intensities have been increasing, reaching the highest values north of domain while wet spell intensities follow the reverse gradients. In most cases, the results of the SPI lead to divide the chronological time series into two periods. The first one before 1970 and the second one after 1970 characterized by a high frequency of severe/extremely wet spells and severe/extreme dry spells respectively. Stations located inner the country like Ngaoundere and Bertoua have known more intensive wet spells before 1970 and less intensive dry spells after 1970 as compared to the two other stations. Normal climatic conditions (SPI falling between -0.5 and 0.5), wet and dried spells usually alternate. Particular extremely wet spells have been experienced in the neighboring area of the Atlantic Ocean after 1990. This is clearly shown up at Kribi (30), where the SPI diagram reveals that the preceded decades had registered more frequent drought events than at other stations.

For long time scales (greater than 6-month), moderate/severe drought and extremely wet episodes are reproduced with lower frequency (with a periodicity of about ten year) than for short time scales. Extremely wet and extreme drought episodes last less and are observed on decadal scale. Generally, the frequency of wet/drought event decreases when increasing their intensification. Moderate and severe drought began effectively after 1970, excepted at the neighboring station of the Atlantic Ocean (Kribi), where they began earlier (since 1960). Before the beginning of these drought episode, climate was moderately wet, mixed with severe wet conditions. This was observed about twice on a time period long of two decades. These observations lead to deduce that as time is passing, droughts are becoming more frequent and intense showing the effect of climate change that certainly had affected socio-economic sector negatively. Long episodes of severe droughts and short episode of extreme droughts are identified in the decades 1970

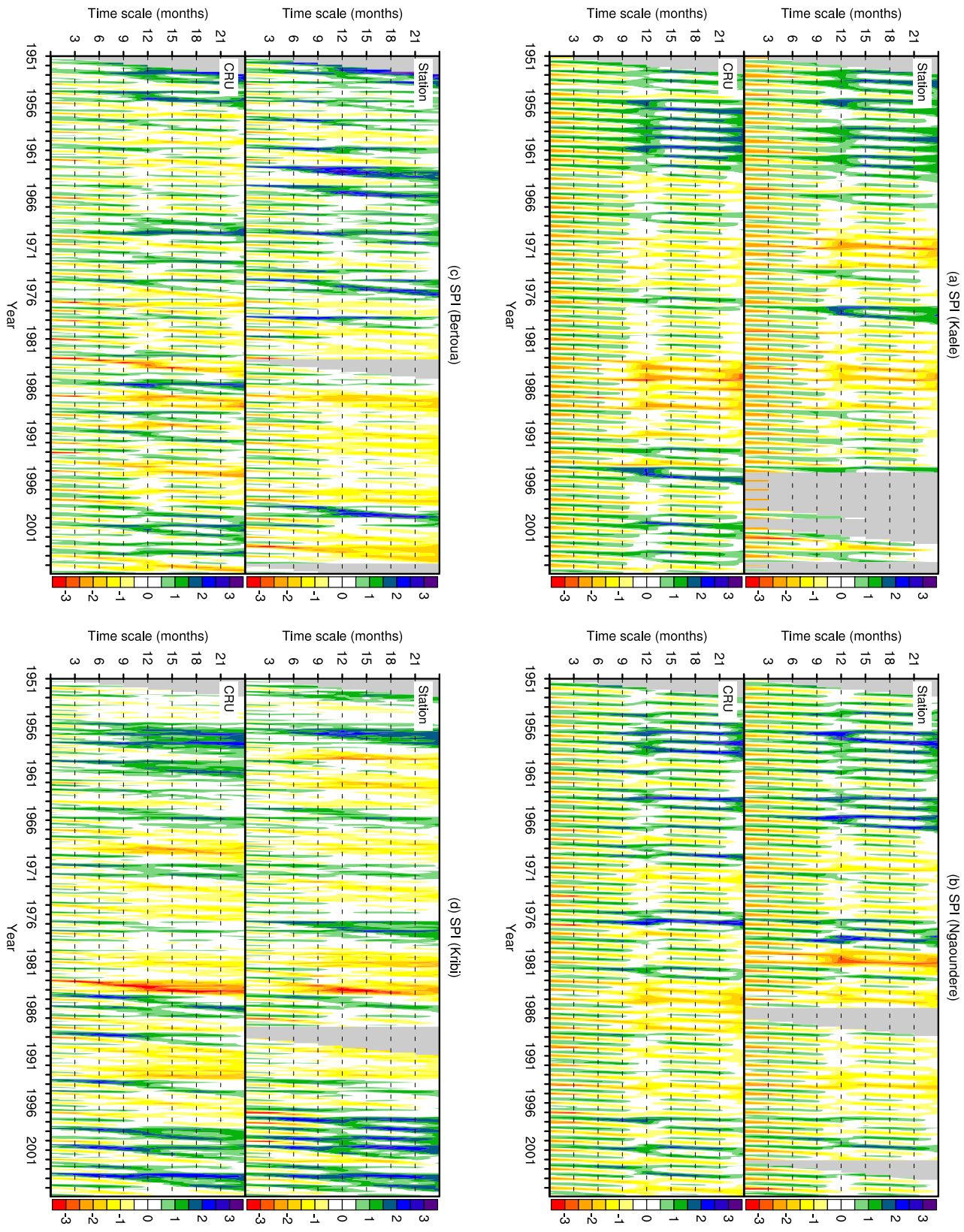

Figure 30: *Station and CRU multiscalar SPI for Kaele, Ngaoundere, Bertoua and Kribi. Horizontal dashed lines show focused time scales.*

and 1980 in all stations. When other stations recorded drought or wet conditions on long time scale, Kribi experienced the opposite climate condition.

For time scales less than 6-month, it was recorded severe drought episode every year alternated with moderately wet and mild climate conditions (mild drought/wet). Therefore, there is a yearly periodicity of the reproductivity of climate events along the chronological precipitation time series. It is noticed that these periodic droughts for short time scales (less than 6-month) are becoming more intense after 1977 while moderate wet predominated before. From this figure, it appears that below the 9-month time scale, drought episodes are mostly intra-annual. They become multi-annual above, lasting up to five years.

Figure 30 also shows that SPI calculated using CRU gridpoint data close to a station properly identify wet and dry sequences over all timescales. The CRU precipitation derived SPI has the added advantage of not having missing points. The similarity between the two datasets were checked by the correlation coefficients shown in Figure 31. The results reveal high correlation between observed and CRU precipitation and calculated SPIs for time scale less than 9-month and between 15- and 21-month. Station of the northern part of the domain (Kaele and Ngaoundere) having highest correlations (greater than 0.8). Correlations on 12- and 24-month time scale are lower falling down to 0.35 at Bertoua observatory.

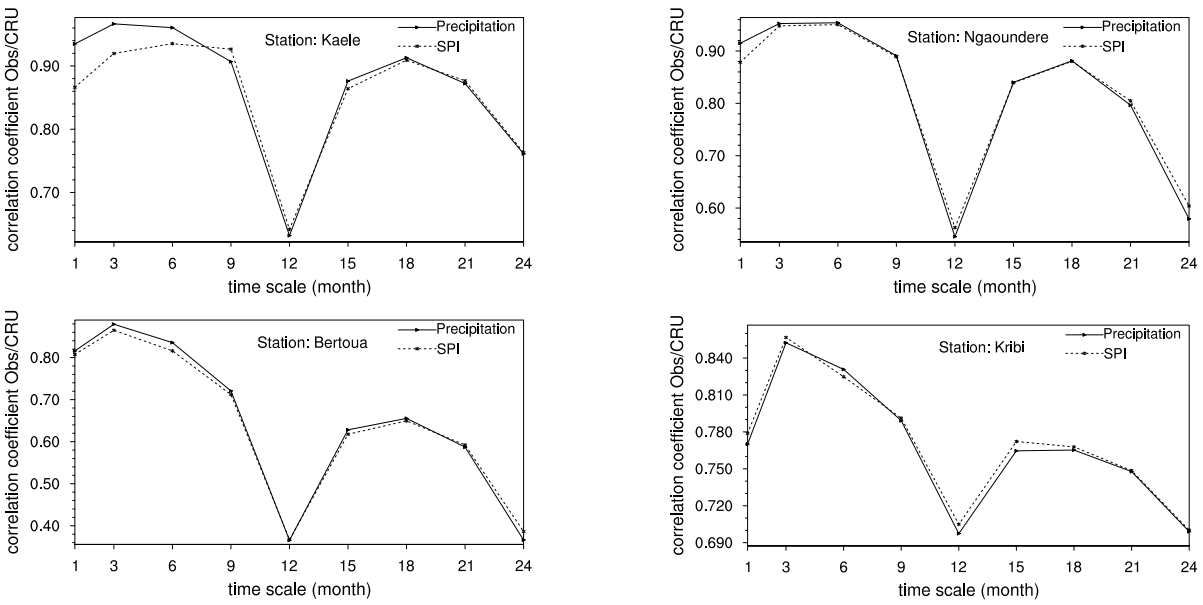

Figure 31: *Correlation coefficients between Stations and CRU for both precipitation and SPI.*

Discussion

It was found that the suitable distribution function fitting the data depends on station location and on the length of the time interval used for aggregation of precipitation. The weibull and gamma are the functions that best fit precipitation in the area. In most studies on SPI, the gamma distribution is chosen without any testing. The need for such an evaluation is even clearer for longer time scales where weibull, gamma and lognormel distributions are found, with no discernable pattern. We also found that objective drought thresholds are station specific for subannual scales, but the spatial distributions are quite coherent. Thus, regional values can be defined. For longer scales (above 12-month), most stations in the domain have the same threshold values. In most stations, drought magnitude and duration increased with time for both short and long time scales. This can be the consequences of a reduction in precipitation due to climate change as suggested by Sergio et al. (2009). Such an increase in dryness probably affected crop development and river runoff negatively. The SPI based only on precipitation can not explain the influence of temperature change in drought condition. Thus, Sergio et al. (2009) suggested the calculation of a new index, the Standardized Precipitation Evapotranspiration Index (SPEI) suited to detecting, monitoring, and exploring the consequences of global warming on drought conditions. Further studies taking into account this approach are necessary in other to better understand drought climatology. With the increase of global warming, an increase in drought magnitude, duration and frequency is to be feared and studies including climate models intended to guide adaptive measure also need to be done. CRU precipitation distribution functions and derived SPI corroborate the results of many stations. Therefore it may be recommended for further investigations to use CRU data on areas where observations are not possible or where they have high proportions of missing data.

Summary of the chapter

The principal results of our investigation were presented and discussed in this chapter. We found that precipitation indices change with space and time and can be well simulated by many climate models. For the future climate, it is projected a slight modification in many indices due to the greenhouse gas effect.

General Conclusion

The complex interactions and feedbacks that occur within Earth's climate system make it difficult to establish how large the human-induced effects will be or how soon we may be able to detect the climate change. However, the increase of our understanding of the natural variability of the climate system can help to built better climate models that more explicitly and more accurately represent weather phenomena, and to reduce uncertainties in predictions and adaptability. The present work contributes to this challenge. Using daily precipitation data from 24 stations in Cameroon and from four general circulation models (MPI-echam5, CSIRO-mk3.5, BCCR-bcm2.0 and MRI-cgcm2.3.2a), we analyzed some rainfall statistical parameters, onset, retreat and length of the rainy season under current and perturbed climates. The standardized precipitation index was also analyzed using monthly precipitation from stations and CRU grids.

For the study of onset, retreat and length of the rainy season, climatic zones were first defined, each of them characterized by stations with close onset and retreat dates of the rainy season. Next, onset and retreat dates and lengths of the rainy season for the current climate (1962-1993) calculated from both observations and IPCC model outputs were studied and compared. Projections of impacts of climate change on onset and retreat dates and length of the rainy season were assessed with these same models under the SRES A2 greenhouse gas emission scenario over the period 2082-2098. Results show that rainy season begins earliest and ends latest south of the domain while earliest retreat dates are registered north of the domain. Thus, the length of the rainy season increases southwards. Amplitudes of fluctuations are stronger for onset date than for retreat. Model results for current climate are close to observations when they are considered with their corresponding standard deviations. The climate models CSIRO-mk3.5 and MPI-echam5, perhaps because of their higher spatial resolution, show the best performances and are then more appropriate than the two other models for determining onset, retreat and length of the rainy season over Cameroon and neighboring areas. The low spatial resolution of BCCR-bcm2.0 and MRI-cgcm2.3.2a may have contributed to their poor results in most

cases. For future climate (2082-2098) and according to three of the four climate models results, onset and retreat dates are expected in most cases to be later by about 1 pentad (5 days) than in the present climate and for the duration of the rainy season, an increase of approximately 1 pentad (5 days) is expected in the northern part of the domain and a decrease of the same range elsewhere.

As for annual total amounts, MPI-echam5 and CSIRO-mk3.5 well reproduce observed pattern and trends, but precipitation intensities are slightly underestimated in the southern part by MPI-echam5 and overestimated in the northern part by CSIRO-mk3.5. But combining the two model outputs, simulation of the mean annual total amount is improved. MRI-cgcm2.3.2a and BCCR-bcm2.0 are successful only in some parts of the domain. MPI-echam5 shows best results during the seasons MAM and JJA while CSIRO-mk3.5 and MRI-cgcm2.3.2a give good spatial representation during MAM and SON. All models well simulate dry periods and overestimate the number of rainy days. The study of the maximum length of dry spells shows that extreme southern area is the least dry while the Sudano Sahelian area is the driest and the four models well represent spatial pattern of this parameter. Only CSIRO-mk3.5 and MPI-echam5 succeed in representing intensities over the entire domain while other models do well only below 8°N and overestimate above. All models tend to underestimate extreme events. As concerned interannual trends, most rainfall statistical parameters reflect a passage from the dry 1980 years to a wetter period. Orography and geographical position are some of the factors causing inhomogeneity of spatial trends. The student's t-statistic and the Mann-Kendall statistic were used to test trends at 0.05 significant level. Studies reveal that the models BCCR-bcm2.0 and CSIRO-mk3.5 show best results of signs of trends for the fraction of annual precipitations contributed by daily events above the 90^{th} percentile of daily values and only BCCR-bcm2.0 succeed for annual number of rain days in the three zones. It is noticed that models with high resolution (CSIRO-mk3.5 and MPI-echam5) show best results of the mean current climate. Trend magnitude for mean annual total amounts is best simulated by BCCR-bcm2.0 and the fraction of annual precipitation contributed by daily events above the 90^{th} percentile of daily values is best simulated by both BCCR-bcm2.0 and CSIRO-mk3.5 at the order of 10^{-3}. For the future climate in the late of 21^{st} century (2082-2098), no changes in rainfall statistical parameters are expected around Adamawa Plateau and East of the domain. The results of this part reveal that high spatial resolutions seem to positively impact simulations of general circulation models. This points to the need in future investigations to assess the performances of regional climate model. Being able to predict onset and retreat dates within days would be of more benefit

to local farmers. Also, recasting results in terms of probabilities is necessary to evaluate risks of false starts of rain which are problematic for the sowing season (Hess et al. 1995).

We also used four statistical distribution functions to fit precipitation data recorded in 24 observation stations in Cameroon. The Anderson-Darling statistic was used to choose the best distribution function describing each station precipitation that was then used for the calculation of the standardized precipitation index (SPI). It was found that the best distribution changes with location and time scale. In most cases, the weibull and the gamma distributions better fit empirical precipitation. For short time scale (equal to 6 months or less), stations above 10°N have the gamma distribution function as the best fit while below this belt, stations show bias to the weibull distribution except for very few cases. Above 6-month time scale, there is a lot of spatial inconsistencies of fitted distributions. The results of the SPI show that droughts are generally rarer than wetness. Long episodes of severe droughts and short episodes of extreme droughts are identified in the decades 1970 and 1980 in many stations. Drought episodes are mostly intra-annual for short time scale (9 months or less). They become multi-annual above, lasting up to five years. CRU grid precipitation show good results of the SPI with the best performances on short time scales. The necessity to objectively define the operational drought thresholds in order to expect the triggering of true drought responses was shown.

The results of the current work, the observation of the climate and consensus of the results produced by many models in many areas in the world show the evidence that climate is changing and give an increased confidence in the credibility of the models. Some forms of air pollution (e.g. emissions of CO_2 and other greenhouse gases) resulting from human activities significantly alter the climate, in the sense of global warming. The risk of destabilizing the Earth's climate system is growing every day with the increase of the emissions of global warming gases as the world burns ever more coal, oil and gas for energy. It is reported that for many areas on Earth, climate change causes significant damage: sea level rise (Vellinga et van Verseveld 2000), accentuation of extreme weather events (droughts, floods, hurricanes, ...), destabilization of forests, threats to freshwater resources, agricultural problems, desertification, reduction of biodiversity, expansion of tropical diseases, ecosystems, etc. (Vellinga et van Verseveld 2000). Improved forecasts of regional climate change, aimed to better understand the responses of trees and characterize the adaptive capacities of forestry sector, will provide new information on the likely impacts of climate change on forests. This new information should be gradually used by development policies in order to improve resilience of forests to future climates. It is therefore important to disseminate knowledge on appropriate adaptation measures

to all policymakers. Society should develop appropriate responses to help manage and reduce vulnerability to extreme meteorological events. It is likely that increasing frequency and/or intensity of severe weather as a result of climate change will put more lives and property at risk, particularly in coastal and inland areas close to coastlines. Around the world, these areas have already become very vulnerable over the past several decades as human populations and development have grown dramatically in coastal and near-coastal regions (Kevin et al. 2000).

bibliography

Abramowitz, M., and A.e. Stegun, 1965: Handbook of Mathematical Formulas, Graphs, and Mathematical Tables. *Dover Publications, Inc.: New York.*

Adejuwon, J.O., 2006: Variability and the Severity of the Little Dry Season in Southwestern Nigeria. *Journal of Climate*, **19**, 483–493.

Adejuwon, J.O., E.E. Balogun, and S.A. Adejuwon, 1990: On the annual and seasonal patterns of rainfall fluctuations in Sub-Saharan West-Africa. *Int. J. Climatol*, **10**, 839–848.

Ahmad, S., and A.B. Bilal, 2010: Posterior estimates of two parameter exponential distribution using S-PLUS software. *Journal of Reliability and Statistical Studies*, **Vol. 3**, 27–34.

Alan, D.Z., and S. Justin, 2003: Detection of intensification in Global and Continentale Scale Hydrological Cycle: Temporal Scale of Evaluation. *American Meteorological Society.*, **16**, 535–547.

Anderson, T., and D. Darling, 1952: Asymptotic theory of certain goodness-of-fit criteria based on stochastic processes. *Ann. Math. Stat.*, **23**, 193–212.

Anderson, T., and D. Darling, 1954: A test of goodness-of-fit. *J. Amer. Statist. Assoc.*, **49**, 765–769.

Angell, J., 1994: Global, hemispheric and zonal temperature anomalies derived from radiosonde records. , 636–672 In "Trends '93: A compendium of data on global change" (Eds. T. A. Boden et al.), ORNL/CDIAC–65, Oak Ridge, TN.

Ati, O.F., C.J. Stigter, and E.O. Oladipo, 2002: A comparison of methods to determine the onset of the growing season in Northern Nigeria. *Int. J. Climatol*, **22**, 731–742.

Ayoade, J.O., 1974: A statistical analysis of rainfall over Nigeria. *J. Trop. Geogr.*, **39**, 11–23.

Bartošová, J., 2006: Logarithmic-Normal Model of Income Distribution in the Czech Republic. *Austrian Journal of Statistics*, **vol. 35, no. 23**, pp. 215–222.

Benoit, P., 1977: The start of the growing season in Northern Nigeria. *Agric. Met.*, **18**, 91–99.

Bretscher, O., 1995: Linear Algebra With Applications. *Upper Saddle River NJ: Prentice Hall.*, **3rd ed.**

Brunetti, M., M. Colacino, M. Maugeri, and T. Narni, 2001: Trends in the daily intensity of precipitation in Italy from 1951 to 1996. *Int. J. Climatol*, **21**, 299–316.

Burgueño, A., C. Serra, and X. Lana, 2004: Montly and annual statistical distributions of daily rainfall at the Fabra observatory (Barcelona, NE Spain) for the years 1917-1999. *Theor. Appl. Climatol*, **77**, 57–75.

Bussay, A., C. Szinell, M. Hayes, and S. M., 1998: Monitoring drought in Hungary using the standardized precipitation index. *Annales Geophysicae, Supplement 11 to Vol 16, the Abstract Book of 23rd EGS General Assembly, C450. April 1998, Nice; France.*

Cook, K., and E. Vizy, 2006: Coupled Model Simulations of the West African Monsoon System: Twentieth- and Twenty-First-Century Simulations. *J. Climate.*, **19**, 3681–3703.

Daniel, S.W., 2006: Statistical Methods in the Atmospheric Sciences. Second Edition. *International Geophysics Series*, **91**.

Diana, B., 2012: Lognormal distribution and using L-moment method for estimating its parameters. *International Journal of Mathematical Models and Methods in Applied Sciences*, **6**, pp. 30–44.

Douville, H., and J.F. Royer, 1996: Sensitivity of the Asian summer monsoon to an anomalous Eurasian snow cover within the M6t6o-France GCM. *Climate Dynamics.*, **12**, 449–466.

Edwards, D.C., and T. McKee, 1997: Characteristics of 20th Century Drought in the United States at Multiple Time Scales. *Fort Collins, Colorado, Department of Atmospheric Science, Colorado State University.*

Emori, S., A. Hasegawa, T. Suzuki, and K. Dairaku, 2005: Validation, parameterization dependance, and future projection of daily precipitation

simulated with high-resolution atmospheric GCM. *Geophys. Res.*, **32**, L06708, doi:10.1029/2004GL022306, 2005.

Errasti, I., A. Ezcurra, J. Sáenz, and G. Ibarra-Berastegi, 2011: Validation of IPCC AR4 models over the Iberian Peninsula. *Theor Appl Climatol*, **103**, 61–79.

Fowler, A., and J. Hennessy, 1995: Potential impacts of globale warming on the frequency and magnitude of heavy precipitation. *Natural Hazards*, **11**, 282–303.

Frei, C., D. Lüthi, and H. Davies, 1998: Heavy precipitation processes in a warmer climate. *Geophysical Research Letters*, **25**, 1431–1434.

Furevik, T., M. Bentsen, H. Drange, N. Kvamsto, and A. Sorteberg, 2003: Description and evaluation of the Bergen climate model: ARPEGE coupled with MICOM. *Climate Dyn.*, **21**, 27–51.

Gerald, A.M., Z. Francis, E. Jenni, K. Thomas, M. Linda, and P. Whetton, 2000: Trends in Extreme Weather and Climate Events: Issues Related to Modeling Extremes in Projections of Future Climate Change. *Bulletin of the American Meteorological Society*, **81**, 427–436.

Goodman, S.N., 1999: Toward Evidence-Based Medical Statistics. 1: The P Value Fallacy. *Annals of Internal Medicine.*, **130**, 995–1004.

Goodrich, G.B., and A.W. Ellis, 2006: Climtological drought in Arizona: An analysis of indicators for guiding the Governor's Drought Task Force. *Prof. Geogr.*, **58**, 460–469.

Goosse, H., P. Barriat, W. Lefebvre, M. Loutre, and Z. V., 2010: Introduction to climate dynamics and climate modeling. *Online textbook available at http://www.climate.be/textbook.*

Gordon, H., P. Whetton, A. Pittock, A. Fowler, and M. Haylock, 1992: Simulated changes in daily rainfall intensity due to the enhanced greenhouse effet: Implication for extreme rainfall events. *Climate Dynamics*, **8**, 33–102.

Gordon, H.B., L.D. Rotstayn, J.L. McGregor, M.R. Dix, E.A. Kowalczyk, S.P. O'Farrell, L.J. Waterman, A.C. Hirst, S.G. Wilson, M.A. Collier, I.G. Watterson, and T.I. Elliott, 2002: The CSIRO Mk3 Climate System Model [Electronic publication]. *Aspendale: CSIRO Atmospheric Research.*, **(CSIRO Atmospheric Research technical paper; no. 60)**, 130 pp.

Gregory, J., and J. Mitchell, 1995: Simulation of daily variability of surface temperature and precipitation in the current and $2xCO_2$ climate of the UKMO climate model. *Quarterly Journal of the Royal Meteorological Society*, **121**, 1452–1476.

Guenang, G.M., and K.F. Mkankam, 2012: Onset, retreat and length of the rainy season over Cameroon. *Atmospheric Science Letters*, **13**, 120–127.

Guttman, N.B., 1998: Comparing the Palmer Drought Index and the Standardized Precipitation Index. *Journal of the American Water Resources Association*, **34 No. 1**, 113–121.

Guttman, N.B., 1999: Accepting the Standandardized Precipitation Index: a calculation algorithm. *J. Amer. Water Resour. Assoc.*, **35(2)**, 311–322.

Haniyeh, P., and A. Saeid, 2011: Estimation of the Weibull Distribution Based on Type-II Censored Samples. *Applied Mathematical Sciences*, **5(52)**, 2549–2558.

Hansen, J., R. Ruedy, M. Sato, and K. Lo, 2010: Global Surface Temperature Change. *Reviews of Geophysics.*, **48, RG4004**, 1–29.

Helsel, D.R., and R.M. Hirsch, 2002: Statistical Methods in Water Resources. *Science for a Changing World*, 213–216.

Hennessy, K.J., J.M. Gregory, and M.J.F. B., 1997: Changes in daily precipitation under enhanced greenhouse conditions. *Climate Dyn.*, **13**, 667–680.

Hess, T.M., W. Stephens, and U.M. Maryah, 1995: Rainfall trends in the north east arid zone of Nigeria 1961-1990. *Agricultural and Forest Meteorology*, **74**, 87–97.

Houghton, J.T., L.G. Meira Filho, B.A. Callandar, N. Harris, A. Kattenberg, K. Maskell, and Eds, 1995: Climate Change. *The Science of Climate Change. Cambridge University Press*, 572 pp.

Ilesanmi, O.O., 1972a: An ampirical formulation of the onset, advance and retreat of rainfall in Nigeria. *J. Trop. Geogr.*, **34**, 17–24.

Ilesanmi, O.O., 1972b: Aspect of the precipitation climatology of the July-August rainfall minimum of southern Nigeria. *J. Trop. Geogr.*, **35**, 51–59.

Indrani, P., and A.T. Abir, 2011: Assessing seasonal precipitation trends in India using parametric and non-parametric statistical techniques. *Theor Appl Climatol*, **103**, 1–11.

IPCC, 1992: Climate change 1992: The Supplementary Report to the IPCC Scientific Assessment. Eds. Houghton, J.T., Callander, B.A., Varney, S.K. *Cambridge*

University Press, Cambridge, Cambridge. 200pp.

IPCC, 1995: Climate change 1995: the science of climate change. *Cambridge University Press, Cambridge.*

IPCC, 2001a: The Scientific Basis.Contribution of Working Group I to the Third Assessment Report of the Intergovernmental Panel on Climate Change. In: Houghton JT, Ding Y, Griggs DJ, Noguer M, VanderLinden PJ, Dai X, Maskell K, Jhonson CA (eds). *Cambridge University Press, Cambridge. U.K.,p.881.*

IPCC, 2001b: The Scientific Basis.Contribution of Working Group I to the Third Assessment Report of the Intergovernmental Panel on Climate Change. In: Houghton JT, Ding Y, Griggs DJ, Noguer M, VanderLinden PJ, Dai X, Maskell K, Jhonson CA (eds). *Cambridge University Press, Cambridge. U.K.,p.881.*

IPCC, 2001c: The Scientific Basis.Contribution of Working Group II to the Third Assessment Report of the Intergovernmental Panel on Climate Change. In: McCarthy, J. J.; Canziani, O. F.; Leary, N. A.; Dokken, D. J.; and White, K. S., ed. *Cambridge University Press, ISBN 0-521-80768-9 (pb: 0-521-01500-6).*

IPCC, 2007a: Synthesis Report, Contribution of Working Groups I, II and III to the Fourth Assessment Report of the Intergovernmental Panel on Climate Change. Core Writing Team; Pachauri, R.K; and Reisinger, A., ed. *Geneva, Switzerland: IPCC, ISBN 92-9169-122-4.*

IPCC, 2007b: The Physical Science Basis, Contribution of Working Group I to the Fourth Assessment Report of the Intergovernmental Panel on Climate Change. In: Solomon, S.; Qin, D.; Manning, M.; Chen, Z.; Marquis, M.; Averyt, K.B.; Tignor, M.; and Miller, H.L., ed. *Cambridge University Press, ISBN 978-0-521-88009-1 (pb: 978-0-521-70596-7).*

IPCC, Climate Change, 2007a: Contribution of Working Group I to the Fourth Assessment Report of the Intergovernmental Panel on Climate Change, 2007. In: Solomon S, Qin D, Manning M, Chen Z, Marquis M, Averyt KB, Tignor M, Miller HL (eds). *Cambridge University Press*, **Cambridge**, p. 996.

IPCC, Climate Change, 2007b: The Physical Sciences Basis. IPCC retrieved 2007-04-30. .

IPCC, Climate Change, 2007c: Working group II contribution to the Intergovernmental Panel on Climate Change Fourth Assessment Report Climate 2007: Climate Change Impacts, Adaptation and Vulnerability. .

Jolliffe, I., and P. Hope, 1996: Representative of daily rainfall distributions using normalised rainfall curves. *Int. J. Climatol*, **16**, 1157–1163.

Jones, R., J. Murphy, M. Noguer, and A. Keen, 1997: Simulation of climate change over europe using a nested regional-climate model. II: Comparison of driving and regional model responses to a doubling of carbon dioxide. *Quarterly Journal of the Royal Meteorological society*, **122**, 265–292.

Karen, C., R. Imtiaz, and L. Jeff, 2011: The drought monitor. *Feature Article From Intermountain West Climate Summary, July 2011 Intermountain West Climate Summary*, **7 (5)**, 1–7.

Karl, T.R., and R.W. Knight, 1998: Secular trends of precipitation amount, frequency, and intensity in the United States. *Bull. Amer. Meteor. Soc.*, **79**, 231–241.

Kevin, E.T., M. Kathleen, M. Linda, and R. Steven, 2000: Effects of changing climate on weather and human activities. *University science books. Sausalito, California.*

Kothavala, Z., 1997: Extreme precipitation events and the applicability of global climate models to study floods and droughts. *Math. Comput. Simul.*, **43**, 261–268.

Lehmann, E., and J.P. Romano, 2005: Testing Statistical Hypotheses (3E ed.). *New York: Springer.*, **New York: Springer. ISBN 0-387-98864-5.**

Leonard, M.D., 2010: Review Studies of 21st-century precipitation trends over West Africa. *Int. J. Climatol.*, **10**, DOI: 10.1002/joc.2180.

Lloyd-Hughes, B., and M.A. Saunders, 2002: A Drought Climatology For Europe. *International Journal of Climatology*, **22**, 1571–1592.

Mann, H.B., 1945: Non parametric tests against trend. *Econometrica*, **13**, 245–259.

McKee, T., N.J. Doesken, and J. Kliest, 1993: The relationship of drought frequency and duration to time scales. In Proceedings of the 8th Conference of Applied Climatology, 17-22 January, Anaheim, CA. *American Meterological Society, Boston, Massachusetts*, pp. 179–184.

Meehl, G.A., C. Covey, T. Delworth, M. Latif, B. McAvaney, J.F.B. Mitchell, R.J. Stouffer, and K.E. Taylor, 2007: The WCRP CMIP3 multimodel dataset: A new era in climate change research. *Bulletin of the American Meteorological Society.*, **88**, 1383–1394.

Mkankam, K.F., 2000: Validation of general circulation climate models and projections of temperature and rainfall changes in Cameroon and some of its neighboring areas. *Theoretical and Applied Climatology*, **67**, 97–107.

Mugalavai, E.M., E.C. Kipkorir, D. Raes, and M.S. Rao, 2008: Analysis of rainfall onset, cessation and length of growing season for western Kenya. *Agricultural and Forest Meteorology*, **148**, 1123–1135.

Murphy, A., and R. Winkler, 1987: A general framework for forecast verification. *Monthly Weather Review*, **115**, 1330–1338.

Ndomba, P.M., 2010: Development of Rainfall Curves for Crops Planting Dates: A Case Study of Pangani River Basin in Tanzania. *Nile Basin Water Science and Engineering Journal*, **3**, 13–27.

Nityanand, S., and A.R. Ashwini, 2009: Climatic and Hydroclimatic Features of Wet and Dry Spells and their Extremes across India. *Indian Institute of Tropical Meteorology.*

Odekunle, T.O., 2004: Rainfall and the length of the growing season in Nigeria. *Int. J. Climatol.*, **24**, 467–479.

Odekunle, T.O., 2006: Determining rainy season onset and retreat over Nigeria from precipitation amount and number of rainy days. *Theor. Appl. Climatol.*, **83**, 193–201.

Odekunle, T.O., E.E. Balogun, and O.O. Ogunkoya, 2005: On the prediction of rainfall onset and retreat dates in Nigeria. *Theor. Appl. Climatol.*, **81**, 101–112.

Olaniran, O.J., 1983a: The 0nset of the rains and the start of the growing season in Nigeria. *Nigerian Geographical Journal*, **26(1 and 2)**, 81–88.

Olaniran, O.J., 1983b: The monsoon factor and the seasonality of rainfall distribution in Nigeria. *Malaysian J. Trop. Geogr.*, **7**, 38–45.

Olaniran, O.J., 1989: A study of climatic variability in Nigeria based on the onset, retreat, and length of the rainy season. *Int. J. Climatol*, **9**, 253–269.

Omotosho, J.B., 1990a: Onset of thunderstorms and precipitation over Northern Nigeria. *Int. J. Climatol*, **10**, 849–860.

Omotosho, J.B., 1990b: Synoptic meteorology: pathway to seasonal rainfall prediction for sustainable agriculture and effective water resource management in West

Africa but Nigeria in particular. *Journal of the Nigerian Meteorological Society (NMS)*, **3(2)**, 81–86.

Omotosho, J.B., 2002: Synoptic meteorology: pathway to seasonal rainfall prediction for sustainable agriculture and effective water resources management in West Africa but Nigeria in particular. *Journal of the Nigerian Meteorological Society*, **3**, 81–89.

Osborn, TJ.and Hulme, M., P. Jones, and B. TA., 2000: Observed trends in the daily intensity of United Kingdom precipitation. *Int. J. Climatol*, **20**, 347–364.

Parker, D.J., R.R. Burton, A. Diongue-Niang, R.J. Ellis, M. Felton, C.M. Taylor, C.D. Thorncroft, P. Bessemoulin, and A.M. Tompkins, 2005: The diurnal cycle of the West African monsoon circulation. *Royal Meteorological Society*, **131**, 2839–2860.

Penlap, K.E., C. Matulla, H.V. Storch, and F. Mkankam Nkamga, 2004: Downscaling of GCM scenarios to assess precipitation changes in the little rainy season (March-June) in Cameroon. *Climate Research*, **26**, 85–96.

Quiring, S.M., 2009: Developing Objective Operational Definitions for Monitoring Drought. *Journal Of Applied Meteorology And Climatology.*, **48**, 1217–1229.

Ratan, R., and V. Venugopal, 2013: Wet and dry spell characteristics of global tropical rainfall. *Water resources research.*, **49 (6)**, 3830–3841.

Roeckner, E., K. Arpe, L. Bengtsson, M. Christoph, M. Claussen, L. Dumenil, M. Esch, M. Giorgetta, U. Schlese, and U. Schulzweida, 1996: The atmospheric general circulation model ECHAM4: model description and simulation of present day climate. *Max Planck Institute for Meteorology,*, **Report No.218, Hamburg, Germany**, 90 pp.

Sadiki, W., and C. Fischer, 2005: A Posteriori Validation applied to the 3D-VAR Arpege and Aladin data assimilation systems. *Tellus.*, **57A**, 21–34.

Salack, S., B. Muller, and A.T. Gaye, 2011: Rain-based factors of high agricultural impacts over Senegal. Part I: integration of local to sub-regional trends. *Theor. Appl. Climatol.*, **DOI: 10.1007/s00704-011-0414-z**.

Seleshi, Y., and U. Zanke, 2004: Recent changes in rainfall and rainy day in Ethiopia. *Int. J. Climatol*, **24**, 973–983.

Sergio, M.V.S., S. Begueria, and I.L.M. Juan, 2009: A Multiscalar Drought Index Sensitive to Global Warming: The Standardized Precipitation Evapotranspiration

Index. *Journal of Climate*, **23**, 1696–1718.

Shuo-Jye, W., 2002: Estimations of the parameters of the Weibull distribution with progressively censored data. *J. Japan Statist. Soc.*, **Vol. 32 No. 2**, 155–163.

Stewart, J.L., 1991: Principle and performance of response farming. In Climatic Risk in Crop Production. Models and Management for the Semi-Arid Tropics and Sub-Tropics. Ford W, Muchow RC, Bellamy ZA (eds). *CAB International: Wallingford.*

Svoboda, M., D. LeComte, M. Hayes, R. Heim, K. Gleason, J. Angel, B. Rippey, R. Tinker, M. Palecki, D. Stooksbury, D. Miskus, and S. Stephens, 2002: The drought monitor. *Bulletin of the American Meteorological Society*, **83**, 1181–1190.

Syed, F.S., J.H. Yoo, H. Körnich, and F. Kucharski, 2010: Are intraseasonal summer rainfall events micro monsoon onsets over the western edge ofthe South-Asian monsoon? *Atmospheric Research.*, **88**, 341–346.

Szalai, S., and C. Szinell, 2000: Comparison of two drought indices for drought monitoring in Hungary - a case study. *In Drought and Drought Mitigation in Europe, Vogt JV, Somma F (eds). Kluwer: Dordrecht; 161–166.*

Tarhule, A., Z. Saley-Bana, and P. Lamb, 2009: A prototype GIS for rainfall monitoring in West Africa. *Bulletin of American Meteorological Society*, **90**, 1607–1614.

Thom, H., 1958: A note on the gamma distribution. *Monthly Weather Review*, **86**, 117–122.

Trenberth, K., D. Stepaniak, and J. Caron, 2000: The global monsoon as seen through the divergent atmospheric circulation. *Journal of Climate*, **13**, 3969–3993.

UNEP, 2004: United Nations Environment Program. *African environment outlook: past, present and future perspectives. Geneva.*, **ISBN No. 92-807-2458-4**, 16 pp.

Vellinga, P., and W.J. van Verseveld, 2000: Climate change and extreme weather events. *WWF-World Wide Fund For Nature (Formerly World Wildlife Fund), Gland, Switzerland.*

Vicente-Serrano, S.M., 2006: Spatial and temporal analysis of droughts in the Iberian Peninsula (1910-2000). *Hydrological Sciences Journal*, **51(1)**, 83–97.

Voss, R., W. May, and E. Rocckner, 2002: Enhanced resolution modeling study on anthropogenic climate change: changes in extreme of the hydrological cycle. *Int.*

J. Climatol, **22**, 755–777.

WAN, G., X. CAO, F. LI, and K. LI, 2013: Sphere Shell Space 3D Grid. *International Archives of the Photogrammetry, Remote Sensing and Spatial Information Sciences.*, **XL-4**, 77–82.

Wigley, T.M.L., 1999: The science of climate change, global and u.s. perspectives. *National Center for Atmospheric Research, Pew Center on Global Climate Change.*

Wilks, D., 1995: Statistical Methods in the Atmospheric Sciences. *Academic Press: London.*

Wilks, D., 2006: Statistical methods in the atmospheric sciences. Second Edition. *International geophysics series. Academic Press*, **91**.

Woodward, W.A., and H.L. Gray, 1993: Global Warming and the problem of testing for trend in time series data. *J. Climate*, **6**, 953–962.

Yukimoto, S., A. Noda, A. Kitoh, M. Hosaka, H. Yoshimura, T. Uchiyama, K. Shibata, O. Arakawa, and S. Kusunoki, 2006: Present-Day Climate and Climate Sensitivity in the Meteorological Research Institute Coupled GCM Version 2.3 (MRI-CGCM2.3). *Journal of the Meteorological Society of Japan.*, **84**, 333–363.

Zwiers, F.W., and V.V. Kharin, 1998: Changes in the extremes of the climate simulated by CCC GCM2 under CO_2 doubling. *J. Climate*, **11**, 2200–2222.

Appendix

Annexe A: *Grouping based on onset and retreat dates of the rainy season*

The following Figure (Fig. 32) were not inserted in the original manuscript, but they were useful to define criteria of the grouping and to delimitate sub-domains of our study domain. The 4 pentad interval (results on Fig. 4) appeared to be the one giving reasonable separate zones (stations spatially grouped) as compared to interval of 1, 2 or 3 pentads. These zones were then retained for the study.

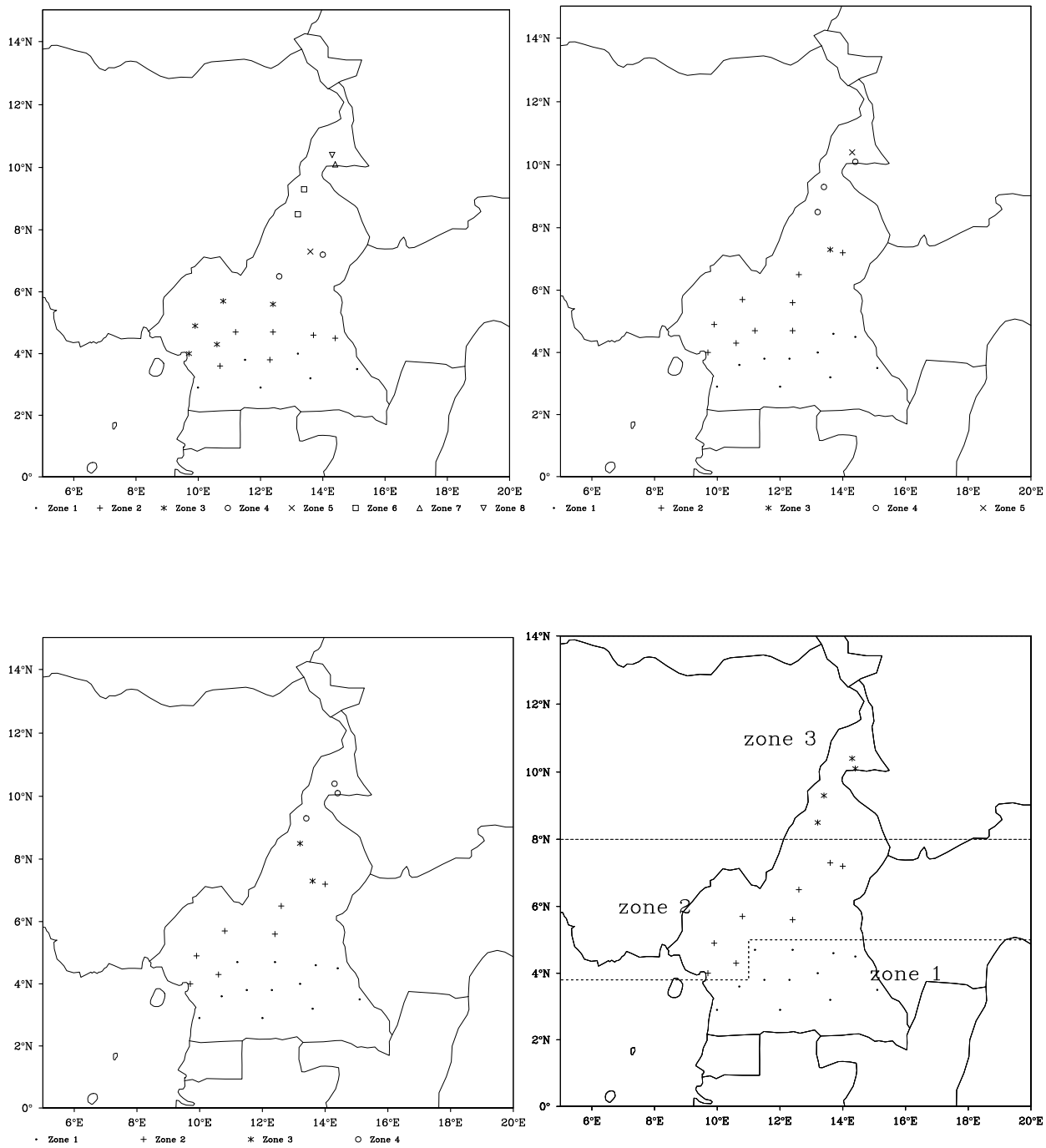

Figure 32: Classification of stations in different sub-domains. Stations where both onset and retreat dates are different by 1 pentads at most (Figure top left), 2 pentads at most (Figure top right), 3 pentads at most (Figure bottom left) or 4 pentads at most (Figure bottom right) were assigned the same marker and constitute stations of a same zone.

Annexe B: *Interannual trends magnitudes in mean annual total amounts and fraction of annual precipitations contributed by daily events above the 90^{th} percentile*

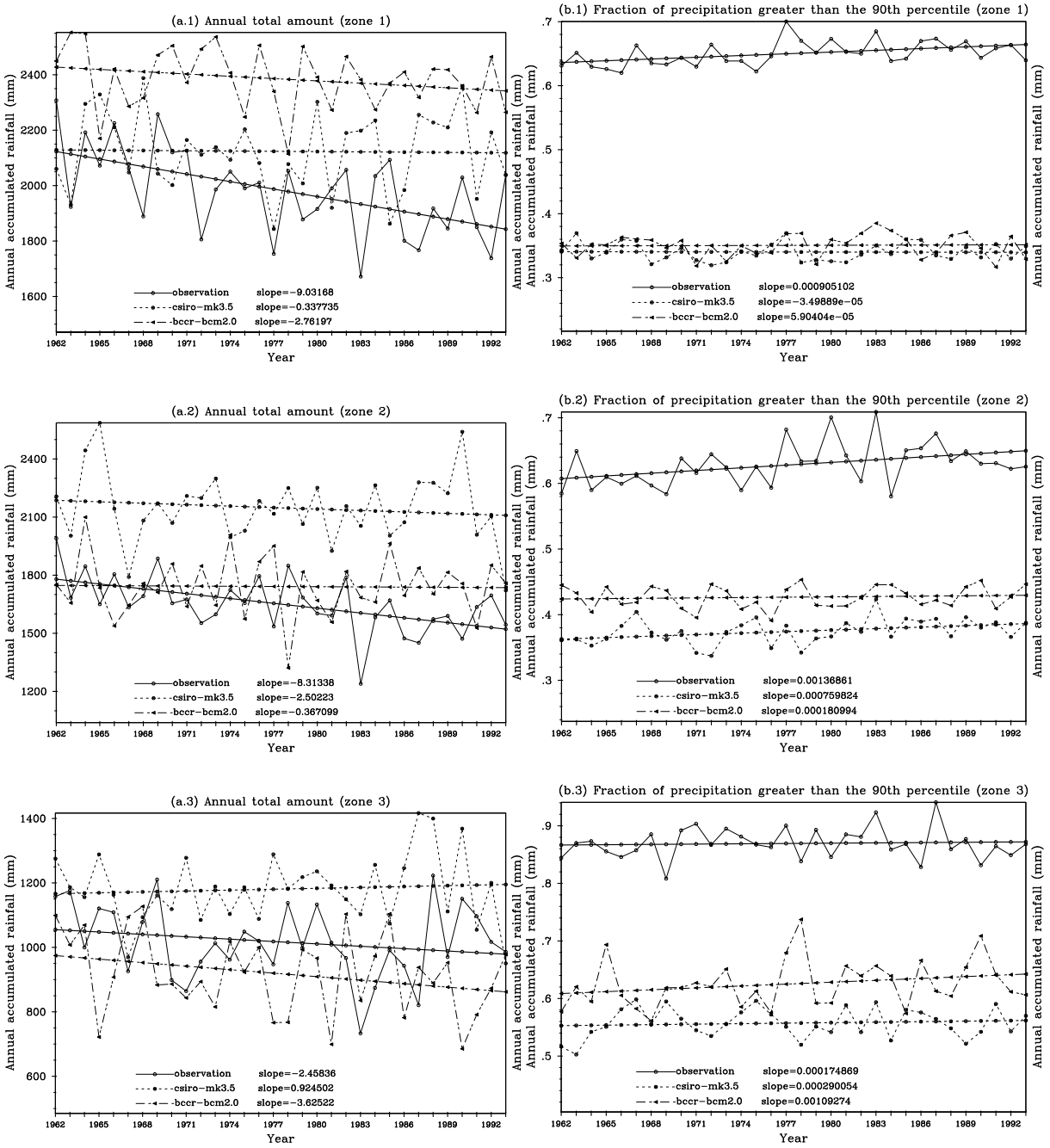

Figure 33: Interannual trends magnitudes in mean annual total amounts ((a.1), (a.2), (a.3)) and in fraction of annual precipitations contributed by daily events above the 90^{th} percentile ((b.1), (b.2), (b.3)).

Annexe C: *Value of the Kolmogorov-Smirnov test statistic for the normality of SPIs.*

Table 18: Value of the Kolmogorov-Smirnov test statistic for the normality of SPIs. Test were done at 5% significant level. Bold characters indicate significant values and underlined characters indicate that the H_0 hypothesis were accepted.

No	Station	Value of D for n-month time scale					
		values of n					
		1	3	6	12	18	24
1	Maroua	0.4095	0.2421	0.1388	**0.0411**	0.0675	**0.0335**
2	Kaele	0.4131	0.2392	0.1179	0.064	**0.0473**	0.0925
3	Garoua	0.4061	0.2391	0.1052	**0.052**	**0.0542**	**0.0409**
4	Poli	0.3546	0.1978	0.1001	**0.0449**	**0.0597**	**0.0577**
5	Ngaoundere	0.3105	0.162	0.0803	**0.0402**	**0.0535**	**0.0544**
6	Meiganga	0.223	0.1011	0.0748	**0.0356**	**0.0444**	0.0714
7	Tibati	0.2559	0.107	0.08	**0.0353**	**0.0403**	**0.0537**
8	Koundja	0.1916	0.0878	0.0846	**0.0427**	**0.0561**	**0.0549**
9	Yoko	0.1799	0.1199	**0.0481**	**0.0395**	**0.0445**	**0.0386**
10	Nkongsamba	0.0921	0.0635	0.0795	**0.0441**	**0.053**	**0.0484**
11	Bafia	0.1385	0.1103	**0.0321**	**0.05**	**0.0359**	0.0605
12	Nanga-eboko	0.115	0.0797	**0.0319**	**0.0386**	**0.0313**	**0.0323**
13	Bertoua	0.0915	0.0849	**0.0252**	**0.0278**	**0.0463**	**0.0384**
14	Batouri	0.0865	0.0855	**0.0313**	**0.0487**	**0.0332**	**0.0541**
15	Ngambe	0.0803	**0.0532**	0.0727	0.0708	**0.0357**	**0.0495**
16	Douala	**0.048**	0.0643	0.0815	0.0775	**0.0312**	0.0931
17	Abong-mbang	0.0898	0.073	**0.0301**	**0.041**	**0.0389**	**0.0348**
18	Yaounde	0.0674	0.0814	**0.0322**	**0.0289**	**0.0322**	0.0682
19	Akonolinga	0.0879	0.0868	**0.0321**	**0.0457**	**0.0315**	0.091
20	Eseka	0.0711	0.0722	**0.023**	**0.0303**	**0.0315**	**0.0569**
21	Yokadouma	0.0773	0.0894	**0.0293**	**0.0561**	**0.0407**	**0.0289**
22	Lomie	0.0691	0.076	**0.0338**	**0.0397**	**0.0355**	**0.0452**
23	Kribi	**0.0195**	**0.0397**	**0.0278**	**0.0314**	**0.0271**	**0.0572**
24	Sangmelima	0.0648	**0.0595**	**0.0213**	**0.027**	**0.0268**	**0.0529**

Annexe D: *GLOSSARY*

Aerosol: Microscopic particles suspended in the atmosphere, originating from either a natural source (e.g., volcanoes) or human activity (e.g., coal burning).

Albedo: The reflectivity of the Earth.

Anaerobic: Occurring in the absence of free oxygen; an example of an anaerobic process is digestion in cattle.

Annual cycle: The sequence of seasons over a full year.

Anthropogenic climate change: Climate change arising from human influences.

Anticyclone: A high-pressure weather system. The wind rotates clockwise around these in the Northern Hemisphere and counterclock- wise in the Southern Hemisphere. They usually give rise to fine, settled weather.

Atmospheric chemistry: The science of the chemical composition of the atmosphere.

Atmospheric instability: The growth of small disturbances into large disturbances through internal processes.

Baroclinic instability: An atmospheric instability associated with horizontal temperature gradients such as between the equator and the poles.

Biomass burning: The burning of organic matter from plants, animals, and other organisms.

Carbon dioxide (CO_2): A naturally occurring, colorless atmospheric greenhouse gas. It arises in part from decay of organic matter. Plants take up carbon dioxide during photosynthesis. Animals breathe it out during respiration. Humans contribute to carbon dioxide concentrations in the atmosphere by burning fossil fuels and plants.

Chaos: In a technical sense, a process whose variations look random even though their behavior is governed by precise physical laws.

Chlorofluorocarbon (CFC): One of a family of greenhouse gas compounds containing chlorine, fluorine, and carbon. CFCs do not occur naturally; all are made by humans. They are generally used as propellants, refrigerants, blowing agents (for producing foam), and solvents.

Climate: The average weather together with the variability of weather conditions for a specified area during a specified time interval (usually decades).

Climate change: Long-term (decadal or longer) changes in climate, whether from natural or human influences.

Climate model: A computer model that uses the physical laws of nature to predict the evolution of the climate system.

Climate system: The interconnected atmosphere-ocean-land-biosphere-ice components of the Earth involved in climate processes.

Climate variation: A fluctuation in climate lasting for a specified time interval, usually many years.

Cold front: A transition zone where a cold air mass advances, pushing warmer air out of the way. Warm air is forced to rise, commonly creating convection and thunderstorms, so that a period of "bad weather" occurs as the temperatures drop.

Composition of the atmosphere: The makeup of the atmosphere, including gases and aerosols.

Convection: In weather, the process of warm air's rising rapidly while cooler air subsides, usually more gradually, over broader regions elsewhere to take its place. This process often produces cumulus clouds and may result in rain.

Cumulus cloud: A puffy, often cauliflower-like, white cloud that forms as a result of convection.

Cyclone: A low-pressure weather system. The wind rotates around cyclones in a counter clockwise direction in the Northern Hemisphere and clockwise in the Southern Hemisphere. Cyclones are usually associated with rainy, unsettled weather and may include warm and cold fronts.

Dust Bowl era: The period during the 1930s when prolonged drought and dust storms arose in the central Great Plains of the United States.

Dynamics: In climate, the study of the action of forces on the atmospheric and oceanic fluids and their response in terms of winds and currents.

Ecosystem: A system involving a living community and its nonliving environment, considered as a unit.

El Niño: The occasional warming of the tropical Pacific Ocean off South America. Associated warming from the west coast of South America to the central Pacific typically lasts a year or so and alters weather patterns around the world.

Electromagnetic spectrum: The spectrum of radiation at different wavelengths, including ultraviolet, visible, and infrared rays.

Enhanced greenhouse effect: The increase in the greenhouse effect from human activities.

Evapotranspiration: The evaporation of moisture from the surface together with transpiration, the release of moisture from within plants.

Feedback: The transfer of information on a system's behavior across the system that modifies behavior. A positive feedback intensifies the effect; a negative feedback reduces the effect.

Fossil fuel: A fuel derived from living matter of a previous era; fossil fuels include coal, petroleum, and natural gas.

General circulation model: A computer model, usually of the global atmosphere or the oceans; GCMs are often used as part of even more complex climate models.

Glacier: A mass of ice, commonly originating in mountainous snow fields and flowing slowly down-slope.

Global warming: The increasing heating of the atmosphere caused by increases in greenhouse gases from human activities and their "entrapment" of heat. It produces increases in global mean temperatures and an increased hydrological cycle. This phenomenon is also popularly known as the greenhouse effect.

Greenhouse effect: The effect produced as certain atmospheric gases allow incoming solar radiation to pass through to the Earth's surface but reduce the escape of outgoing (infrared) radiation into outer space. The effect is responsible for warming the planet.

Greenhouse gas: Any gas that absorbs infrared radiation in the atmosphere.

Groundwater: Water residing underground in porous rock strata and soils.

Hydrological cycle: The cycle by which water moves and changes state through the atmosphere, oceans, and Earth. Evaporation and transpiration of moisture produce water vapor, which is moved by winds and falls out as precipitation to become groundwater, which in turn may run off in streams or in glaciers into the seas or become stored below ground.

Infrared radiation: The longwave part of the electromagnetic spectrum, corresponding to wavelengths of 0.8 microns to 1,000 microns. For the Earth, it also corresponds to the wavelengths of thermal emitted radiation. Also known as longwave radiation.

Jet stream: The strong core of the midlatitude westerly winds, typically at about 8 to 10 km above the surface of the Earth, in each hemisphere.

Land surface exchange: An exchange of gases from the land surface into the atmosphere or vice versa. The most common is evaporation of water into water vapor.

Little Ice Age: A prolonged cool period, especially in Europe, occurring primarily in the 16th and 17th centuries.

Longwave radiation: See infrared radiation.

Mean: The average of a set of values.

Methane (CH_4): A naturally occurring greenhouse gas in the atmosphere produced

from anaerobic decay of organisms. Common sources include marshes (thus the name *marsh gas*), coal deposits, petroleum fields, and natural gas deposits. Human activities contribute to increased amounts of methane, which can come from the diges tive system of domestic animals (such as cows), from rice paddies, and from landfills.

Natural greenhouse effect: The part of the greenhouse effect that does not result from human activities.

Negative feedback: See feedback.

Net radiation: The sum of all the shortwave and longwave radiation passing through a level in the atmosphere.

Nitrous oxide (N_2O): A naturally occurring greenhouse gas in the atmosphere produced by microbes in the soil and ocean. Humans contribute to concentrations through burning wood, using fertilizers, and manufacturing nylon.

Nonlinear: Not linear. Linear relationships between two variables can be plotted as a straight line on a graph. Nonlinear relationships involve curved or more complex lines.

Normal distribution: A bell-shaped curve of the distribution of the frequency with which values occur, defined by the mean and the standard deviation.

Ozone (O_3): A molecule consisting of three bound atoms of oxygen. Most oxygen in the atmosphere, consists of only two oxygen atoms (O_2). Ozone is a greenhouse gas. It is mostly located in the stratosphere, where it protects the biosphere from harmful ultraviolet radiation. Human activities contribute to near-surface ozone through car exhaust and coal-burning power plants; ozone in the lower atmosphere has adverse affects on trees, crops, and human health.

Phenology: The study of natural phenomena that occur in a cycle, such as growth stages in crops.

Photosynthesis: The process by which green plants make sugar and other carbohydrates from carbon dioxide and water in the presence of light.

Positive feedback: See feedback.

Runoff: Excess rainfall that flows into creeks, rivers, lakes, and the sea.

Scattering radiation: The dispersion of incoming radiation into many different directions by molecules or particles in the atmosphere. Radiation scattered backwards is equivalent to reflected radiation.

Solar radiation: Radiation from the sun, most of which occurs at wavelengths shorter than the infrared.

Southern Oscillation: A global-scale variation in the atmosphere associated with El Niño events.

Stability: In meteorology, a property of the atmosphere, making it resistant to displacements. The atmosphere is stable if a perturbation decays and it returns to its former state. It is unstable if the perturbation grows.

Standard deviation: A measure of the spread of a distribution. For a normal distribution, 68

Stratosphere: The zone of the atmosphere between about 10–15 and 50 kilometers above the Earth's surface. Most of the ozone in the atmosphere is in the stratosphere. The stratosphere is separated from the troposphere below by the tropopause.

Temperature gradient: The differences in temperature across a specified region.

Thermal: A rising pocket of warm air.

Thermal radiation: Longwave (infrared) radiation from the Earth.

Transpiration: The giving off of water vapor through the leaves of plants.

Troposphere: The part of the atmosphere in which we live, ascending to about 15 km above the Earth's surface, in which temperatures generally decrease with height. The atmospheric dynamics we know as weather take place within the troposphere.

Urban heat island: The region of warm air over built-up cities associated with the presence of city structures, roads, etc.

Visible radiation: Electromagnetic radiation, lying between wavelengths of 0.4 and 0.7 microns, to which the human eye is sensitive.

Warm front: A transition zone where a warm air mass pushes cooler air out of the way over a broad region. The warm air tends to rise, often creating stratiform clouds and rain as the temperatures rise.

Weather: The condition of the atmosphere at a given time and place, usually expressed in terms of pressure, temperature, humidity, wind, etc. Also, the various phenomena in the atmosphere occurring from minutes to months.

Weather systems: Cyclones and anticyclones and their accompanying warm and cold fronts.

Wind shear: Large differences in wind speed and/or direction over short distances.

Publications list

Publications

1. **G. M. Guenang**, F. Mkankam Kamga, (2012): Onset, retreat and length of the rainy season over Cameroon, *Atmospheric Science Letters of the Royal Meteorological Society*, **13: 120-127**

2. **G. M. Guenang**, F. Mkankam Kamga, (2013) : Computation of the Standardized Precipitation Index (SPI) and its use to assess drought occurrences in Cameroon over recent decades, *Journal of Applied Meteorology and Climatology of the American Meteorology Society*, **53 (10): 2310-2324**

ATMOSPHERIC SCIENCE LETTERS
Atmos. Sci. Let. **13**: 120–127 (2012)
Published online 22 February 2012 in Wiley Online Library
(wileyonlinelibrary.com) **DOI:** 10.1002/asl.371

RMetS
Royal Meteorological Society

Onset, retreat and length of the rainy season over Cameroon

G. M. Guenang* and F. Mkankam Kamga
Laboratory for Environmental Modelling and Atmospheric Physics, Department of Physics, University of Yaounde 1, Yaounde, Cameroon

**Correspondence to:*
G. M. Guenang, Laboratory for Environmental Modelling and Atmospheric Physics, Department of Physics, University of Yaounde 1, Yaounde, Cameroon.
E-mail: merlin.guenang@yahoo.fr

Received: 30 July 2011
Revised: 28 December 2011
Accepted: 29 December 2011

Abstract

Observed precipitation from 24 stations in Cameroon during 1962–1993 were used to study onset, retreat and length of the rainy season. Results were compared to control simulations by four IPCC 4AR AOGCMs. CSIRO-mk3.5 and MPI-echam5 AOGCMs best captured onset, retreat and duration of the rainy season. Projections for 2082–2098 under the SRES A2 emission scenario were also analysed. For that period, onset dates are expected to be later by 1 pentad or more than in the current climate and retreat by less than half a pentad in zones 1 and 2. This will lead to a slight decrease in the duration of the rainy season. The situation is reverse in zone 3, where the season will be longer. Copyright © 2012 Royal Meteorological Society

Keywords: rainfall onset; rainfall retreat; length of the rainy season; climate change; Cameroon; climate projection

1. Introduction

Rainfall onset and retreat dates are important parameters in the agricultural calendar in most tropical regions. As defined by Odekunle *et al.* (2005), the rainfall onset is the period at the beginning of the rainy season, when rainfall distribution has become adequate for crop development, while rainfall retreat refers to the period, towards the end of the rainy season, when rainfall distribution may no longer sustain crop growth. Many regions over the world are expected to suffer substantial climate modifications as a result of global warming. These changes will affect the onset and retreat of the rainy season which has become irregular over the years (Salack *et al*., 2011), making it difficult for farmers to optimize the seed planting period and adjust to the length of the growing season (Olaniran, 1983a; Mugalavai *et al*., 2008; Ndomba, 2010). The immediate consequences are the decrease of agricultural production and an increase risk of hunger. Therefore, the determination of the onset and retreat dates of the rainy season in various regions throughout the world have become a challenge for many researchers.

Various methods have been developed to determine onset and retreat dates of the rainy season. Odekunle(2006) classified these methods into five main categories: (1) Intertropical Discontinuity (ITD)-rainfall model (Ilesanmi, 1972a), (2) rainfall-evapotranspiration relation model (Benoit, 1977), (3) percentage cumulative mean rainfall model, based on rainfall data alone (Ilesanmi, 1972b; Adejuwon *et al*., 1990; Adejuwon, 2006), (4) wind shear model (Omotosho, 1990a, 1990b), (5) the theta-E technique (Omotosho, 2002). Odekunle(2006) used two different methods based on rainfall data, to determine onset and retreat dates of the rainy season in Nigeria. The study established that both rainfall amount and rainy days are equally effective in the determination of the mean rainfall onset and retreat dates, but the latter method is more efficient for individual year. Omotosho(1992) proposed a simple empirical scheme for predicting onset and retreat in the West African Sahel, using upper atmosphere wind data. He considered that the poleward retreat of the subtropical jet is linked to the start of rain, whereas the destruction of the wind shear is a forerunner to the cessation of rainfall. The percentage cumulative mean rainfall is the most used method. It has the advantage of depending only on rainfall data that are readily available from direct measurements rather than other rainfall-associated factors (Odekunle *et al*., 2005). This method was used by Olaniran(1983a) to study the onset of rains and the start of the growing season in Nigeria. The results revealed that there is no significant difference between the mean onset date obtained and the mean start of the growing season.

Most studies on rainfall onset and retreat in African countries were performed on a limited number of stations or on short time periods because of the lack of complete data series in observation. The use of satellite data or of models outputs are some palliative solutions to this issue. However, satellite data are limited to recent periods while model outputs can cover longer periods in both present and future. In view of the present global warming and its consequences on local climate variability, the use of model outputs to investigate characteristics of the rainy season (e.g. rainfall totals, rainy day frequencies, onset, retreat and length of the rainy season) is necessary in order to assess future changes and guide adaptation measures. Global and regional climate models with various

IPCC emission scenarios have been used by many authors for projecting future climate change. In the Iberian Peninsula, it was found that 5/24 IPCC GCMs (MIROC3.2-HIRES, MPI-ECHAM5, GFDL-CM2.1, BCCR-BCM2.0 and UKMO-HADGEM1) best reproduce current climate (Errasti *et al*., 2011) and could be used for future projections. Mkankam (2000) noted that two IPCC-coupled atmosphere-ocean general circulation models (ECHAM4 and HADCM2) simulated well the present climate in Cameroon and neighbouring areas. Thus, he used their outputs to evaluate projected changes in rainfall and temperature resulting from increased concentration of greenhouse gases (GHGs) in the atmosphere for the period 2040–2070. The results revealed changes in annual rainfall within the range of present climate variability while the projected temperature increases were larger than observed variability. An evaluation of the ability of 18 GCMs to capture the West African monsoon system, found that three models (among them MPI-ECHAM5) gave reasonable simulations of the twentieth-century climate while others comprising CSIRO-Mk3.0 and MRI-CGCM2.3.2 failed to do so (Cook and Vizy, 2006). Errasti *et al*. (2011) revealed that all IPCC models do not describe the present climate with similar accuracy. Furthermore, the best models for a particular region of the earth do not always achieve the same degree of performance in other regions. Additionally, the skill of the models is different according to the meteorological variables examined.

The objectives of this paper are to evaluate the performances of some IPCC-4AR model in reproducing onset, retreat and length of the rainy season in the study area, and to assess future changes under the SRES A2 GHG emission scenario. Simulations of current climate and of future perturbed climate under this emission scenario were carried out for the IPCC 4th Assessment Report (IPCC-4AR) using several GCMs. The method of the percentage cumulative mean rainfall amount was used to determine present and future climate rainfall onset and retreat dates over Cameroon. Analyses for pertubed climate were extended to the country's neighbouring areas to increase the number of model grid points used as theses areas have similar climate (Figure 1).

The work is organized as follows. In Section 2, the study area is described. In Section 3, we present data used and define the methodology. The results on stations grouping, the analysis of mean onset, retreat and length of the rainy season for both current and future climates, are in Section 4. Section 5 is devoted to concluding remarks and perspectives.

2. Study area

The study domain is located in Equatorial Central Africa between 1–13 °N and 7–18 °E. This area

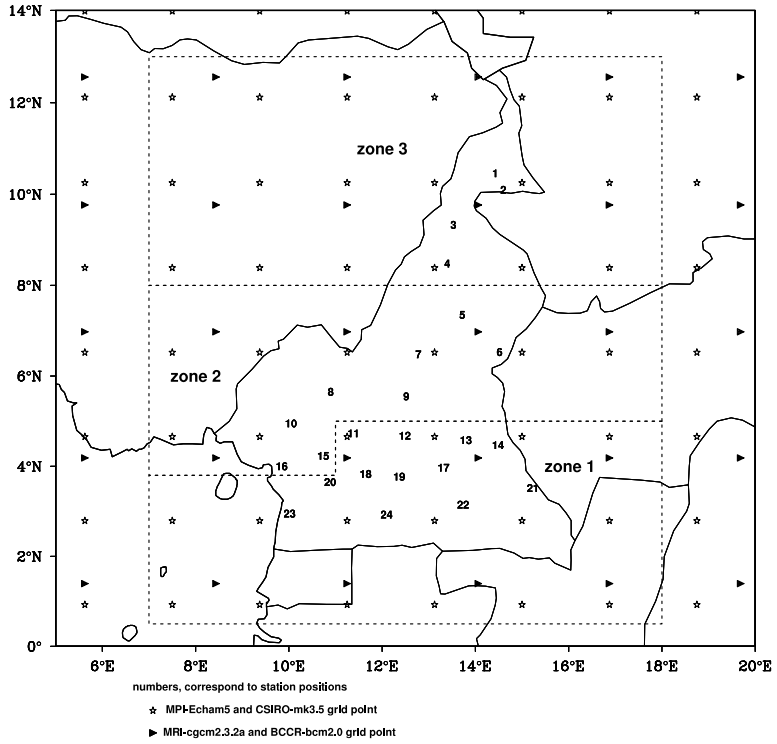

Figure 1. Study area with the geographical locations of rainfall stations (indicated by numbers) and of climate models grid points (BCCR-bcm2.0, CSIRO-mk3.5, MPI-echam5 and MRI-cgcm2.3.2a). Grid point locations for each model are indicated by a specific marker. Dashed lines show delimited zones.

encompasses the Cameroon territory. GCMs results are discussed on a wider domain including areas bordering the country (Figure 1). The climate of the area is not uniform, varying from tropical humid in the south to semi-arid and hot in the north. The southern part of the country is bordered in the west by Atlantic Ocean and is covered by dense rain forest. The northern part has a dry to arid Sahelian type climate depending on latitude. Economic activities in the area are based mostly on agriculture, generally at subsistence levels. Cacao, coffee, bananas, rubber, palm oil and cotton are the main cash crops raised by farmers. Main food crops are cassava, corn, yams, sweet potatoes and millet. Logging is another important resource in Cameroon with heavy timber exportation. More information on the country can be found in Penlap *et al*. (2004). All these activities are rainfed and almost no irrigation.

3. Data and methodology

3.1. Data used

Five data sets were used in the study: daily rainfall data from 24 measuring stations in Cameroon and simulated daily rainfall from MPI-echam5, MRI-cgcm2.3.2a, BCCR-bcm2.0 and CSIRO-mk3.5. Station rainfall data provided by the Cameroon Meteorological Services are the same successfully used by Penlap *et al*. (2004). The geographical positions of the stations are shown in Figure 1. Table I indicates their names, locations and altitudes. Some stations have missing values, representing at most less than 4% of total data. Simulated rainfall were obtained from the World Climate Research Program's (WCRP's) Coupled Model Inter-comparison Project phase 3 (CMIP3) multi-model dataset at the Lawrence Livermore National Laboratory, USA. They were produced for IPCC 4th Assessment Report (4AR) (Meehl *et al*., 2007). Echam5 is a model of the Max Planck Institute (MPI-echam5) for Meteorology in Germany (Roeckner *et al*., 1996) while cgcm2.3.2a and mk3.5 are respectively from the Meteorological Research Institute (MRI-cgcm2.3.2a) in Japan (Yukimoto *et al*., 2006) and the Australian Commonwealth Science and Industrial Research Organization (CSIRO-mk3.5) (Gordon *et al*., 2002). Model bcm2.0 is from the Bjerknes Centre for Climate Research (BCCR-bcm2.0), University of Bergen, Norway (Furevik *et al*., 2003). A 32-year data for the current climate (1962–1993) and a 19-year (2082–2098) of the future climate under the SRES A2 emission scenario were analysed. Grid points for each of the four IPCC 4AR models are shown in Figure 1. Echam5 and Mk3.5 have the same grid spacing (208 km) while Cgcm2.3.2a and Bcm2.0 have spacings of 310 km.

Table I. Geographical positions and altitudes of the 24 rainfall stations used. Stations are grouped per defined climatic zones. They are also assigned numbers used to represent them in Figure 1.

Region	N°	Station name	Lon (°E)	Lat (°N)	Alt (m)
Zone 1	11	Bafia	11.25	4.73	500
	12	Nanga-éboko	12.37	4.68	623
	13	Bertoua	13.68	4.58	668
	14	Batouri	14.37	4.47	650
	17	Abong-mban	13.20	3.97	693
	18	Yaoundé	11.53	3.83	753
	19	Akonolinga	12.25	3.77	671
	20	Eséka	10.77	3.65	228
	21	Yokadouma	15.10	3.52	534
	22	Lomié	13.62	3.15	624
	23	Kribi	09.99	2.95	10
	24	Sangmélima	11.98	2.93	712
Zone 2	5	Ngaoundéré	13.57	7.35	1104
	6	Meiganga	14.0	7.20	1027
	7	Tibati	12.63	6.48	873
	8	Koundja	10.75	5.65	1210
	9	Yoko	12.37	5.55	1027
	10	Nkongsamba	09.93	4.95	816
	15	Ngambé	10.62	4.23	610
	16	Douala	09.73	04.00	5
Zone 3	1	Maroua	14.26	10.46	423
	2	Kaélé	14.45	10.10	386
	3	Garoua	13.38	9.33	241
	4	Poli	13.25	8.48	436

3.2. Methodological approach

The method adopted in this study for the determination of onset and retreat dates was the cumulative percentage mean rainfall amount (Ilesanmi, 1972a). Daily rainfall data for each year were grouped into 5-day means (pentads). This grouping was performed on non-overlapping 5-day means starting at pentad 1 (1 to 5 January) and ending at pentad 73 (27 to 31 December). In the first step of the method, the percentage of mean annual rainfall was determined at 5-day intervals. Next, cumulative percentages were calculated for the full year. Finally, the timings of the accumulation of 7–8% and of 90% of the annual rainfall were taken as onset and retreat of rains respectively. The length of the rainy season was defined simply as the period between onset and retreat dates. According to the method adopted here, the monsoon rainy season, between onset and retreat accounts for 83.5% of annual rainfall.

In the first part of the analysis, the temporal mean onset and retreat dates of the rainy season were first calculated for each station of the domain. Second, the following criteria were used to divide the study domain into sub-domains or zones: stations where both onset and retreat dates are different by 4 pentads at most were assigned to a common climatic zone. The 4-pentad interval appeared to be the one giving reasonable separate zones (stations spatially grouped) as compared to interval of 1, 2 or 3 pentads (Figures not shown). For model outputs, zone definitions were extended to neighbouring areas of Cameroon in order to increase the number of grid points used. Some studies on domains comprising our study area (Olaniran,

1989, 1983b) can justify this extension. Next, observed and simulated data were analysed in every zone by calculating for each year and at each station (grid point) onset and retreat dates and length of the rainy season. Annual results were averaged for stations (grid points) within each zone giving a 32-year time series per zone for both observations and model outputs. Finally, means, standard deviations and interannual variability were analysed and compared. Statistics on how each model reproduces the observed parameters (onset and retreat dates and duration of the rainy season) were estimated as the ratio of the observed number of parameters simulated correctly to the total number of cases.

Climate change evaluations were based on comparisons between current climate and future SRES A2 scenario perturbed climate. The A2 scenario recognized as the most severe (Cook and Vizy, 2006) assumes strong CO2, CH4 and SO2 increases throughout the twenty-first century (except for SO2, which declines after 2030) (IPCC, 2001). Knowledge about how models respond to these changes are useful for predictions of economic impacts.

4. Results and discussion

4.1. Grouping based on onset and retreat dates of the rainy season

A total of three zones were defined in the study domain (Figure 1) using the criteria presented in the methodology section. These zones are similar to those defined using other criteria (Olaniran, 1989, 1983b). Thus we can consider:

(1) The equatorial forest zone (zone 1) mostly covered by dense forests and having two rainy seasons;
(2) The Midland zone (zone 2) which predominantly covers highlands where topography effectively extends the length of the humid period, due to localized convection and orographic effects (Olaniran, 1983b);
(3) The Sahelian zone (zone 3), where the tropical continental air mass predominates, except during the Monsoon season when the tropical maritime air mass covers the area for 3 to 5 months at most (Olaniran, 1983b).

Table II shows the range of onset and retreat dates for each zone.

4.2. Comparative study of mean onset and retreat dates and lengths of the rainy season under the current climate (1962–1993)

Mean onset and retreat dates and lengths of the rainy season as well as associated standard deviations for each zone are shown in Table III for observed and simulated data. As expected, rainfall onset and retreat follow the northward move of the ITD during the months of March to August and its southward retreat between September and October, respectively. Similar spatial migrations of onset and retreat dates were observed in many African countries, for example in Nigeria, Senegal and western Kenya (Odekunle, 2004; Mugalavai *et al*., 2008; Salack *et al*., 2011). Retreat is more abrupt as it takes only 8 pentads compared to 12 for onset. This rapid retreat was also observed in neighbouring Nigeria (Ayoade, 1974; Odekunle, 2006). Earliest onset is in zone 1, south of the study domain, on the 16th pentad of the year (17th–21st March), followed by zone 2 four pentads (20 days) later, and latest onset, close to 2 months (11 pentads) after zone 1, is in the northernmost stations (Table III(a)). Retreat starts in the North and moves South (Table III(b)) and time lags between zones are less than for onset dates. Uncertainties are higher (higher standard deviations) on onset than on retreat dates. The length of the rainy season (Table III(c)) decreases from South to North: 25 consecutive pentads (4 months) in zone 3, 37 (6 months) in zone 2 and 45 (7.5 months) in zone 1. This is in agreement with annual rainfall amounts observed in theses areas. The spatial variation in duration affects the choice of crop types and farming techniques, depending on zones in order to avoid losses due to insufficient number of rainy days. That is why in Kenya where the maximum length of the growing season is about 4 months, irrigation is recommended during the short rainy season as a way of supplementing the limited rainfall (Mugalavai *et al*., 2008)). The increase in the length of the rainy season from zone 3 to zone 1 may be explained by the annual migration of the ITD, which controls the Monsoon influx of humid maritime air into the continent. This favourable rainfall-producing factor has the least residence period over zone 3.

The value of standard deviation of a time series can be used to elucidate temporal variability (Syed *et al*., 2010). For onset date, observed standard deviations of 2 pentads in zone 1 and 3 pentads in zones 2 and 3 indicate that interannual variability of this parameter is lower in the Equatorial forest zone. Retreat dates

Table II. Range of mean onset and retreat dates of the rainy season for each zone. Results are given in pentad number and the corresponding calendar dates are in parentheses. The first pentad is the period from January 1 to January 5.

Sub-domain	Onset date range	Retreat date range
Zone 1	15th–17th pentad (12 March–26 March)	60th–62th pentad (23 October–6 November)
Zone 2	19th–21st pentad (1 April–15 April)	55th–59th pentad (22 September–22 October)
Zone 3	25th–29th pentad (1 May–25 May)	52nd–54th pentad (13 September–27 September)

Table III. Mean onset and retreat dates and lengths of the rainy season for the period 1962–1993 in the three zones. Onset and retreat dates are in pentads number ± standard deviation. The corresponding calendar ranges dates are between brackets without the standard deviations. Lengths of the rainy season are in pentads and the equivalent number of days are indicated in parentheses.

	(a) Onset date			(b) Retreat date			(c) Length (*retreat–onset*)		
Data	**Zone 1**	**Zone 2**	**Zone 3**	**Zone 1**	**Zone 2**	**Zone 3**	**Zone 1**	**Zone 2**	**Zone 3**
Observation	16^{th} pentad ± 2 (17–21 March)	20^{th} pentad ± 2 (6–10 April)	28^{th} pentad ± 3 (16–20 May)	61^{st} pentad ± 1 (22 October–1 November)	57^{th} pentad ± 1 (8–12 October)	53rd pentad ± 2 (18–22 September)	45 pentads ± 2 (225 days)	37 pentads ± 3 (185 days)	25 pentads ± 3 (125 days)
BCCR-bcm2.0	12^{th} pentad ± 2 (25 February–1 March)	22nd pentad ± 2 (16–20 April)	29^{th} pentad ± 3 (21–25 May)	64^{th} pentad ± 1 (12–16 November)	59^{th} pentad ± 1 (18–22 October)	54^{th} pentad ± 2 (23–27 September)	52 pentads ± 2 (260 days)	36 pentads ± 2 (180 days)	25 pentads ± 4 (125 days)
CSIRO-mk3.5	14^{th} pentad ± 2 (7–11 March)	20^{th} pentad ± 2 (6–10 April)	24^{th} pentad ± 2 (26–30 April)	63rd pentad ± 1 (7–11 November)	57^{th} pentad ± 1 (8–12 October)	52^{th} pentad ± 1 (13–17 September)	49 pentads ± 2 (245 days)	37 pentads ± 2 (185 days)	28 pentads ± 2 (140 days)
MPI-echam5	14^{th} pentad ± 2 (7–11 March)	19^{th} pentad ± 2 (1–5 April)	26^{th} pentad ± 2 (6–10 May)	63^{th} pentad ± 1 (7–11 November)	60^{th} pentad ± 1 (23–27 October)	56^{th} pentad ± 1 (3–7 October)	49 pentads ± 2 (245 days)	40 pentads ± 2 (200 days)	30 pentads ± 2 (150 days)
MRI-cgcm2.3.2a	6^{th} pentad ± 2 (26–30 January)	16^{th} pentad ± 2 (17–21 March)	29^{th} pentad ± 2 (21–25 May)	66^{th} pentad ± 1 (22–26 November)	58^{th} pentad ± 1 (13–17 October)	49^{th} pentad ± 1 (29 August–2 September)	60 pentads ± 2 (300 days)	42 pentads ± 2 (210 days)	20 pentads ± 2 (100 days)

and lengths of the rainy season in all the three zones show lower amplitudes of fluctuations than onset dates (Figures not shown). Extreme values (minima and maxima) observed in the interannual variability of onset dates are much farther from their means, compared to retreat and duration of the rainy season. In general, models outputs poorly reproduce these interannual variations (correlation coefficient $|r| < 0.5$). However MPI-echam5 in most cases do the best job.

Of the four general circulation models, only MPI-echam5 has an onset date within one standard deviation of observations in all the three zones. A similar analysis shows that CSIRO-mk3.5 gives good onset in zones 1 and 2, while BCCR-bcm2.0 and MRI-cgcm2.3.2a succeed in only one zone. Based on this criterion, three models have the right simulation in zone 3 and two in the other zones. Because there is less dispersion on retreat dates (standard deviation of 1), no model is on target in zone 1, one is in zone 2 and two are in zone 3. For both onset and retreat, boxplot diagrams (Figure 2(a) and (b)) indicate that dispersion between models is low, the models tending to agree more among them than with observations. Their poor performance on retreat dates translates into poor results for the length of the season (Figure 2(c)) which are mostly off target in zone 1 but slightly better in zones 2 and 3. It is also to be noted that MRI-cgcm2.3.2a is often even out of the range of extreme observations.

A quantitative verification of the model simulations are needed in order to objectively analyse and compare their performances. In Figure 2, numbers expressed in percentages and represented below each model boxplots are statistical probabilities for models to capture the observed parameters (onset and retreat dates and length of the rainy season). In zone 1, CSIRO-mk3.5 and MPI-echam5 show better results than the other two models. While their statistical probabilities for predicting onset date are greater than 50% (61% for CSIRO-mk3.5 and 58% for MPI-echam5), they give poor results for retreat date and duration (less than 10%). In zone 2, CSIRO-mk3.5 shows best results and also has the greatest statistical probability (100% for both onset date and duration, 81% for retreat date). The second best performance is by MPI-echam5 for onset (94% of statistical probability for prediction) and by BCCR-bcm2.0 for duration (85%). Other models show poorer results (less than 50%). In zone 3, the best statistical probability for prediction is by MPI-echam5 for onset date (74%), CSIRO-mk3.5 for retreat date (75%) and BCCR-bcm2.0 for duration of the rainy season (78%). For onset and retreat dates, the second best is BCCR-bcm2.0. Overall, CSIRO-mk3.5 shows highest combined statistical probability for prediction of onset and retreat dates and duration of the rainy season, followed by MPI-echam5. MRI-cgcm2.3.2a shows lowest statistical probability.

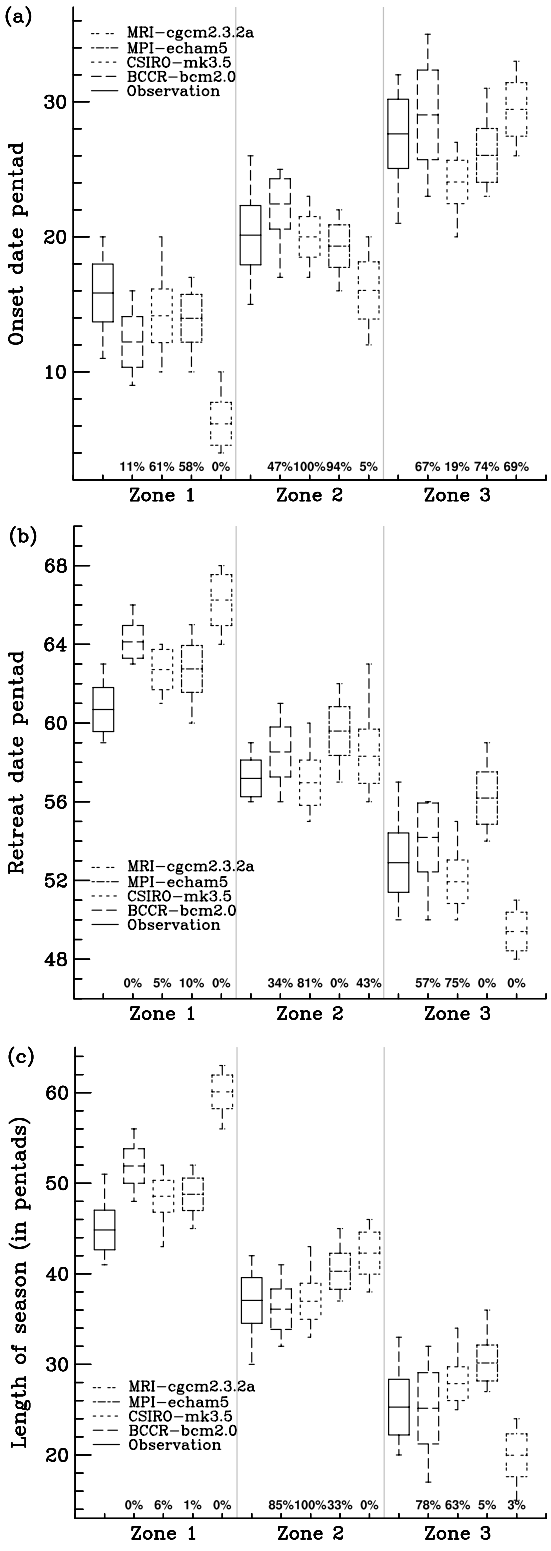

Figure 2. Onset date, retreat date and duration of the rainy season for observation and models simulations. Numbers expressed in percentage and presented below each model boxplot represent the statistical probability for each model to forecast the observed onset date (a), retreat date (b) and duration of the rainy season (c).

4.3. Onset and retreat dates and length of the rainy season under a perturbed climate

To assess the effect of increased GHG concentration in the atmosphere on onset and retreat dates and length of the rainy season, projected dates for the period 2082–2098 were analysed. These were determined from the outputs of GCM simulations using the same methodology presented earlier.

Results under the perturbed climate of a given GCM were compared to its own simulation of current climate. Differences in onset and retreat dates of the rainy season and in duration between future and present climates are shown in Figure 3(a), (b) and (c), respectively. Surprisingly there are no great changes

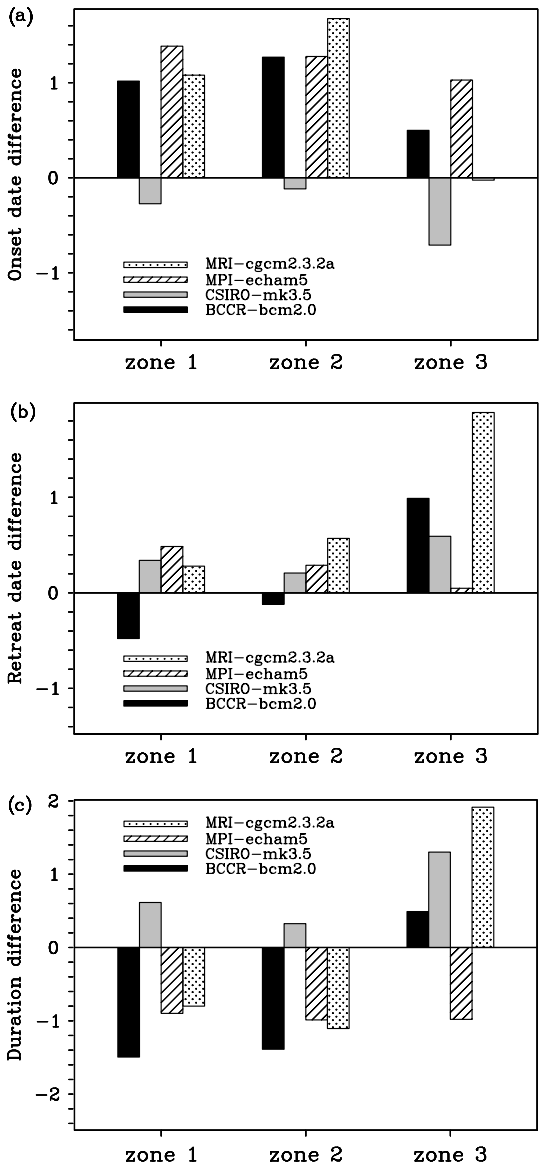

Figure 3. Gap between mean future and mean current climate dates for onset (a), retreat (b) and differences in the duration (c) of the rainy season. Vertical axis are graduated in pentads.

in either onset or retreat dates. Three of the models (MPI-echam5, BCCR-bcm2.0 and MRI-cgcm2.3.2a) show late onset of 1 pentad in all zones, while CSIRO-mk3.5 has approximately normal start in zones 1 and 2 and early start of about 1 pentad in zone 3. Retreat occurs mostly earlier, but by less than 1 pentad, except for MRI-cgcm2.3.2a in zone 3 where it is almost 2 pentads earlier. Rainy seasons are shorter by approximately 1 pentad in zones 1 and 2 and longer in zone 3 by up to 2 pentads. These changes are all within the range of variability of current climate simulated by each model and could not be considered significant. This result corroborates that of Mkankam (2000) given the strong relationship between onset and rainfall attributes (Stewart, 1991; Ati *et al*., 2002). The shortening of the rainy season is one of the most feared result of anthropogenic climate change. But projections under the SRES A2 scenario by the four models used here indicate that to the end of the twenty-first century, no major perturbations of the seasons are expected, and it will be possible to continue growing the same crops as at present time in Cameroon.

5. Concluding remarks and perspectives

Daily precipitations for 24 meteorological stations in Cameroon were used to define climatic zones in the domain 1–13 °N and 7–18 °E located in Equatorial Central Africa. Zones were defined, each of them characterized by stations with close onset and retreat dates of the rainy season. Next, onset and retreat dates and lengths of the rainy season for the current climate (1962–1993) calculated from both observations and four IPCC 4AR AOGCMs (BCCR-bcm2.0, CSIRO-mk3.5, MPI-echam5 and MRI-cgcm2.3.2a) outputs were studied and compared for each zone. Projections of impact of climate change on onset and retreat dates and length of the rainy season were assessed with these same models under the SRES A2 GHG emission scenario over the period 2082–2098.

In general, the rainy season begins earliest and ends latest south of the domain while earliest retreat dates are seen north of the domain. Thus, the length of the rainy season increases southwards. Amplitudes of fluctuations are stronger for onset date than for retreat. Model results for current climate are close to observations when they were considered with the corresponding standard deviations. CSIRO-mk3.5 and MPI-echam5 perhaps because of their higher spatial resolution, show the best performances and are then more appropriate than the two other models for determining onset, retreat and length of the rainy season over Cameroon and neighbouring areas. The low spatial resolution of BCCR-bcm2.0 and MRI-cgcm2.3.2a may have contributed to their poor results in most cases. For future climate (2082–2098) and according to three of the four models results, onset and retreat dates are expected in most cases to be later by about 1 pentad (5 days) than in the present climate. The CSIRO-mk3.5 and BCCR-bcm2.0 models are not part of the consensus for onset and retreat dates respectively. As for the duration of the rainy season, an increase of approximately 1 pentad (5 days) is expected in zone 3 and a decrease of the same range elsewhere. MPI-echam5 in zone 3 and CSIRO-mk3.5 in zones 1 and 2 however disagree.

The results of this study reveal that high spatial resolutions seem to positively impact simulations of general circulation models. This point to the need in future investigations to assess the performances of regional climate model. Being able to predict onset and retreat dates within days would be of more benefit to local farmers. Also recasting results in terms of probabilities is necessary to evaluate risks of false starts of rain which are problematic for sowing season (Hess *et al*., 1995).

Acknowledgements

Many thanks to the National Meteorological Services of Cameroon (DNMC) for providing observed daily precipitations data. Many more thanks also go to the following: the modelling groups for making their model output available for analysis, the Program for Climate Model Diagnosis and Inter-comparison (PCMDI) for collecting and archiving this data, and the WCRP's Working Group on Coupled Modelling (WGCM) for organizing the model data analysis activity. The WCRP CMIP3 multi-model dataset is supported by the Office of Science, U.S. Department of Energy. We are also grateful to the anonymous reviewers who helped improve the content, grammar and syntax of this manuscript.

References

Adejuwon JO. 2006. Variability and the severity of the little dry season in Southwestern Nigeria. *Journal of Climate* **19**: 483–493.

Adejuwon JO, Balogun EE, Adejuwon SA. 1990. On the annual and seasonal patterns of rainfall fluctuations in Sub-Saharan West-Africa. *International Journal of Climatology* **10**: 839–848.

Ati OF, Stigter CJ, Oladipo EO. 2002. A comparison of methods to determine the onset of the growing season in Northern Nigeria. *International Journal of Climatology* **22**: 731–742.

Ayoade JO. 1974. A statistical analysis of rainfall over Nigeria. *Journal of Tropical Geography* **39**: 11–23.

Benoit P. 1977. The start of the growing season in Northern Nigeria. *Agricultural Meteorology* **18**: 91–99.

Cook K, Vizy E. 2006. Coupled model simulations of the West African monsoon system: twentieth- and twenty-first-century simulations. *Journal of Climate* **19**: 3681–3703.

Errasti I, Ezcurra A, Sáenz J, Ibarra-Berastegi G. 2011. Validation of IPCC AR4 models over the Iberian Peninsula. *Theoretical and Applied Climatology* **103**: 61–79.

Furevik T, Bentsen M, Drange H, Kvamsto N, Sorteberg A. 2003. Description and evaluation of the Bergen climate model: ARPEGE coupled with MICOM. *Climate Dynamics* **21**: 27–51.

Gordon HB, Rotstayn LD, McGregor JL, Dix MR, Kowalczyk EA, O'Farrell SP, Waterman LJ, Hirst AC, Wilson SG, Collier MA, Watterson IG, Elliott TI. 2002. *The CSIRO Mk3 Climate System Model [Electronic publication].* CSIRO Atmospheric Research: Aspendale (CSIRO Atmospheric Research technical paper; no. 60), 130 pp.

Hess TM, Stephens W, Maryah UM. 1995. Rainfall trends in the north east arid zone of Nigeria 1961–1990. *Agricultural and Forest Meteorology* **74**: 87–97.

Ilesanmi OO. 1972a. An ampirical formulation of the onset, advance and retreat of rainfall in Nigeria. *Journal of Tropical Geography* **34**: 17–24.

Ilesanmi OO. 1972b. Aspect of the precipitation climatology of the July–August rainfall minimum of southern Nigeria. *Journal of Tropical Geography* **35**: 51–59.

IPCC. 2001. *The Scientific Basis*. Contribution of Working Group I to the Third Assessment Report of the Intergovernmental Panel on Climate Change, In Houghton JT, Ding Y, Griggs DJ, Noguer M, VanderLinden PJ, Dai X, Maskell K, Jhonson CA (eds). Cambridge University Press: Cambridge, UK; p. 881.

Meehl GA, Covey C, Delworth T, Latif M, McAvaney B, Mitchell JFB, Stouffer RJ, Taylor KE. 2007. The WCRP CMIP3 multi-model dataset: a new era in climate change research. *Bulletin of the American Meteorological Society* **88**: 1383–1394.

Mkankam KF. 2000. Validation of general circulation climate models and projections of temperature and rainfall changes in Cameroon and some of its neighboring areas. *Theoretical and Applied Climatology* **67**: 97–107.

Mugalavai EM, Kipkorir EC, Raes D, Rao MS. 2008. Analysis of rainfall onset, cessation and length of growing season for western Kenya. *Agricultural and Forest Meteorology* **148**: 1123–1135.

Ndomba PM. 2010. Development of rainfall curves for crops planting dates: a case study of Pangani River Basin in Tanzania. *Nile Basin Water Science and Engineering Journal* **3**: 13–27.

Odekunle TO. 2004. Rainfall and the length of the growing season in Nigeria. *International Journal of Climatology* **24**: 467–479.

Odekunle TO. 2006. Determining rainy season onset and retreat over Nigeria from precipitation amount and number of rainy days. *Theoretical and Applied Climatology* **83**: 193–201.

Odekunle TO, Balogun EE, Ogunkoya OO. 2005. On the prediction of rainfall onset and retreat dates in Nigeria. *Theoretical and Applied Climatology* **81**: 101–112.

Olaniran OJ. 1983a. The onset of the rains and the start of the growing season in Nigeria. *Nigerian Geographical Journal* **26**(1 and 2): 81–88.

Olaniran OJ. 1983b. The monsoon factor and the seasonality of rainfall distribution in Nigeria. *Malaysian Journal of Tropical Geography* **7**: 38–45.

Olaniran OJ. 1989. A study of climatic variability in Nigeria based on the onset, retreat, and length of the rainy season. *International Journal of Climatology* **9**: 253–269.

Omotosho JB. 1990a. Onset of thunderstorms and precipitation over Northern Nigeria. *International Journal of Climatology* **10**: 849–860.

Omotosho JB. 1990b. Synoptic meteorology: pathway to seasonal rainfall prediction for sustainable agriculture and effective water resource management in West Africa but Nigeria in particular. *Journal of the Nigerian Meteorological Society (NMS)* **3**(2): 81–86.

Omotosho JB. 1992. Long-range prediction of the onset and end of the rainy season in the West African Sahel. *International Journal of Climatology* **12**: 369–382.

Omotosho JB. 2002. Synoptic meteorology: pathway to seasonal rainfall prediction for sustainable agriculture and effective water resources management in West Africa but Nigeria in particular. *Journal of the Nigerian Meteorological Society* **3**: 81–89.

Penlap KE, Matulla C, Storch HV, Mkankam Nkamga F. 2004. Downscaling of GCM scenarios to assess precipitation changes in the little rainy season (March–June) in Cameroon. *Climate Research* **26**: 85–96.

Roeckner E, Arpe K, Bengtsson L, Christoph M, Claussen M, Dumenil L, Esch M, Giorgetta M, Schlese U, Schulzweida U. 1996. The atmospheric general circulation model ECHAM4: model description and simulation of present day climate. Max Planck Institute for Meteorology, Report No.218, Hamburg, Germany, 90 pp.

Salack S, Muller B, Gaye AT. 2011. Rain-based factors of high agricultural impacts over Senegal. Part I. Integration of local to sub-regional trends. *Theoretical and Applied Climatology* **106**: 1–22, DOI: 10.1007/s00704-011-0414-z.

Stewart JL. 1991. Principle and performance of response farming. In *Climatic Risk in Crop Production. Models and Management for the Semi-Arid Tropics and Sub-Tropics*, Ford W, Muchow RC, Bellamy ZA (eds). CAB International: Wallingford.

Syed FS, Yoo JH, Körnich H, Kucharski F. 2010. Are intraseasonal summer rainfall events micro monsoon onsets over the western edge of the South-Asian monsoon? *Atmospheric Research* **88**: 341–346.

Yukimoto S, Noda A, Kitoh A, Hosaka M, Yoshimura H, Uchiyama T, Shibata K, Arakawa O, Kusunoki S. 2006. Present-day climate and climate sensitivity in the Meteorological Research Institute Coupled GCM Version 2.3 (MRI-CGCM2.3). *Journal of the Meteorological Society of Japan* **84**: 333–363.

JOBNAME: JAM 00#00 2014 PAGE: 1 SESS: 8 OUTPUT: Tue Sep 2 04:21:49 2014 Total No. of Pages: 15
/ams/jam/0/jamCD140032

Journal of Applied Meteorology and Climatology (Proof Only)

Computation of the Standardized Precipitation Index (SPI) and Its Use to Assess Drought Occurrences in Cameroon over Recent Decades

AU1 GUY MERLIN GUENANG AND F. MKANKAM KAMGA

Laboratory for Environmental Modelling and Atmospheric Physics, University of Yaoundé 1, Yaoundé, Cameroon

(Manuscript received 16 January 2014, in final form 22 July 2014)

ABSTRACT

The standardized precipitation index (SPI) is computed and analyzed using 55 years of precipitation data recorded in 24 observation stations in Cameroon along with University of East Anglia Climate Research Unit (CRU) spatialized data. Four statistical distribution functions (gamma, exponential, Weibull, and lognormal) are first fitted to data accumulated for various time scales, and the appropriate functions are selected on the basis of the Anderson–Darling goodness-of-fit statistic. For short time scales (up to 6 months) and for stations above 10°N, the gamma distribution is the most frequent choice; below this belt, the Weibull distribution predominates. For longer than 6-month time scales, there are no consistent patterns of fitted distributions. After calculating the SPI in the usual way, operational drought thresholds that are based on an objective method are determined at each station. These thresholds are useful in drought-response decision making. From SPI time series, episodes of severe and extreme droughts are identified at many stations during the study period. Moderate/severe drought occurrences are intra-annual in short time scales and interannual for long time scales (greater than 9 months), usually spanning many years. The SPI calculated from CRU gridded AU2 precipitation shows similar results, with some discrepancies at longer scales. Thus, the spatialized dataset can be used to extend such studies to a larger region—especially data-scarce areas.

1. Introduction

Agriculture is the main socioeconomic activity in sub-Saharan African countries. According to Tarhule et al. (2009), about 95% of the used land is devoted to agriculture, which is the main occupation of about 65% of the population. Good crop development depends on the needed level of soil water reserve provided by precipitation. Perturbations of the hydrological cycle in response to climate change may involve perturbations of the frequency and intensity of precipitation and then directly affect the availability and quality of freshwater (Pal and Al-Tabbaa 2011). Should there be severe or recurrent droughts, major environmental and economic damage would result, with negative impacts such as soil degradation, decrease in agricultural production, and less hydroelectric energy production. Severe droughts were recorded in the Sahel region during the 1970s and 1980s and in many countries of the Horn of Africa, where they were more frequent, and the situation has persisted up to the first decade of the twenty-first century (Kandji et al. 2006). The sad consequences are usually widespread starvation and death (Druyan 2011; UNEP 2002). Therefore, there is the need to better understand droughts and to study their temporal and spatial variabilities under the current and future perturbed climate so as to guide vulnerability and adaptation assessments and measures.

Droughts are apparent after a long period with a shortage of precipitation or without any precipitation (Vicente-Serrano et al. 2010). Many definitions and related mathematical tools for their quantification have been developed. Among the most widely used are the traditional Palmer drought severity index (PDSI; Palmer 1965) and the standardized precipitation index (SPI; McKee et al. 1993). The PDSI is a soil moisture algorithm that includes terms for water storage and evapotranspiration, whereas the SPI is a probability index that is based solely on precipitation. It was formulated by McKee et al. (1993) to give a better representation of abnormal wetness and dryness than does the PDSI. The SPI can be defined as the number of standard deviations by which a normally distributed

Corresponding author address: G. M. Guenang, Laboratory for Environmental Modelling and Atmospheric Physics, Dept. of Physics, University of Yaoundé 1, P.O. Box 812 Yaoundé, Cameroon.
E-mail: merlin.guenang@yahoo.fr

DOI: 10.1175/JAMC-D-14-0032.1

JOBNAME: JAM 00#00 2014 PAGE: 2 SESS: 8 OUTPUT: Tue Sep 2 04:21:49 2014 Total No. of Pages: 15
/ams/jam/0/jamCD140032

random variable deviates from its long-term mean. For precipitation, it is mostly used to quantify deficits (droughts) on many time scales. The SPI has many advantages over the PDSI (Hayes et al. 1999). It depends only on precipitation and can be used for both dry and rainy seasons. It can describe drought conditions that are important for a range of meteorological, agricultural, and hydrological applications. Studies have shown that the SPI is suitable for quantifying most types of drought events (Bussay et al. 1998; Szalai and Szinell 2000). Calculated at various time scales (from 1 to n months), SPI values can be efficient for the description of streamflow (on 2–6-month time scales), agricultural drought (on 2–3-month time scales), and groundwater level (on 5–24-month time scales) (Lloyd-Hughes and Saunders 2002). Some workers have stated that, because it depends only on precipitation, the SPI is not affected by topography (Hayes et al. 1999; Lloyd-Hughes and Saunders 2002; Lana et al. 2001).

In recent decades, many studies using the SPI were undertaken. Using the SPI extended to the Northern Hemisphere, Bordi and Sutera (2001) showed that there are some interesting spatially remote teleconnections that link the tropical Pacific Ocean with the European area. Lloyd-Hughes and Saunders (2002) found that trends in SPI values indicate significant change in the proportion of Europe experiencing extreme and/or moderate drought conditions during the twentieth century. SPI analysis satisfactorily explained the recurrent floods in the past 25 years that have affected the southern Cordoba Province in Argentina (Seiler et al. 2002). Livada and Assimakopoulos (2007) used the SPI to detect spatial and temporal drought events over Greece and found mild to moderate drought reduction from north to south and from west to east on 3- and 6-month time scales over the 51-yr time period of the study. In that study, the frequency of occurrence of severe and extreme drought conditions was very low on the 12-month time scale. The SPI was also used in China to study drought/wetness episodes in the Pearl River basin, and the results were helpful for basin-scale water resource management under a changing climate (Zhang et al. 2009). Thus, the SPI is widely used (Vicente-Serrano 2006). Its main weaknesses are dependence on the normalization procedure (the probability density function used) (Quiring 2009) and poor definition in arid regions that experience many months with zero precipitation (Wu et al. 2007). For Africa in particular, there are only a few studies on drought monitoring by use of climate indices. Ntale and Gan (2003) used the SPI as a drought indicator in the East African region and compared its performance with the PDSI and the Bhalme–Mooley index. The identification of droughts in Zimbabwe by Manatsa et al. (2008) on the basis of SPI estimation from the regionally averaged rainfall for 1900–2000 revealed that the most extreme droughts of the twentieth century were recorded in 1991 and 1992. Yuan et al. (2013) more recently used dynamical models to obtain probabilistic seasonal drought forecasts in Africa. This low number of past studies is one of the motivations of the current study.

In many studies that use the SPI, the gamma distribution is found to fit the precipitation data very well (Lloyd-Hughes and Saunders 2002) and to provide the best model for describing monthly precipitation. In the study over Cameroon that is presented here, we will go through the full process of distribution selection by fitting many distribution functions to the data and will use an appropriate statistical test to select the best fit for calculating the SPI at time scales of 3, 6, 12, 18, and 24 months. This selection is carried out at every station and at grid points for recorded and gridded University of East Anglia (United Kingdom) Climatic Research Unit (CRU) data. The ultimate purpose is to provide useful information for monitoring and managing water resources in agriculture, domestic/industrial uses, and hydroelectric energy production. The study can also help to understand better the historical variability of drought events and their relative intensity. We will also evaluate the usefulness of a spatialized dataset (CRU gridded precipitation) in reproducing station results and thus guide their use in areas without measuring stations. This paper is organized as follows: In the next section, the study area and data used are described. Section 3 gives details of SPI calculation and statistical distribution functions used to fit the data. Section 3f describes the method. Results are presented in section 4, and the paper ends with discussion and concluding remarks in section 5.

2. Study domain and data used

a. Study domain

Cameroon is located in equatorial central Africa between 1° and 13°N and between 7° and 18°E. The southern part of the country is bordered in the west by the Atlantic Ocean and is covered by dense rain forest. The northern part has a dry to arid Sahelian-type climate, depending on latitude. The main economic activity in the area is agriculture, generally at the subsistence level. Cassava, corn, yam, sweet potato, and millet are grown for food. Cacao, coffee, banana, rubber, palm oil, and cotton are the main cash crops raised by farmers. Logging is another important resource in Cameroon, with heavy timber exportation. These activities are mostly rainfed, and the use of irrigation is very marginal.

JOBNAME: JAM 00#00 2014 PAGE: 3 SESS: 8 OUTPUT: Tue Sep 2 04:21:49 2014 Total No. of Pages: 15
/ams/jam/0/jamCD140032

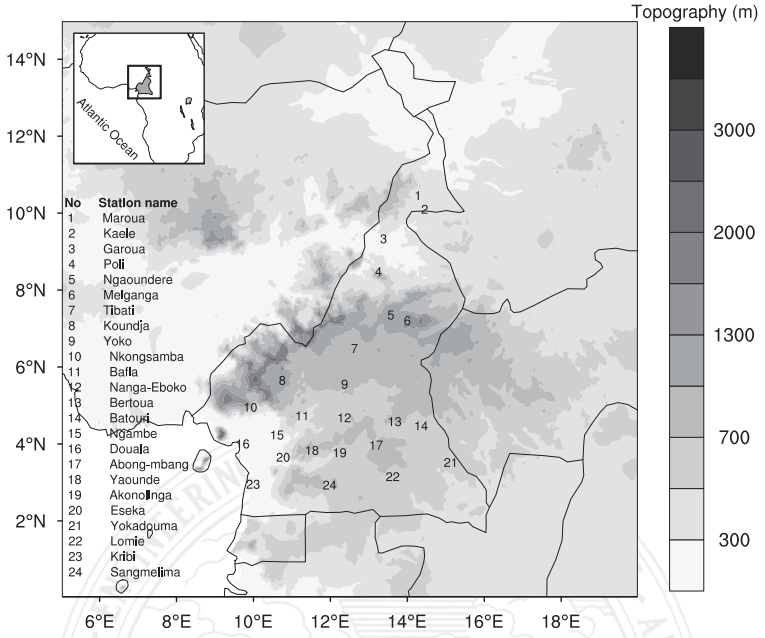

FIG. 1. Study area with the geographical locations of rainfall stations (indicated by numbers). The topography is shaded.

b. *Data used*

Monthly precipitation data used in this study derive from daily precipitation of 24 measuring stations in Cameroon as provided by the Cameroon Meteorological Service. The geographical positions of these stations and the topography of the domain are shown in Fig. 1. The precipitation record extends from 1951 to 2005 (55 yr). Part of this dataset was used by Penlap et al. (2004) and more recently by Guenang and Mkankam Kamga (2012). Overall, approximately 8.6% of the values are missing. One station (Nkongsamba) has no missing values, nine (Douala, Meiganga, Kribi, Ngaoundéré, Koundja, Bertoua, Poli, Yaoundé, and Garoua) have fewer than 4% of values that are missing, and seven (Abong-Mbang, Yokadouma, Sangmélima, Batouri, Yoko, Ngambe, and Lomié) are missing between 4% and 11% of their values. Gridded precipitation data from the CRU were also used to calculate the SPI on the study domain. Since many stations of the domain were used in the construction of the CRU gridded precipitation, these two datasets are not independent (New et al. 1999, 2000). Version 3.0 of the CRU precipitation data (Harris et al. 2014) is available at a monthly time scale on 0.5° × 0.5° longitude/latitude spatial grids. These data are unrestricted and at the time of writing were available for download from the Internet (http://badc.nerc.ac.uk/data/cru/).

3. Method

a. *Calculation procedure for the SPI*

The method used for SPI computation was developed by McKee et al. (1993) and Edwards and McKee (1997) to study relative departures of precipitation from normality. It has been widely applied in many studies (Vicente-Serrano 2006; Vicente-Serrano et al. 2010). It uses monthly precipitation aggregates at various time scales (1, 3, 6, 12, 18, and 24 months, etc.). As an illustration of the procedure, for a 3-month time scale, the precipitation accumulation from month $j - 2$ to month j is summed and attributed to month j. At this time scale, the first two months of the data time series are missing. Next follows the normalization procedure, in which an appropriate probability density function is first fitted to the long-term time series of aggregated precipitation. Then the fitted function is used to calculate the cumulative distribution of the data points, which are finally transformed into standardized normal variates. This procedure is repeated for all needed time scales. Because the processes that generate rainfall in our study domain vary in time and in space, many distributions may be needed to cover all time scales and stations. The maximum-likelihood (ML) estimation method was used to fit four probability distribution functions (i.e., gamma,

JOBNAME: JAM 00#00 2014 PAGE: 4 SESS: 8 OUTPUT: Tue Sep 2 04:21:50 2014 Total No. of Pages: 15
/ams/jam/0/jamCD140032

TABLE 1. Drought classification by SPI value and USDM drought definition.

Drought classification by SPI value		USDM drought definition (Svoboda et al. 2002)		
SPI value	Class	Category	Description	Percentile
2.00 or more	Extremely wet	—	—	—
1.50–1.99	Severely wet	—	—	—
1.00–1.49	Moderately wet	—	—	—
0–0.99	Mildly wet	—	—	—
From 0 to −0.99	Mild drought	D0	Abnormally dry	21%–30%
From −1.00 to −1.49	Moderate drought	D1	Moderate drought	11%–20%
From −1.50 to −1.99	Severe drought	D2	Severe drought	6%–10%
−2 or less	Extreme drought	D3	Extreme drought	3%–5%
—	—	D4	Exceptional drought	<2%

exponential, Weibull, and lognormal) to each time series. The one with the lowest value of the Anderson–Darling goodness-of-fit test statistic (Anderson and Darling 1952, 1954) was retained as representing the underlying distribution of the data.

b. SPI interpretation and operational drought definition

The SPI, often called the z score, is the number of standard deviations from the mean at which an event occurs. Thus, the 3-month SPI value provides a comparison of accumulated precipitation over that specific 3-month period with the mean precipitation total for the same annual period as calculated over the full study period. This applies to any n-month SPI value, where n, the number of months of accumulation, is the time scale. For precipitation, high positive values correspond to wet sequences and high negative values correspond to drought periods. For drought evaluation (negative SPI), short time scales on the order of 3 months may be important for agricultural applications, whereas long time scales of up to many years are of more interest in water-supply management (Guttman 1998). Many classifications of dryness and wetness events as based on the SPI have been proposed in the literature. An example is shown in Table 1 (Lloyd-Hughes and Saunders 2002). To use indices such as the SPI for operational monitoring, it is necessary to define drought threshold levels for preventive or corrective actions. Goodrich and Ellis (2006) proposed using preselected percentiles of the index to determine thresholds, as based on fitted empirical distributions. Quiring (2009) improved on the technique by using percentile values from distributions fitted to the data to define more-objective drought levels. Table 1 (columns 1 and 2) also shows the five-category drought definition from the U.S. Drought Monitor (USDM), with their description and corresponding percentiles (Svoboda et al. 2002). Here, we use the Quiring technique (Quiring 2009) and the percentile intervals of this table to determine drought in our domain.

c. The ML estimation method

The ML estimation method maximizes the probability of the observed data under a selected distribution. Applied to a dataset, it provides values of the distribution parameters that maximize the likelihood function (Wilks 2006).

Let x_i $(i = 1, \ldots, n)$ be a sample of n independent and identically distributed observations coming from a population with an underlying probability density function $f(.\,|\,\theta_0)$, where θ_0 is the unknown distribution parameter. It is desirable to find an estimator $\hat{\theta}$ that would be as close to the true value θ_0 as possible.

The joint density function for an independent and identically distributed sample is defined as

$$f(x_1, x_2, \ldots, x_n\,|\,\theta) = f(x_1\,|\,\theta) \times f(x_2\,|\,\theta) \times \cdots \times f(x_n\,|\,\theta). \tag{1}$$

If x_i are fixed parameters of this function and θ is the function's variable that is allowed to vary freely, then the function will be called the likelihood function:

$$\mathcal{L}(\theta\,|\,x_1, \ldots, x_n) = f(x_1, x_2, \ldots, x_n\,|\,\theta) = \prod_{i=1}^{n} f(x_i\,|\,\theta). \tag{2}$$

In practice, the log-likelihood is more convenient. It is the logarithm of the likelihood function so that

$$\ln\mathcal{L}(\theta\,|\,x_1, \ldots, x_n) = \sum_{i=1}^{n} \ln f(x_i\,|\,\theta). \tag{3}$$

The average log-likelihood can also be used:

$$\hat{\ell} = n^{-1} \ln\mathcal{L}. \tag{4}$$

The term $\hat{\ell}$ estimates the expected log-likelihood of a single observation in the model. The ML method estimates θ_0 by finding a value of θ that maximizes $\hat{\ell}(\theta\,|\,x)$.

JOBNAME: JAM 00#00 2014 PAGE: 5 SESS: 8 OUTPUT: Tue Sep 2 04:21:50 2014 Total No. of Pages: 15
/ams/jam/0/jamCD140032

d. Distributions used to fit the data

1) THE GAMMA DISTRIBUTION FUNCTION

The probability density function of the gamma distribution is defined as

$$g(x) = \frac{1}{\beta^{\alpha}\Gamma(\alpha)} x^{\alpha-1} e^{-x/\beta} \quad \text{for} \quad x > 0, \tag{5}$$

where $\alpha > 0$ is a shape parameter, $\beta > 0$ is a scale parameter, $x > 0$ is the amount of precipitation, and $\Gamma(\alpha)$ is the gamma function. More detailed descriptions of the gamma distribution can be found in Lloyd-Hughes and Saunders (2002) and Guttman (1999).

To fit the distribution parameters, α and β are estimated from the sample data. Using the approximation for ML defined by Thom (1958), they can be estimated as

$$\hat{\alpha} = \frac{1}{4A}\left(1 + \sqrt{1 + \frac{4A}{3}}\right) \quad \text{and} \tag{6}$$

$$\hat{\beta} = \bar{x}/\hat{\alpha}, \tag{7}$$

where $\bar{x}$ is mean precipitation and A is given by

$$A = \ln(\bar{x}) - n^{-1}\sum \ln(x). \tag{8}$$

Under some conditions, α and β can be better estimated by using an iterative procedure as suggested by Wilks (1995).

For a given month and time scale, the cumulative probability $G(x)$ of an observed amount of precipitation is given by

$$G(x) = \frac{1}{\hat{\beta}^{\hat{\alpha}}\Gamma(\hat{\alpha})} \int_0^x x^{\hat{\alpha}} e^{-x/\hat{\beta}}\, dx. \tag{9}$$

Letting $t = x/\hat{\beta}$, we reduce the expression to the following function, called the incomplete gamma function:

$$G(x) = \frac{1}{\Gamma(\hat{\alpha})} \int_0^x t^{\hat{\alpha}-1} e^{-1}\, dt. \tag{10}$$

The gamma distribution is not defined for $x = 0$, and, the probability of zero precipitation $q = P(x = 0)$ being positive, the cumulative probability becomes

$$H(x) = q + (1 - q)G(x). \tag{11}$$

2) THE EXPONENTIAL DISTRIBUTION FUNCTION

The general formula for the probability density function of the exponential distribution is stated as (Ahmad and Bhat 2010)

$$f(x) = \frac{1}{\beta} e^{-(x-\mu)/\beta} \quad \text{for} \quad x \geq \mu \quad \text{and} \quad \beta > 0, \tag{12}$$

where μ is the location parameter and β is the scale parameter. The scale parameter is often referred to as $\lambda = 1/\beta$ and is called the constant failure rate. The terms μ and β can be estimated from an independent and identically distributed sample $x = (x_1, \ldots, x_n)$ drawn from the variable using the ML estimation method (Ross 2009):

$$\hat{\lambda} = 1/\bar{x}, \tag{13}$$

where

$$\bar{x} = n^{-1} \sum_{i=1}^{n} x_i.$$

3) THE LOGNORMAL DISTRIBUTION FUNCTION

In probability theory, a positive random variable x follows the lognormal (μ, σ^2) distribution if the logarithm of the random variable is normally distributed. The probability density function of a lognormal distribution is defined as (Bartosova 2006; Bilkova 2012)

$$f(x; \mu, \sigma) = \frac{1}{x\sigma\sqrt{2\pi}} \exp\left[-\frac{(\ln x - \mu)^2}{2\sigma^2}\right], \quad x > 0, \tag{14}$$

where $x > 0$, $-\infty < \mu < +\infty$, and $\sigma > 0$. The term μ is the scale parameter that stretches or shrinks the distribution, and σ is the shape parameter that affects the shape of the distribution. They can be determined by the ML estimators:

$$\hat{\mu} = n^{-1} \sum_k \ln x_k \quad \text{and} \tag{15}$$

$$\hat{\sigma}^2 = n^{-1} \sum_k (\ln x_k - \hat{\mu})^2. \tag{16}$$

4) THE WEIBULL DISTRIBUTION FUNCTION

The probability density function of a Weibull random positive variable x is (Wu 2002; Panahi and Asadi 2011)

$$f(x; \alpha, \beta) = \alpha\beta x^{\alpha-1} e^{-\beta x^{\alpha}}, \tag{17}$$

where α and β are the shape and scale parameters, respectively. Its complementary cumulative distribution function is a stretched exponential function. The Weibull distribution is related to a number of other probability distributions; in particular, it interpolates between the exponential distribution ($k = 1$) and the Rayleigh distribution ($k = 2$). There are no closed-form expressions of the parameters $\hat{\alpha}$ and $\hat{\beta}$, and therefore

JOBNAME: JAM 00#00 2014 PAGE: 6 SESS: 8 OUTPUT: Tue Sep 2 04:21:51 2014 Total No. of Pages: 15
/ams/jam/0/jamCD140032

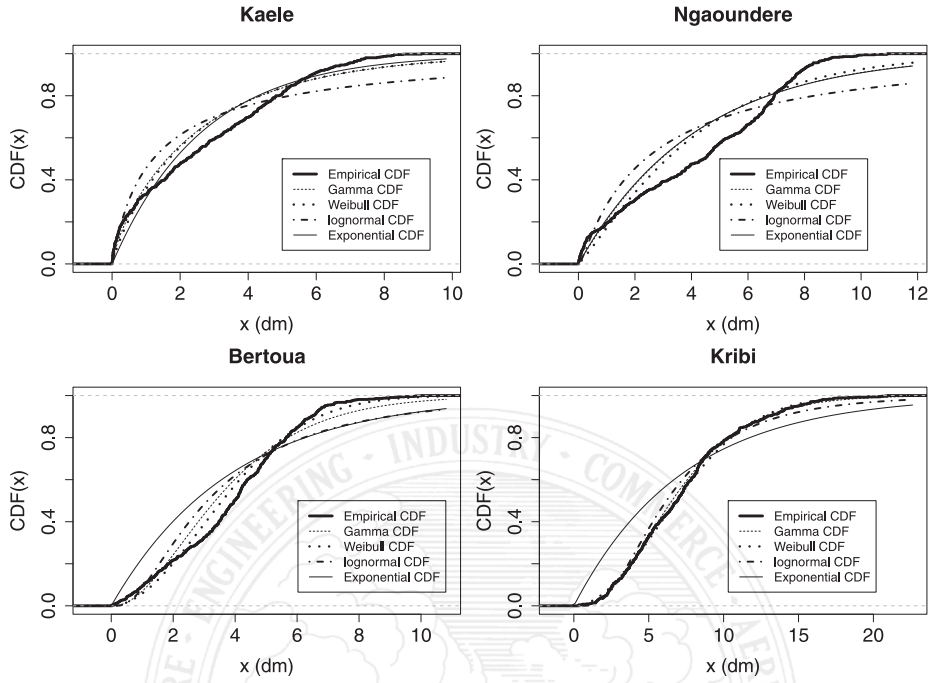

FIG. 2. Cumulative distribution functions for 3-month aggregated precipitation showing the empirical cumulative distribution function and gamma, Weibull, lognormal, and exponential distributions fitted to the data.

they are estimated by maximizing the log-likelihood expression of Eq. (3) (Panahi and Asadi 2011).

e. Statistical tests used

1) THE ANDERSON AND DARLING STATISTICAL TEST

The Anderson–Darling statistic A^2 measures how well a given data sample X_i ($i = 1, \ldots, n$) follows a particular distribution function F. The statistic is defined as (Anderson and Darling 1952, 1954)

$$A^2 = -n - n^{-1} \sum_{i=1}^{n} (2i-1)\{\ln[F(X_i)] + \ln[1 - F(X_{n+1-i})]\}. \quad (18)$$

For a given dataset and distribution function, the better that the distribution fits the data, the smaller this statistic will be. The hypothesis regarding the distributional form is rejected at the chosen significance level α if the test statistic A^2 is greater than the critical value obtained from a table.

2) THE KOLMOGOROV–SMIRNOV GOODNESS OF FIT

The Kolmogorov–Smirnov (K–S) test is a nonparametric test that can be used to compare a sample with a reference probability distribution or to compare two samples. It quantifies a distance between the empirical distribution function of the sample and the cumulative distribution function of the reference distribution or between the empirical distribution functions of two samples.

For a given cumulative distribution function $F(x)$, the K–S statistic is defined as (Stephens 1970)

$$D_n = \max_x |F_n(x) - F(x)|, \quad (19)$$

where n is the number of observations in the population x, $F_n(x)$ is the empirical cumulative distribution function, and $F(x)$ is the theoretical cumulative distribution function. The K–S test can be modified to serve as a goodness-of-fit test. In the special case of testing for normality of the distribution, samples are standardized and are compared with a standard normal distribution.

f. Study steps

SPI time series were calculated for all stations and for the CRU grid point nearest to each station. This procedure is expected to lead to normally distributed SPI, but this is not always the case. Since the Quiring technique (Quiring 2009) requires fitting a statistical distribution to the SPI, five distributions including the normal were tested, and then the K–S goodness-of-fit test

JOBNAME: JAM 00#00 2014 PAGE: 7 SESS: 8 OUTPUT: Tue Sep 2 04:21:51 2014 Total No. of Pages: 15
/ams/jam/0/jamCD140032

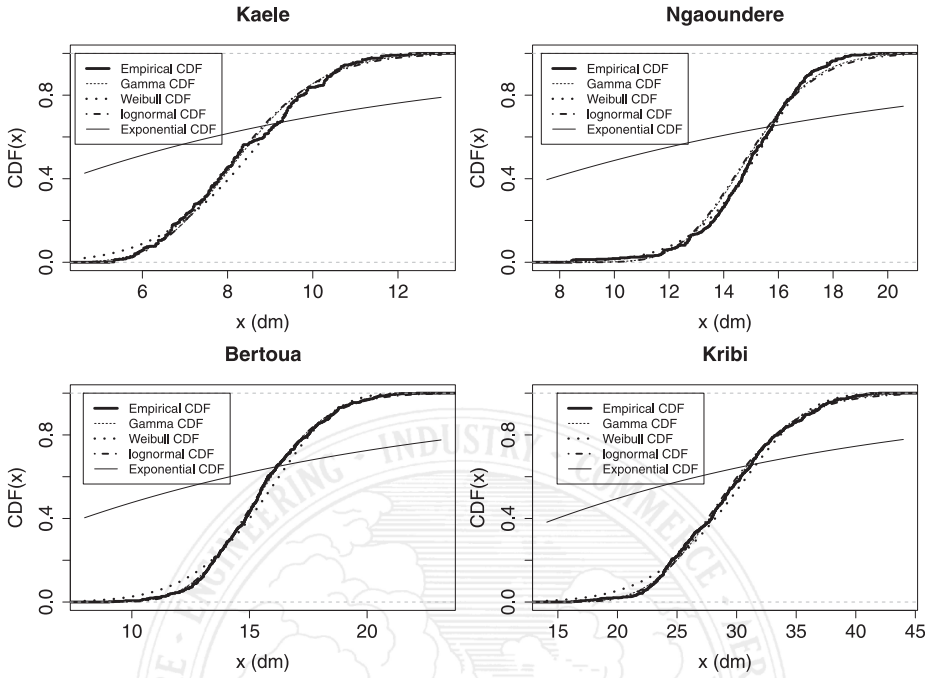

FIG. 3. As in Fig. 2, but for 12-month aggregated precipitation.

statistic was used at the 5% significant level. In almost all instances, the Weibull and normal distributions had the lowest (and also close) K–S test statistics. Operational drought thresholds were therefore calculated on the basis of the normal distribution and on percentiles defined by Svoboda et al. (2002) (Table 1). Analyses of the results focused on four stations (Kaélé, Ngaoundéré, Bertoua, and Kribi), one in each of four different known climatic zones of the study domain. These zones are characterized by similar rain and physical atmospheric processes. Each station has the least amount of missing data in its zone. The station of Kaélé is located north of the domain in the Sahelian zone, Ngaoundéré is in the Adamawa Plateau is in the middle part of the domain, Bertoua is in the eastern part in dense forest, and Kribi is in the southwestern part closest to the Atlantic Ocean (Fig. 1).

4. Results

a. *Suitable distribution functions for precipitation data*

1) DISTRIBUTION FUNCTIONS FOR STATION PRECIPITATION

Four statistical distribution functions (gamma, exponential, Weibull, and lognormal) were fitted to station precipitation data aggregated at various time scales. Figures 2 and 3 show results of the cumulative distribution function for empirical precipitation and for each of the trial distribution functions. Figures were shown for four stations (Kaélé, Ngaoundéré, Bertoua, and Kribi) at 3- and 12-month time scales. The choice of the suitable distribution function describing precipitation data in each case was based on the minimum value of the Anderson–Darling statistic, as illustrated in Table 2 for 3- and 12-month time scales. The exponential function shows worse results as the number of months in the time scale increases. Table 3 recapitulates these results, extended to other stations and to various time scales. The functions are represented by letters [i.e., gamma (g), Weibull (w), exponential (e), and logormal (ln)]. It appears that, for time scales equal to 6 months and less, the distribution of station precipitation shows a bias for the Weibull function to be suitable for the highest number of stations (21 for both 1- and 3-month time scales and 16 for 6-month time scale) of the 24 studied stations. The gamma function outperformed the others in very few cases. One exceptional case of exponential and lognormal being best is observed for 1- and 6-month time scales, respectively. Above the 6-month time scale, the number of station precipitation distributions being best fitted by the

JOBNAME: JAM 00#00 2014 PAGE: 8 SESS: 8 OUTPUT: Tue Sep 2 04:21:52 2014 Total No. of Pages: 15
/ams/jam/0/jamCD140032

TABLE 2. Anderson–Darling test statistics calculated at 95% confidence level for the four distributions and two time scales; the distribution function key is given in the text. The smallest value at each station is in boldface.

		For 3-month time scale				For 12-month time scale			
No.	Station	g	w	e	ln	g	w	e	ln
1	Maroua	**8.12**	9.24	11.16	18.72	1.48	9.45	184	**1.13**
2	Kaélé	**8.91**	10.20	13.36	21.50	**2.03**	3.84	171	2.22
3	Garoua	13.10	**12.19**	14.08	25.52	1.58	9.31	195.8	**1.04**
4	Poli	18.88	**18.35**	18.58	35.65	**1.08**	3.46	207.7	1.59
5	Ngaoundéré	24.21	**23.20**	24.43	41.22	4.84	**1.36**	218	6.76
6	Meiganga	17.36	**16.08**	18.51	34.30	1.03	6.96	223.9	**0.91**
7	Tibati	19.37	**17.15**	21.09	37.43	**0.72**	3.88	199.8	1.24
8	Koundja	16.22	**12.87**	22.70	35.21	**0.90**	4.35	223.8	1.12
9	Yoko	16.40	**13.01**	23.83	30.83	1.08	5.10	167.9	**0.91**
10	Nkongsamba	8.15	**7.099**	14.15	19.84	**1.20**	3.60	229	1.89
11	Bafia	20.55	**13.62**	45.14	36.81	**1.81**	5.99	200	2.24
12	Nanga-Eboko	12.36	**6.65**	43.15	26.78	4.97	**0.72**	179	6.91
13	Bertoua	15.19	**7.65**	58.47	30.30	**0.47**	5.41	210.8	0.53
14	Batouri	11.48	**6.02**	49.79	21.08	**1.21**	2.68	165.9	1.57
15	Ngambe	5.50	**4.18**	12.81	14.85	**2.35**	3.09	172	2.59
16	Douala	4.62	**4.32**	14.37	10.63	**3.58**	4.15	213	3.9
17	Abong-Mbang	10.99	**5.02**	54.07	22.15	**1.46**	5.78	183	2.03
18	Yaoundé	11.41	**5.69**	58.96	22.46	**0.51**	4.24	217.7	0.96
19	Akonolinga	10.98	**5.58**	56.85	21.06	2.30	**1.43**	186	3.12
20	Eséka	11.61	**5.37**	58.21	22.31	0.81	7.75	183.7	**0.48**
21	Yokadouma	11.51	**5.61**	61.34	20.96	**2.50**	5.82	187	3.67
22	Lomié	8.04	**3.12**	58.36	15.48	**1.03**	8.48	161.7	1.05
23	Kribi	**0.70**	0.84	61.56	4.77	**0.94**	4.24	200	1.15
24	Sangmélima	6.25	**1.63**	70.84	13.34	0.86	10.6	184	**0.56**

Weibull function decreases, falling to three and seven (three stations for 12 and 18 months, and seven for 24 months) to the benefit of the gamma function, which is suitable for up to 18 stations at the 18-month time scale. The number of station precipitation distributions following the lognormal function also increases with the number of months in the time scale, reaching 8 stations of 24.

F4 Figure 4 shows the spatial pattern of the suitable distribution functions over the domain of study for 3- (Fig. 4a), 6-,and 12- (Fig. 4b), and 18- and 24-month (Fig. 4c) time scales. For not more than a 3-month time scale (illustration for 3 months in Fig. 4a), the gamma distribution function is suitable north of the domain (Sahelian region), particularly above 10°N, while below that the Weibull function is the best fit, except for a single case at the boundary of the Atlantic Ocean that shows a bias to the gamma function. The Weibull function remains the most suitable at the 6-month time scale between 4° and 10°N, which represents the transition zone between the Sahelian and equatorial forest zones. Stations of the equatorial forest zone, covering the southern plateau (below 4°N), mostly show a bias for the gamma distribution. At a 12-month time scale and beyond, there is a mixture of gamma, lognormal, and Weibull distributions in different zones, leading to no apparent spatial organized pattern (Figs. 4b,c). The pattern for the 18-month time scale looks more like that of 6 months but with the gamma function in place of the Weibull function. An almost equal number of gamma [(9)], lognormal [(8)], and Weibull [(7)] functions fit the 24-month time scale, with no particular spatial organization. These apparent inconsistencies are due to the fact that in most cases more than one distribution was adequate and the Anderson–Darling statistics may not have been significantly different. Between 18- and 24-month time scales, the number of station data showing a bias for the lognormal function increases up to 8 in the southwestern part of the domain (right of the Atlantic Ocean).

2) DISTRIBUTION FUNCTIONS FOR CRU PRECIPITATION

Distribution functions were also fitted to precipitation time series of the CRU grid point that is nearest to each station of the study domain. The results are in Table 3, where the last column indicates the number of cases of the six time scales analyzed for which the same distribution functions fitted both station and CRU data. The highest number of agreements across time scales between the two datasets is obtained in the southeastern part of the domain (Batouri and Yokadouma stations).

JOBNAME: JAM 00#00 2014 PAGE: 9 SESS: 8 OUTPUT: Tue Sep 2 04:21:54 2014 Total No. of Pages: 15
/ams/jam/0/jamCD140032

TABLE 3. Selected distribution functions for station precipitation data at various time scales. In the last column is the number of times the same distribution fits both the station and the CRU data.

No.	Station	Best distribution for n-month time scale						No. of CRU agreement of six possible
		$n = 1$	$n = 3$	$n = 6$	$n = 12$	$n = 18$	$n = 24$	
1	Maroua	g	g	g	ln	w	g	3
2	Kaélé	g	g	w	g	g	ln	5
3	Garoua	w	w	w	ln	w	g	4
4	Poli	w	w	w	g	g	w	4
5	Ngaoundéré	w	w	w	w	g	w	3
6	Meiganga	w	w	w	ln	g	ln	1
7	Tibati	w	w	w	g	g	w	5
8	Koundja	w	w	w	g	g	g	3
9	Yoko	w	w	w	ln	g	ln	3
10	Nkongsamba	w	w	w	g	g	g	4
11	Bafia	w	w	w	g	g	g	5
12	Nanga-Eboko	w	w	w	w	w	w	3
13	Bertoua	w	w	w	g	g	w	5
14	Batouri	w	w	w	g	g	ln	6
15	Ngambe	e	w	w	g	g	w	4
16	Douala	w	w	w	g	g	ln	5
17	Abong-Mbang	w	w	g	g	g	w	4
18	Yaoundé	w	w	g	g	g	g	2
19	Akonolinga	w	w	g	w	g	g	4
20	Eséka	w	w	g	ln	ln	ln	2
21	Yokadouma	w	w	w	g	g	g	6
22	Lomié	w	w	g	g	g	g	5
23	Kribi	w	g	ln	g	ln	ln	3
24	Sangmélima	w	w	g	ln	ln	ln	3

In three instances, there was agreement on fewer than three time scales, that is, Yaoundé and Eseka in the south and Ngaoundéré on the Adamawa Plateau. Overall, stations and CRU gridded precipitation are mostly fitted by the same functions.

b. Analysis of the SPI for different time scales

1) OPERATIONAL DROUGHT THRESHOLDS

The operational drought thresholds as described in section 3 were calculated for all stations for the five

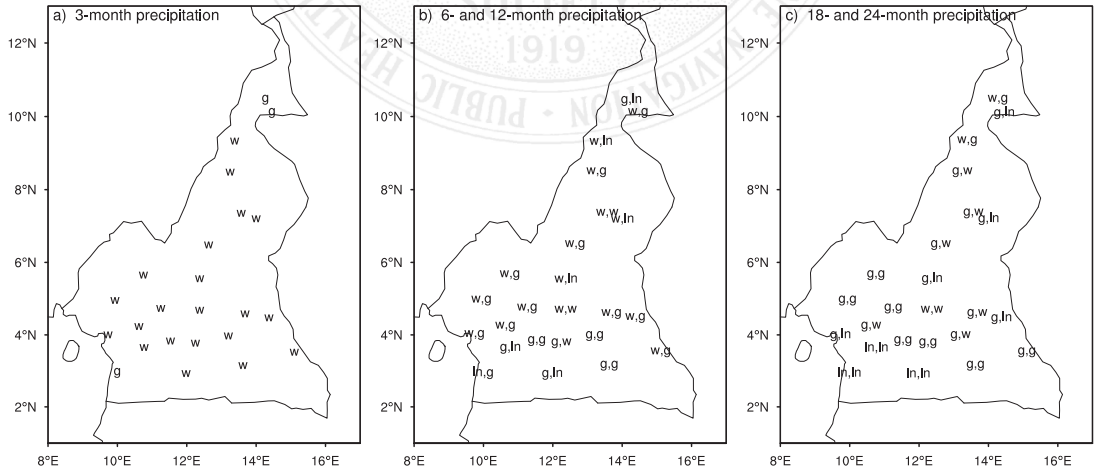

FIG. 4. Spatial pattern of chosen distribution function for (a) 3-month, (b) 6- and 12-month, and (c) 18- and 24-month precipitation; the distribution key is given in the text. In (b) and (c), the first letter refers to the first time scale and the second letter to the second time scale in the figure.

JOBNAME: JAM 00#00 2014 PAGE: 10 SESS: 8 OUTPUT: Tue Sep 2 04:21:57 2014 Total No. of Pages: 15
/ams/jam/0/jamCD140032

TABLE 4. Operational drought thresholds for various time periods and for all stations, calculated using 3- and 12-month SPI.

No.	Station name	Drought category for 3 month					Drought category for 12 month				
		D4	D3	D2	D1	D0	D4	D3	D2	D1	D0
1	Maroua	−2.03	−1.74	−1.5	−1.02	−0.59	−1.64	−1.47	−1.32	−0.94	−0.71
2	Kaélé	−2.08	−1.86	−1.47	−1.04	−0.62	−1.64	−1.47	−1.32	−0.94	−0.71
3	Garoua	−2.25	−1.92	−1.49	−1.09	−0.51	−2.28	−1.61	−1.19	−0.74	−0.48
4	Poli	−2.49	−2.21	−1.58	−0.91	−0.55	−1.64	−1.47	−1.32	−0.94	−0.71
5	Ngaoundéré	−2.55	−2.05	−1.69	−0.93	−0.49	−2.05	−1.63	−1.2	−0.73	−0.47
6	Meiganga	−2.35	−1.9	−1.56	−0.99	−0.54	−1.64	−1.47	−1.32	−0.94	−0.71
7	Tibati	−2.66	−1.99	−1.54	−0.9	−0.47	−1.64	−1.47	−1.32	−0.94	−0.71
8	Koundja	−2.55	−1.83	−1.49	−0.9	−0.45	−1.57	−1.4	−1.24	−0.83	−0.61
9	Yoko	−2.44	−1.91	−1.48	−0.91	−0.45	−1.64	−1.47	−1.32	−0.94	−0.71
10	Nkongsamba	−1.97	−1.64	−1.45	−1.01	−0.55	−1.79	−1.57	−1.17	−0.83	−0.51
11	Bafia	−2.36	−1.94	−1.44	−0.99	−0.32	−1.64	−1.47	−1.32	−0.94	−0.71
12	Nanga-Eboko	−2.27	−1.74	−1.38	−0.9	−0.45	−1.64	−1.47	−1.32	−0.94	−0.71
13	Bertoua	−2.31	−1.77	−1.42	−0.9	−0.41	−1.64	−1.47	−1.32	−0.94	−0.71
14	Batouri	−2.2	−1.74	−1.45	−0.88	−0.5	−1.64	−1.45	−1.28	−0.92	−0.6
15	Ngambe	−1.98	−1.67	−1.37	−1	−0.54	−1.75	−1.61	−1.29	−0.85	−0.59
16	Douala	−1.73	−1.5	−1.31	−0.97	−0.62	−1.76	−1.5	−1.19	−0.9	−0.63
17	Abong-Mbang	−2.18	−1.71	−1.38	−0.84	−0.48	−1.64	−1.47	−1.32	−0.94	−0.71
18	Yaoundé	−2.16	−1.74	−1.45	−0.88	−0.49	−1.64	−1.47	−1.32	−0.94	−0.71
19	Akonolinga	−2.13	−1.7	−1.4	−0.94	−0.47	−1.93	−1.7	−1.44	−0.88	−0.46
20	Eséka	−2.06	−1.78	−1.46	−0.81	−0.46	−2.09	−1.65	−1.32	−0.85	−0.54
21	Yokadouma	−1.97	−1.71	−1.41	−0.91	−0.46	−1.64	−1.47	−1.32	−0.94	−0.71
22	Lomié	−1.94	−1.62	−1.32	−0.9	−0.51	−1.64	−1.47	−1.32	−0.94	−0.71
23	Kribi	−1.82	−1.46	−1.27	−0.83	−0.55	−1.64	−1.47	−1.32	−0.94	−0.71
24	Sangmélima	−1.85	−1.6	−1.24	−0.85	−0.52	−2.05	−1.58	−1.32	−0.85	−0.47

USDM categories of Table 1 (columns 3–5) and for 3- and 12-month time scales. All the values are shown in Table 4. In considering the extreme-drought category D4 for the 3-month time scale, it is seen that there is a range from a maximum of −1.73 in the coastal city of Douala to a minimum of −2.66 in Tibati on the Adamawa Plateau. The spatial distribution of D4 thresholds is coherent, with values of lower than −2.40 on the high grounds of the Adamawa Plateau. Continental stations located between latitudes 2° and 7°N have thresholds between −2.10 and −2.40. In the southern part of the domain and in the coastal area in the southwest, values are higher than −2.0. Values for the three Sahelian stations of Kaélé, Maroua, and Garoua are respectively −2.08, −2.03, and −2.25. At this scale, extreme-drought category D3 follows the general pattern of D4. For the 12-month SPI, most of the stations have a D4 threshold of −1.64, with only three stations below −2.0. From the spatial analysis of category D4, there is no strong dependence on topography, although most stations have very similar thresholds (−1.64) at a 12-month time scale.

2) FREQUENCY OF DROUGHT EVENTS

Objective drought thresholds were also used to examine frequency in the SPI time series. In Fig. 5, appropriate D4-category threshold values are represented by dashed horizontal lines and exceedances corresponding to drought occurrences. For the 3-month SPI (left column in Fig. 5), each station had at least one event with a value that was lower than −3. For the first 25 yr of the study period the four stations differ markedly in D4-category drought frequency (10 in Kaélé, 6 in Kribi, only 2 in Ngaoundéré, and none in Bertoua), whereas in the second half of the period these episodes are more frequent (two stations had 13 events each, and the other two had 8 events each). For the 12-month SPI, all categories of drought events are frequent, especially from the mid-1960s. The dramatic drought episodes of the 1970s and 1980s are clearly visible, with each station recording at least one D4 event. Table 5 summarizes drought occurrences in all categories, with the number of events and the percentage with respect to the total number of time steps in the data. For the 3-month time scale, this percentage is 1%–2% for exceptional droughts and around 5% for extreme droughts. For the 12-month time scale, the percentage remains low for all categories, ranging from 1% for D4 to 5% for D0 events.

3) STATION VS CRU SPI

Figure 6 presents 3- and 12-month scale SPI time series from the CRU grid point that is nearest to each of the four observations stations of Fig. 5. This choice is

JOBNAME: JAM 00#00 2014 PAGE: 11 SESS: 8 OUTPUT: Tue Sep 2 04:21:58 2014 Total No. of Pages: 15
/ams/jam/0/jamCD140032

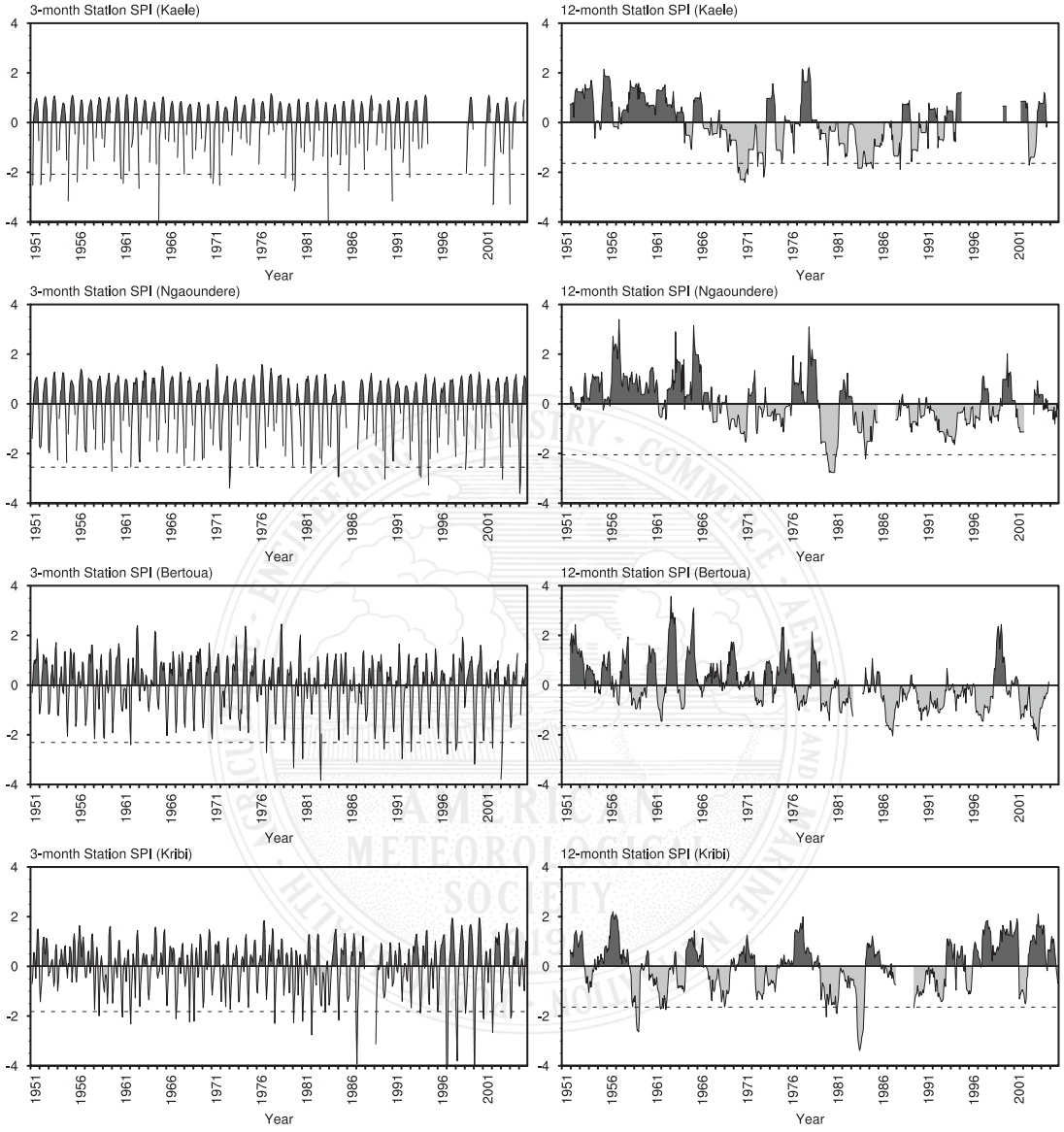

FIG. 5. Station SPI time series for the (left) 3- and (right) 12-month time scales. The horizontal dashed lines indicate operational drought thresholds for the exceptional-drought category (D4).

justified by the fact that the angular distance–weighted interpolation technique used to construct the CRU set gives more weight to the station that is nearest to the grid point, thus making it the best representative of the station. In this analysis, we compare these time series with those of the stations in Fig. 5 to access how well the gridded data reproduce drought characteristics obtained from station observations. For the 3-month-scale SPI, the two time series agree overall, with some discrepancies occurring at dates that differ from station to station: in Kaélé in the early 1950s, the 1970s, and the late 1980s; in Bertoua in the late 1990s; and in Kribi in the late 1990s, except for the drought of 1997. Most strong events that are present in the observations for at least

JOBNAME: JAM 00#00 2014 PAGE: 12 SESS: 8 OUTPUT: Tue Sep 2 04:21:58 2014 Total No. of Pages: 15
/ams/jam/0/jamCD140032

TABLE 5. Number of drought events from 1951 to 2005 and for the five drought categories (D0, D1, D2, D3, and D4). Results in parentheses represent the percentage of realization of the event over the considered time period.

	No. of events for 3-month time scale				No. of events for 12-month time scale			
	Kaélé	Ngaoundéré	Bertoua	Kribi	Kaélé	Ngaoundéré	Bertoua	Kribi
D4	21 (4%)	11 (1%)	14 (2%)	23 (3%)	9 (1%)	2 (0%)	3 (0%)	8 (1%)
D3	26 (5%)	32 (5%)	32 (4%)	36 (5%)	10 (1%)	3 (0%)	2 (0%)	14 (2%)
D2	39 (8%)	53 (9%)	41 (6%)	45 (6%)	13 (2%)	6 (0%)	7 (1%)	20 (3%)
D1	59 (12%)	76 (13%)	53 (8%)	55 (8%)	16 (2%)	21 (3%)	24 (3%)	21 (3%)
D0	81 (17%)	90(15%)	62 (9%)	66 (10%)	21 (3%)	32 (5%)	33 (5%)	27 (4%)

three stations are reproduced in the gridded data, noticeably in 1962, 1967, 1983, 1987, 1997, and 2004. Of more concern are the results of Kaélé, where station data show high year-to-year variability of drought intensities, with six events with an SPI of less than −3, when CRU has an excessively large number of events of magnitude −2. At the same station, three strong events of the early 1950s are much weaker in the gridded data, whereas weak ones in the 1970s are amplified. For the other stations, CRU tends to show more severe droughts. Thus, for events with SPI values of less than −3, there are 12 against 5 in Bertoua, 11 against 7 in Ngaoundéré, but only 3 against 5 in Kribi. This reverse situation in Kribi is due to the underestimation of strong drought events between 1997 and 2000. For the 12-month-scale SPI, the main wet (1950s and late 1990s) and dry (1970s and 1980s) periods show up in both time series. Most drought events last many years, and CRU indicates more extreme values than do stations. The discrepancies noted at shorter time scales tend to be amplified at this and higher scales. Thus, in Kaélé, gridded data show a wet (against dry) episode in the mid-1960s and early 2000s and the reverse in 1994. This phase opposition between the two datasets is also found for the late 1960s in Ngaoundéré and the early 1970s and the 1990s in Bertoua. Amplification of disagreement between station and CRU data is better seen in Fig. 7, which shows multitime-scale SPI. A case in point is the 1996–2000 period in Kribi. On the 3-month scale (Fig. 6), the four years of severe droughts indicated by the station are underestimated by CRU. At the 12-month scale, the period is wet for both and more so for the station. This reversal is due to the strong wet peaks occurring in the same period at the station but not on the CRU grid, and that contributes to the longer-scale SPI. Overall, the CRU gridded data give a fair representation of drought events in the study area and can be used where no local station observations are available. The absence of missing data points is an additional advantage. It may, however, be of interest to evaluate the merits of using more than one grid point at a given site.

5. Discussion and conclusions

We tested four statistical distribution functions on precipitation data recorded at 24 stations in Cameroon for the time period extending from 1951 to 2005. The Anderson–Darling statistic was used to select the suitable distribution functions that were then used in the calculation of the standardized precipitation index. Results were compared with those obtained using CRU grid precipitation. Operational drought thresholds were also calculated for the five defined drought categories, and results were used to study the frequency of drought events at four stations that represent different climatic zones in the study domain. Multiscalar SPI for both station and CRU were finally compared to show the usefulness of gridded data.

It was found that the suitable distribution function underlying the data changes depended on station location and on the length of the time interval used for aggregation of precipitation. The Weibull and gamma are the functions that best fit precipitation in the area. In most studies on the SPI, the gamma distribution is chosen without any testing. The need for such an evaluation is even clearer for longer time scales where Weibull, gamma, and lognormal distributions are found, with no discernable pattern. We also found that objective drought thresholds are station specific for subannual scales but that the spatial distributions are coherent. Thus, regional values can be defined. For longer scales (above 12 months), most stations in the domain have the same threshold values. For most stations, drought magnitude and duration increased with time for both short and long time scales. This can be the consequence of a reduction in precipitation resulting from climate change as suggested by Vicente-Serrano et al. (2010). Such an increase in dryness probably affected crop development and river runoff negatively. The SPI, which is based only on precipitation, cannot explain the influence of temperature change on drought condition. Thus, Vicente-Serrano et al. (2010) suggested the calculation of a new index—the

JOBNAME: JAM 00#00 2014 PAGE: 13 SESS: 8 OUTPUT: Tue Sep 2 04:21:58 2014 Total No. of Pages: 15
/ams/jam/0/jamCD140032

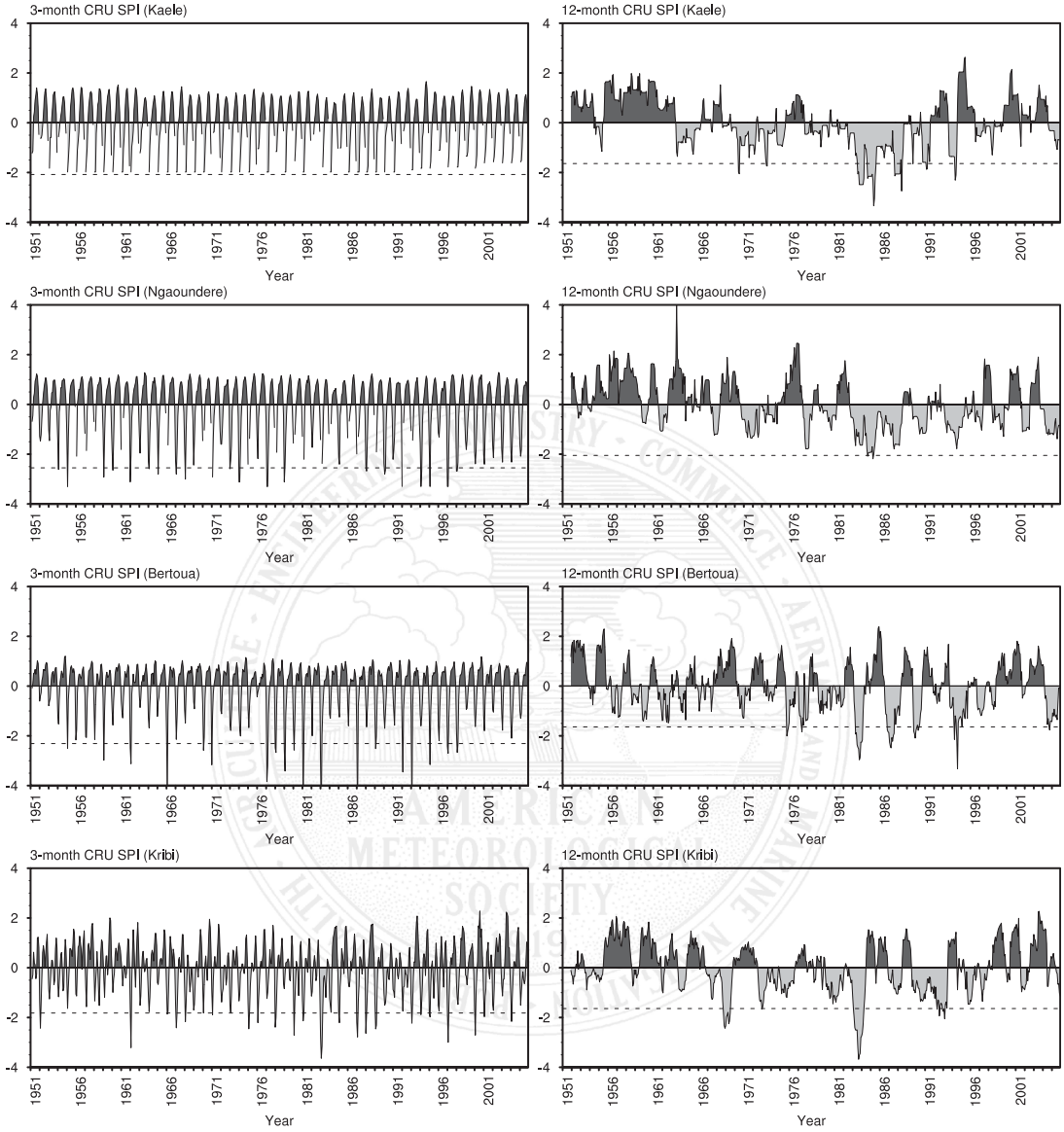

FIG. 6. The (left) 3- and (right) 12-month-scale SPI time series from the CRU grid point that is nearest to each of the four chosen stations.

standardized precipitation evapotranspiration index—that is suited to detecting, monitoring, and exploring the consequences of global warming on drought conditions. Further studies taking into account this approach are necessary to better understand the climatological features of drought. With the increase in global warming, an increase in drought magnitude, duration, and frequency is to be feared, and studies that include climate models and that are intended to guide adaptive measures also need to be done. CRU precipitation distribution functions and derived SPI corroborate the results of many stations, with some discrepancies at longer scales. Therefore, it is recommended that further investigations use CRU data for

JOBNAME: JAM 00#00 2014 PAGE: 14 SESS: 8 OUTPUT: Tue Sep 2 04:21:58 2014 Total No. of Pages: 15
/ams/jam/0/jamCD140032

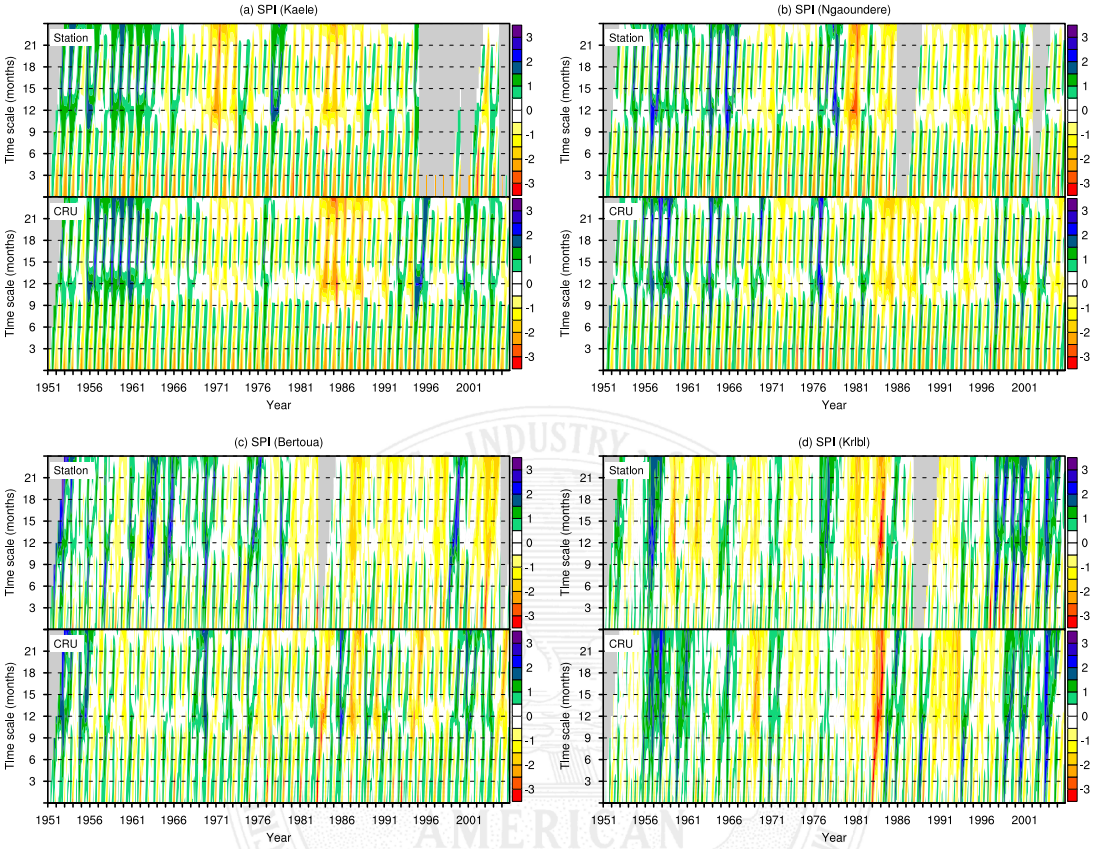

FIG. 7. Station and CRU SPI for four stations.

areas where observations are not possible or where they have high proportions of missing data.

Acknowledgments. The authors are grateful to the National Meteorological Service of Cameroon (DNMC) for providing station precipitation data. The CRU monthly precipitation data were produced by the Climatic Research Unit of the University of East Anglia.

REFERENCES

Ahmad, S., and B. A. Bhat, 2010: Posterior estimates of two parameter exponential distribution using S-PLUS software. *J. Reliab. Stat. Stud.*, **3,** 27–34. [Available online at http://www.jrss.in/data/323.pdf.]

Anderson, T. W., and D. A. Darling, 1952: Asymptotic theory of certain goodness-of-fit criteria based on stochastic processes. *Ann. Math. Stat.*, **23,** 193–212, doi:10.1214/aoms/1177729437.

——, and ——, 1954: A test of goodness-of-fit. *J. Amer. Stat. Assoc.*, **49,** 765–769, doi:10.1080/01621459.1954.10501232.

Bartosova, J., 2006: Logarithmic-normal model of income distribution in the Czech Republic. *Austrian J. Stat.*, **35,** 215–222. [Available online at http://www.stat.tugraz.at/AJS/ausg062+3/062Bartosov.pdf.]

Bilkova, D., 2012: Lognormal distribution and using L-moment method for estimating its parameters. *Int. J. Math. Models Methods Appl. Sci.*, **6,** 30–44. [Available online at http://naun.org/main/NAUN/ijmmas/17-079.pdf.]

Bordi, I., and A. Sutera, 2001: Fifty years of precipitation: Some spatially remote teleconnnections. *Water Resour. Manage.*, **15,** 247–280, doi:10.1023/A:1013353822381.

Bussay, A. M., C. Szinell, M. Hayes, and M. Svoboda, 1998: Monitoring drought in Hungary using the standardized precipitation index. *Ann. Geophys.*, **16** Supp. 11 (abstract book of 23rd EGS Gen. Assembly, Nice, France, C450), xx–xx. AU3

Druyan, L. M., 2011: Studies of 21st-century precipitation trends over West Africa. *Int. J. Climatol.*, **31,** 1415–1424, doi:10.1002/joc.2180.

Edwards, D. C., and T. B. McKee, 1997: Characteristics of 20th century drought in the United States at multiple time scales. Colorado State University Dept. of Atmospheric Science Climatology Rep. 97-2/Atmospheric Science Paper 634, 174 pp. [Available online at http://ccc.atmos.colostate.edu/edwards.pdf.]

Goodrich, G. B., and A. W. Ellis, 2006: Climatological drought in Arizona: An analysis of indicators for guiding the governor's

Fig(s). 7 live 4/C

JOBNAME: JAM 00#00 2014 PAGE: 15 SESS: 8 OUTPUT: Tue Sep 2 04:22:00 2014 Total No. of Pages: 15
/ams/jam/0/jamCD140032

Drought Task Force. *Prof. Geogr.,* **58,** 460–469, doi:10.1111/j.1467-9272.2006.00582.x.

Guenang, G. M., and F. Mkankam Kamga, 2012: Onset, retreat and length of the rainy season over Cameroon. *Atmos. Sci. Lett.,* **13,** 120–127, doi:10.1002/asl.371.

Guttman, N. B., 1998: Comparing the Palmer drought index and the standardized precipitation index. *J. Amer. Water Resour. Assoc.,* **34,** 113–121, doi:10.1111/j.1752-1688.1998.tb05964.x.

——, 1999: Accepting the standardized precipitation index: A calculation algorithm. *J. Amer. Water Resour. Assoc.,* **35,** 311–322, doi:10.1111/j.1752-1688.1999.tb03592.x.

Harris, I., P. D. Jones, T. J. Osborn, and D. H. Lister, 2014: Updated high-resolution grids of monthly climatic observations—The CRU TS3.10 dataset. *Int. J. Climatol.,* **34,** 623–642, doi:10.1002/joc.3711.

Hayes, M. J., M. D. Svoboda, D. A. Wilhite, and O. V. Vanyarkho, 1999: Monitoring the 1996 drought using the standardized precipitation index. *Bull. Amer. Meteor. Soc.,* **80,** 429–438, doi:10.1175/1520-0477(1999)080<0429:MTDUTS>2.0.CO;2.

Kandji, T. S., L. Verchot, and J. Mackensen, 2006: Climate change and variability in the Sahel region: Impacts and adaptation strategies in the agricultural sector. United Nations Environment Programme/World Agroforestry Centre Rep., 48 pp. [Available online at http://www.unep.org/Themes/Freshwater/Documents/pdf/ClimateChangeSahelCombine.pdf.]

Lana, X., C. Serra, and A. Burgueno, 2001: Patterns of monthly rainfall shortage and excess in terms of the standardized precipitation index for Catalonia (NE Spain). *Int. J. Climatol.,* **21,** 1669–1691, doi:10.1002/joc.697.

Livada, I., and V. D. Assimakopoulos, 2007: Spatial and temporal analysis of drought in Greece using the standardized precipitation index (SPI). *Theor. Appl. Climatol.,* **89,** 143–153, doi:10.1007/s00704-005-0227-z.

Lloyd-Hughes, B., and M. A. Saunders, 2002: A drought climatology for Europe. *Int. J. Climatol.,* **22,** 1571–1592, doi:10.1002/joc.846.

Manatsa, D., W. Chingombe, H. Matsikwa, and C. H. Matarira, 2008: The superior influence of Darwin Sea level pressure anomalies over ENSO as a simple drought predictor for southern Africa. *Theor. Appl. Climatol.,* **92,** 1–14, doi:10.1007/s00704-007-0315-3.

McKee, T. B., N. J. Doesken, and J. Kliest, 1993: The relationship of drought frequency and duration to time scales. *Proc. Eighth Conf. of Applied Climatology,* Anaheim, CA, Amer. Meteor. Soc., 179–184.

New, M., M. Hulme, and P. Jones, 1999: Representing twentieth-century space–time climate variability. Part I: Development of a 1961–90 mean monthly terrestrial climatology. *J. Climate,* **12,** 829–856, doi:10.1175/1520-0442(1999)012<0829:RTCSTC>2.0.CO;2.

——, ——, and ——, 2000: Representing twentieth-century space–time climate variability. Part II: Development of 1901–96 monthly grids of terrestrial surface climate. *J. Climate,* **13,** 2217–2238, doi:10.1175/1520-0442(2000)013<2217:RTCSTC>2.0.CO;2.

Ntale, H. K., and T. Y. Gan, 2003: Drought indices and their application to East Africa. *Int. J. Climatol.,* **23,** 1335–1357, doi:10.1002/joc.931.

Pal, I., and A. Al-Tabbaa, 2011: Assessing seasonal precipitation trends in India using parametric and non-parametric statistical techniques. *Theor. Appl. Climatol.,* **103,** 1–11, doi:10.1007/s00704-010-0277-8.

Palmer, W. C., 1965: Meteorological drought. U.S. Dept. of Commerce Weather Bureau Research Paper 45, 65 pp. [Available online at http://www.ncdc.noaa.gov/temp-and-precip/drought/docs/palmer.pdf.]

Panahi, H., and S. Asadi, 2011: Estimation of the Weibull distribution based on Type-II censored samples. *Appl. Math. Sci.,* **5,** 2549–2558.

Penlap, K. E., C. Matulla, H. Von Storch, and F. Mkankam Nkamga, 2004: Downscaling of GCM scenarios to assess precipitation changes in the little rainy season (March-June) in Cameroon. *Climate Res.,* **26,** 85–96, doi:10.3354/cr026085.

Quiring, S. M., 2009: Developing objective operational definitions for monitoring drought. *J. Appl. Meteor. Climatol.,* **48,** 1217–1229, doi:10.1175/2009JAMC2088.1.

Ross, S. M., 2009: *Introduction to Probability and Statistics for Engineers and Scientists.* 4th ed. Associated Press, 664 pp.

Seiler, R. A., M. Hayes, and L. Bressan, 2002: Using the standardized precipitation index for flood risk monitoring. *Int. J. Climatol.,* **22,** 1365–1376, doi:10.1002/joc.799.

Stephens, M. A., 1970: Use of the Kolmogorov–Smirnov, Cramér–Von Mises and related statistics without extensive tables. *J. Roy. Stat. Soc.,* **32B,** 115–122. [Available online at http://www.jstor.org/stable/2984408.]

Svoboda, M., and Coauthors, 2002: The Drought Monitor. *Bull. Amer. Meteor. Soc.,* **83,** 1181–1190. [Available online at http://journals.ametsoc.org/doi/abs/10.1175/1520-0477%282002%29083%3C1181%3ATDM%3E2.3.CO%3B2.]

Szalai, S., and C. Szinell, 2000: Comparison of two drought indices for drought monitoring in Hungary—A case study. *Drought and Drought Mitigation in Europe,* J. V. Vogt and F. Somma, Eds., Springer, 161–166.

Tarhule, A., Z. Saley-Bana, and P. J. Lamb, 2009: A prototype GIS for rainfall monitoring in West Africa. *Bull. Amer. Meteor. Soc.,* **90,** 1607–1614, doi:10.1175/2009BAMS2697.1.

Thom, H. C. S., 1958: A note on the gamma distribution. *Mon. Wea. Rev.,* **86,** 117–122, doi:10.1175/1520-0493(1958)086<0117:ANOTGD>2.0.CO;2.

UNEP, 2002: *African Environment Outlook: Past, Present and Future Perspectives.* United Nations Environment Programme, 422 pp. [Available online at http://www.unep.org/dewa/africa/publications/aeo-1/.]

Vicente-Serrano, S. M., 2006: Spatial and temporal analysis of droughts in the Iberian Peninsula (1910-2000). *Hydrol. Sci. J.,* **51,** 83–97, doi:10.1623/hysj.51.1.83.

——, S. Begueria, and J. I. López-Moreno, 2010: A multiscalar drought index sensitive to global warming: The standardized precipitation evapotranspiration index. *J. Climate,* **23,** 1696–1718, doi:10.1175/2009JCLI2909.1.

Wilks, D. S., 1995: *Statistical Methods in the Atmospheric Science: An Introduction.* Academic Press, 467 pp.

——, 2006: *Statistical Methods in the Atmospheric Sciences.* 2nd ed. Academic Press, 627 pp.

Wu, H., M. D. Svoboda, M. J. Hayes, D. A. Wilhite, and F. Wen, 2007: Appropriate application of the standardized precipitation index in arid locations and dry seasons. *Int. J. Climatol.,* **27,** 65–79, doi:10.1002/joc.1371.

Wu, S.-J., 2002: Estimations of the parameters of the Weibull distribution with progressively censored data. *J. Japan Statist. Soc.,* **32,** 155–163, doi:10.14490/jjss.32.155.

Yuan, X., E. F. Wood, N. W. Chaney, J. Sheffield, J. Kam, M. Liang, and K. Guan, 2013: Probabilistic seasonal forecasting of African drought by dynamical models. *J. Hydrometeor.,* **14,** 1706–1720, doi:10.1175/JHM-D-13-054.1.

Zhang, Q., X. Chong-Yu, and Z. Zengxin, 2009: Observed changes of drought/wetness episodes in the Pearl River basin, China, using the standardized precipitation index and aridity index. *Theor. Appl. Climatol.,* **98,** 89–99, doi:10.1007/s00704-008-0095-4.